THEORETICAL STUDY OF RESONANT TERAHERTZ GENERATION IN ANHARMONIC CARBON NANOTUBES

A Thesis

Submitted in partial fulfillment of the requirements for the

award of the degree of

DOCTOR OF PHILOSOPHY

in

Physics

By

Sandeep Kumar

41800798

Supervised By

DR. VISHAL THAKUR
(Associate Professor)

Department of Physics
Lovely Professional University
Phagwara.

Co-Supervised by

DR. SHIVANI VIJ
(Assistant Professor)

Department of Applied Sciences,
DAV Institute of Engineering & Technology
Jalandhar.

LOVELY PROFESSIONAL UNIVERSITY
PUNJAB
2022

DECLARATION BY THE SCHOLAR

I hereby declare that the research work reported in the Ph.D. thesis entitled **"Theoretical Study of Resonant Terahertz Generation in Anharmonic Carbon Nanotubes"** submitted at **Lovely Professional University, Phagwara, Punjab, India,** is an authentic record of my work carried out under the able guidance and supervision of **Dr. Vishal Thakur** and **Dr. Shivani Vij**. I have not submitted this work elsewhere for any other degree or diploma or any other professional certificate. I am fully responsible for the matter and contents of my Ph. D Thesis.

Sandeep Kumar

Department of Physics

Lovely Professional University, Phagwara, Punjab, India

Date-15-July, 2022

SUPERVISOR'S CERTIFICATE

This is to certify that the research work reported in the Ph.D. thesis entitled **"Theoretical Study of Resonant Terahertz Generation in Anharmonic Carbon Nanotubes"**, submitted by **Sandeep Kumar** at **Lovely Professional University, Phagwara, Punjab, India** is a bonafide record of his novel and original work carried out under my able guidance and supervision. This work has not been submitted elsewhere for any other degree or diploma or any other professional certificate.

Dr. Vishal Thakur

Associate Professor

Department of Physics

Lovely Professional University, Phagwara, Punjab, India

Date-15-July-2022

CO-SUPERVISOR'S CERTIFICATE

This is to certify that the research work reported in the Ph.D. thesis entitled **"Theoretical Study of Resonant Terahertz Generation in Anharmonic Carbon Nanotubes"**, submitted by **Sandeep Kumar** at **Lovely Professional University, Phagwara, Punjab, India** is a bonafide record of his novel and original work carried out under my able co-guidance and co-supervision. This work has not been submitted elsewhere for any other degree or diploma or any other professional certificate.

Dr. Shivani Vij

Assistant Professor

Department of Physics

DAV Institute of Engineering and Technology Jalandhar, Punjab, India

Date-15-July-2022

Abstract

The stretch between the microwave and infrared regions of the electromagnetic wave spectrum results in the formation of terahertz (THz) region. The frequency of THz radiation lies in the frequency range $\sim 10^{11}$ Hz to $\sim 10^{13}$ Hz. The THz radiation on an average has a time-period, $\tau \sim 1.0$ ps, wavelength $\lambda \sim 300$ μm, wave number $k \sim 33.0$ cm^{-1}, frequency $\upsilon \sim 1$THz with photon energy $E = h\upsilon \sim 4.2$ meV. The THz radiation, therefore, interacts strongly with those systems which have their characteristic life-time of the order of ps and energy transition of the order of meV, like bound electrical charges, phonons, free electrons of plasma in the pattern of CNTs, etc. The boundary lines of THz region are not definite and well defined but depend upon the various generation and detection methods used for THz radiation. In the early nineties, due to a lack of efficient generation, detection methods and due to poor research work, the THz region is known as the "THz gap". From the beginning of the 21st century, THz technology has shown immense potential in many applications related to the field of science and research. In the present times, THz technology is used in many fields like industry-manufacturing, pharmaceutical-chemical industry, oncology, dermatology, medical imaging, explosive-chemical detection, safety-security-protection measures, oral healthcare sector, broad hand communication, etc., depending upon their respective special characteristics. To tap the maximum potential of THz technology, it is the need of the hour to create compact, proper, portable, cost effective, reliable, and efficient sources of THz radiation. One of the most recent trends is to employ carbon nanotubes to produce compact, portable and

efficient THz sources. This is because of some extraordinary properties of CNTs like nano dimensions, high thermal and electrical conductivity. The main purpose of the presented thesis is to explore the ways to produce efficient and compact sources of THz generation by using some external parameters and new information about fundamental concepts behind the physical processes. In the present thesis, we have suggested to utilize the array of anharmonic vertically aligned CNTs (VA-CNTs) and horizontally aligned CNTs (HA-CNTs) for the production of economical, portable, and efficient THz sources. In this theoretical research work, various mechanisms of resonant THz generation by the propagation of laser beams through the array of vertically or horizontally aligned anharmonic CNTs has been provided. For this, different schemes by using different conditions and parameters are presented in the thesis. In the thesis, various lasers like plane-polarized and amplitude modulated lasers, etc. are used to interact with the array of CNTs to generate THz radiation. The present thesis consists of four distinct and novel objectives. Each objective has been explained by using the paraxial ray approximation (PRA). Methodology and formulation of hypothesis have been explained in the 2nd chapter of the thesis. The proposed novel terahertz generation schemes can be combined with different laser-plasma and CNTs parameters to increase the power and efficiency of emitted THz radiation.

In the first chapter named Introduction of the thesis, Terahertz gap, THz radiations, special characteristics of THz waves, technological advancements of THz science with the time, research motivation, research objectives, literature review and unique theories of THz generation has been explained. In the second chapter, we have provided a

detailed explanation of the research methodology and formulation of the hypothesis used by us in the present THz generation research work. In the third chapter of the thesis, THz radiation is generated by the propagation of laser beams through the magnetized anharmonic CNTs. Here the static magnetic field is applied transverse to the longitudinal axis of CNTs and to the direction of propagation of lasers. The anharmonicity produced in the CNTs results in increasing the THz generation. In the fourth chapter, we have provided two analytical models for the generation of efficient THz radiations by employing laser filaments under the influence of externally applied transverse static electric and magnetic fields. In the first model, low-intensity THz radiations are generated, which are found to be useful in medical diagnosis of the human beings. In the second model, we provide the interaction of the amplitude-modulated and filamented beam with an array of anharmonic VA-CNTs under the effect of electric and magnetic fields. The anharmonicity plays a very significant role in this scheme to enhance the efficiency and normalized amplitude of THz generation. The fifth chapter of this thesis presents the effect of the cross-focusing of laser beams on the array of vertically aligned anharmonic and magnetized CNTs to generate efficient THz radiation. In the last chapter of the thesis, the prospects and scope of the present research work in futuristic applications have been explained. In this chapter, several insights, and inferences obtained from the above analysis are discussed collectively for the futuristic advancement of the THz science and technology in various fields of the scientific research. In the proposed research work, the unconventional and unorthodox schemes has been developed by using CNTs to obtain the novel THz source to generate efficient THz radiations. This novel THz source can provide

excellent support in upgrading the THz applications. It can also provide a helping hand in making more understanding of nonlinear effects involving THz-matter interactions. This can also open up the doors for many unrevealed nonlinear effects. During the laser-plasma interactions in the array of VA-CNTs and HA-CNTs, the generation of THz radiations is also accompanied by some highly energetic particles and radiations. Most of the time, these highly energetic sub-atomic particles and radiations are electrons, neutrons, protons, positive ions, negative ions, x-rays, γ-rays, etc. By using these additionally generated particles and radiations, we can develop a multipurpose THz pump, x-ray probe, THz probe. These pumps and probes can be further used in many applications of material science and strong-field physics. The highly energetic THz radiations produced by powerful and efficient THz sources can be used to accelerate electrons in accelerators. Such accelerators can be further used in many investigations of particle physics. This can also help reduce the size of high-energy particle accelerators. Researchers from the fields of chemistry and biology are likely to use such a THz source as a unique and powerful research tool to investigate chemo-catalysis and hydration, respectively. THz applications in phase transition and spintronics are also the most active research areas of modern material science. The average energy of the THz photon (4.2 meV) is comparable to the energy of excitons, magnons, and phonons in various systems. Thus, THz technology acts as an anchor to control transient states of matter such as photonics, spintronics, etc. The novel THz sources can be used in the research work of previously inaccessible transients in materials.

ACKNOWLEDGEMENTS

CONTENTS

List of Symbols

$-e$	Electric charge
m	Rest mass of the electron
n_0	Equilibrium plasma density
ω_P	Plasma frequency
ω_1	Frequency of first beating laser
ω_2	Frequency of second beating laser
k_1	Wavenumber of first beating laser
k_2	Wavenumber of second beating laser
ω, ω_{TH}	Frequency of emitted terahertz waves
k, k_{TH}	Wavenumber of terahertz wave
B	External static magnetic field
ω_c	Cyclotron frequency of the electrons of CNTs
E_{ion}	Electric field due to ion cylinder
E_{ele}	Electric field due to electron cylinder
E_s	Space charge electric field
$E_{D.C}$	External static electric field
F_{PM}	Ponderomotive force
β_0	Periodicity of ripples
$n_{\alpha 0}$	The amplitude of density ripples
a	The inner radius of each CNT

b	The outer radius of each CNT
d	Inter-separation distance of CNTs in the array
f_1, f_2	Dimensionless beam width parameters of two lasers
ζ	Normalized distance of propagation
μ	Modulation index of laser
r_{10}, r_{20}	Initial radii of laser beams
ϵ	Electric Permittivity
Δ	Displacement of electrons and ions
ν, ν_e	Collisional Frequency of electrons and neutrals
b_0	Non-uniformity Factor
n_c	Number density of CNTs
α	Anharmonicity Factor
β	Characteristic Parameter
χ	Magnetic Susceptibility
J	Nonlinear Current Density
$\cdot$	Dot product
$\times$	Cross product
$*$	Complex Conjugate
∇	Operator

Abberivations

- EM wave : Electromagnetic wave
- MW : Micro Wave
- CW : Continuous Wave
- THz : Terahertz
- DC : Direct Current
- CUR : Coherent Undulator Radiation
- CSR : Coherent Synchrotron Radiation
- FEL : Free Electron Laser
- LWFA : Laser Wake Field Accelerator
- QCL : Quantum Cascade Laser
- GL : Gas Laser
- HFO : High Frequency Oscillator
- CNTs : Carbon Nanotubes
- SWCNTs : Single Walled Carbon Nanotubes
- MWCNTs : Multi Walled Carbon Nanotubes
- VA-CNTs : Vertically Aligned Carbon Nanotubes
- HA-CNTs : Horizontally Aligned Carbon Nanotubes
- PRA : Paraxial Ray Approximation

LIST OF FIGURES

Chapter 1
Introduction

1.1. Overview and History

Terahertz (THz) waves also known as T-rays or sub-millimeter waves or far infrared waves or T-lux or T-Light or tremendously high frequency waves lie in the region of the electromagnetic wave spectrum with a frequency range $\sim 10^{11}$ Hz to $\sim 10^{13}$ Hz. These waves were, first of all, come into an observation about 120 years ago. The THz region is defined as a sandwich region between the high-frequency band of microwave (MW) (known as electronics) and low-frequency band of infrared light (IR) (known as photonics). The location of the THz radiation region is shown in figure 1.1. The THz radiation has a time-period, $\tau \sim 1.0$ ps, wavelength $\lambda \sim 300$ μm, wave number $k \sim 33.0$ cm^{-1}, frequency $\upsilon \sim 1$THz with average photon energy $E = h\upsilon \sim 4.2$ meV [1-4]. THz radiation, therefore, interacts strongly with those systems which have their characteristic lifetime of the order of ps and energy transition of the order of meV, like bound electrical charges, phonons, free electrons of plasma in the pattern of CNTs, etc. The boundary lines of THz region are not definite and well defined but depend upon the various generation and detection methods used for THz radiation. In the early nineties, due to a lack of efficient generation, detection methods and due to poor research work, the THz region is known as the "THz gap" [5, 6]. But in the modern era "THz gap" (also known as the Shadow region in the electromagnetic spectrum) term is not relevant and suitable, as the gap has been filled due to extensive research work and interesting developments in the THz generation. Earlier in the biginning of 20th century, there are lot of difficulties faced by researchers in producing, generating, propagating, tuning, and controlling the THz radiations. However, due to the continuous progressive approach in the THz field, THz technology has become the crown technology of the world. Now at present THz technology is considered as one of the most advanced and futuristic technologies of the modern world for numerous applications in almost every field of science [7-12]. Some of the properties of THz waves are the same as that of other electromagnetic waves like THz waves

can travel along a straight line, speed of THz waves is the same as that of other electromagnetic waves in air or vacuum (3×10^{10} cm/s). The THz waves also have some special characteristics associated with them as explained below
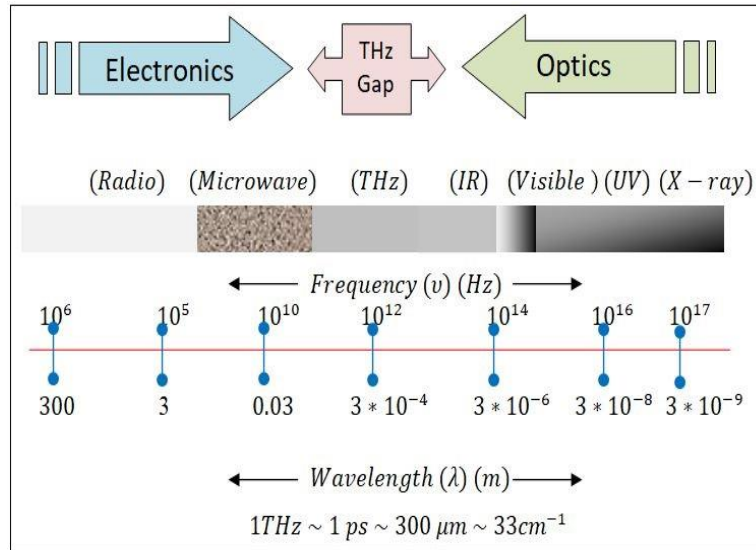
Figure 1.1 Location of THz gap in the electromagnetic spectrum

(i) THz wave can easily make penetration through many non-polar, optically opaque, and non-metallic materials. As a result THz wave can pass though ceramics, paper, books, clothes, wood, plastics, cardboard, etc. [13]. (ii) Most fundamental molecules like O_2, H_2O, CO, and chemical substances have their spectral lines, lying in the THz frequency range, which provides chemical and structural information of chemical substances and organic molecules [14, 15]. (iii) THz radiation can show reflection by the metal surface [16]. (iv) THz radiations are very effectively absorbed by the polar molecules (the molecules in which one end is positively charged and other end is negatively charged) like water. As a result, THz spectroscopy becomes convenient for the investigation of material structures and biological tissues. In medical science, it is well known fact that tumor cells consist of more amount of H_2O as compared to the healthier tissues and THz radiations show different attenuation coefficients in water, or the absorption coefficient in water lies between $100\,\text{cm}^{-1}$ to $1000\,\text{cm}^{-1}$ [17]. (v) THz radiation is non-ionizing, non-destructive, and non-invasive,

resulting in no harm to living cells and tissues of human beings [18, 20]. (vi) The long wavelength of THz radiations is responsible for the very small Rayleigh scattering for THz radiation

The generation of THz radiation has been started even from the early nineties by using various schemes and methods such as optical THz generation, quantum cascade laser, optical rectification, and sources based on laser-plasma interactions [21-26]. The generation of THz radiation by Solid-state electronic devices is limited to lesser than 1 THz. The THz generation by optical rectification can be categorized into two types (i) The THz generation in non-linear media (ii) The THz generation from accelerating electrons. When electromagnetic waves incident in nonlinear media, there occurs non-linear frequency conversion, and it is based on the 2nd order nonlinear optical properties of the materials. Moreover, it has been proved that many nonlinear media like GaAs, GaSe, GaP have a special ability to generate THz radiation through optical excitation techniques [27, 28]. Two types of 2nd order nonlinear processes are involved in THz generation in nonlinear media. One of the processes is known as optical rectification, which is limited to femtosecond laser excitation and another 2nd order nonlinear process is difference frequency generation by laser beating. In this difference frequency generation process, two electromagnetic beams (CW) having frequency difference in the THz region can generate THz waves (CW). THz radiation can also be generated by accelerating electrons. The most popular device to generate THz waves based on the principle of accelerating electrons is photoconductive antennas. The incident laser beam illuminates the slot present between two electrodes on the photoconductive antenna and generates photo carriers. The photo carriers can be accelerated by the D.C. bias field between two electrodes and which further results in photocurrent. This time-varying photocurrent increases with the increase of the intensity of laser beam and vice versa. The another important medium used to generate THz radiation from accelerating electrons is air plasmas. There are two mechanisms involved in air plasma THz radiation generation. One of which is the ponderomotively induced space-charge field created by laser field gradient and the other is the asymmetric laser field by mixing a fundamental beam and its second harmonic beam. In both cases, electric

fields can accelerate the free electrons generated by photoionization via femtosecond laser pulse excitation and as a result, there is the generation of THz radiations. At present, the most powerful THz generation sources are large accelerator-based sources. In these sources, THz generation is possible by employing ultra-relativistic electrons via various schemes CUR (coherent undulator radiation), coherent synchrotron radiations (CSR), and free electrons laser (FEL). FEL employs a strong D.C. magnetic wiggler. This device can produce high powers and is tunable between ~ 0.10 THz to ~ 10.0 THz. Although, the above-mentioned schemes of THz generation can be used to generate THz radiations of ~ 0.10 THz to ~ 10.0 THz, still these are not efficient enough. Moreover, low damage limit, low conversion efficiency, large size, bulky and high cost are associated with these THz sources.

After the discovery of carbon nanotubes in 1999 by Iijima [29], CNTs brought a revolution in many areas of science and technology due to their extraordinary electrical and thermal conductivities [30-37]. In the modern physics world, the latest trend is to use CNTs for the THz generation and detection [38-40], because of their nano-scale dimensions that is compactness. By CNTs, we mean quasi-one-dimensional carbon macromolecule attained by rolling a single or more layers of graphene into a cylindrical structure whose length is in micrometers and diameter is in nanometers. Rolling is represented by two indices n_1 and n_2. If $n_1 = 0$, then CNTs are zigzag, if $n_1 = n_2$, then CNTs are armchair CNTs, If n_1 and n_2 are not equal but greater than zero then CNTs are chiral chair CNTs. The indices n_1, n_2 can also decide the nature of CNTs. Metallic CNTs (MCNTs) are formed if the condition $(n_1 - n_2 = 3p)$, is satisfied where p is an integer. On the same pattern, semiconducting CNTs are formed if the condition $(n_1 - n_2 = 3p + 1)$ is satisfied. With the help of CNTs, we can produce compact sources for THz generation with high efficiency. When a laser beam interacts with the CNTs, the ponderomotive force will act on the electrons of CNTs to produce an oscillatory current. This results in an efficient THz generation. In our research work, we have effectively used the anharmonic effects on carbon nanotubes under the influence of external static fields.

1.2. Technological Advancements and Applications of THz radiations

Based on present and past developments and recent advancements in the field of THz radiation, there has been a huge surge in the applications of THz technology. Therefore, this field is still young and open for some of the futuristic utilizations and applications of THz radiation like THz-tomograpohy, THz-sensor, THz-imaging, THz-spectroscopy, THz-security system, THz-diognostics, etc. are discussed below

1.2.1. Industrial uses

THz radiation can be used in many industrial processes like manufacturing, quality control, maintaining the proper chemical composition and process monitoring, etc. THz radiation in general is preferred to use in those industries in which products are packed in cardboard or plastic packing. In 1995 first time THz time-domain spectroscopy was for producing an image of the wrapped electronic chip [41]. In this system, a pulsed beam with a duration of 10^{-12} seconds is utilized.

1.2.2. Security and Safety Systems

At airport terminals, railway station platforms, VIP places; it is difficult to detect explosives with x-ray detection but distinct signatures of explosives lie in the THz region and we can use THz for the detection of explosives. THz radiation can be reflected by the metal surfaces therefore, can be used for detection of hidden weapons like pistol, knife and any other sharp weapons under the clothes by the terrorists. As these radiations can pass through cardboard, clothes, wood, ceramics, etc., hence can be used to detect letter bombs, parcel bombs, and others. In some countries like Holland, THz security system has become active at some of the airports. In the future, we can upgrade THz security systems to a higher level with new advancements in technology.

1.2.3. Biological and pharmaceutical sciences

When a beam of THz radiations passes through the tissues of human beings (such as the chest, liver, heart, kidney, breast, etc.) there occurs a notable difference between absorption and refractive indices of THz radiations and one can detect easily that which tissue is healthy and which one is infected. When THz beam interacts with living tissues of the human beings, the reflection or transmission of THz pulses provides a significant insight about the molecular structure of healthier or unhealthier biological tissues. This information is quite sufficient to produce the images of the tissues. Nonionizing nature makes THz radiation safe for biological sample diagnostics. In pharmaceutical industries, THz imaging is used to check the integrity and uniform distribution of chemicals of tablets and their coating.

1.2.4. Broad Band Communication

As THz radiations can be effectively absorbed by the earth's atmosphere therefore, the range of THz radiation becomes very small in air. The propagation distance of THz radiation is measured to be very small (only up to ~ 10.0 m). This shows that THz radiation is not suitable for long-distance communication applications. However, within a distance of ~ 10.0 m, the THz band has many applications because of high data transmission rate of the order of 10^2 Gbits/sec. As a result, THz band can be used in indoor wireless networking systems. In 2012, a team of researchers [42] proved that THz radiation can be used as the bandwidth of data transmission in the future. They sent a signal with (~ 542 GHz) resulting in the transfer of Gbits/sec. Optical communication may have problems of scattering and absorption of signals by clouds, rain, dust, etc. But according to Rayleigh scattering, as the wavelength of THz radiation is longer, therefore, scattering is low. As a result, THz can be used for short distances very effectively even in the presence of clouds, smoke, dust, and rain.

The main obstacle in the progressive growth of THz technology is the non-availability of compact, cost effective, efficient and appropriate sources of THz generation. Numerous schemes have been provided by the researchers for the enhancement and improvement in the power, quality, amplitude, tunability and efficiency of THz sources.

1.3. Review of Literature

Hamster *et al.* [43] formulated a theory in which they explained that when a laser beam of power 10^{13} W interacts with gaseous and solid targets, pulsed radiation is generated whose frequency lies in the terahertz region. These radiations are observed to be more intense when laser incident on the solid and form plasma. The emission of these radiations is on the same pattern as that of x-rays and electrons. In this work first time, laser-induced wakefield came into observation. In this, non-linear force (known as ponderomotive force) is responsible for the creation of a large density difference between ions and electrons, and charge separation results in electromagnetic transient. To determine the magnitude of THz radiation hydrodynamic model is used.

Hamster *et al.* [44] again proposed a scheme in which high-intensity ultra-short laser pulses interact with plasmas, resulting in short-pulsed radiation generation which has a frequency in the terahertz region. In this ponderomotive forces results in electromagnetic transient and to find out the magnitude of THz radiation in a more accurate way, the linearized hydrodynamic model was preferred. It results in the enhancement of THz radiation power to a few MW.

Braun *et al.* [45] provided the theory on filamentation action. The filamentation action of laser pulses in the air (as a medium) was observed during 1995. Filamentation is a non-linear optical phenomenon related to the propagation of a beam of light through the medium without significant diffraction. This is possible in accordance with the optical Kerr effect, which results in the change of the refractive index in the medium and proportional to the intensity of the light beam as a result core of the light beam becomes more intense than the wings of the beam.

Chang *et al.* [46] have predicted that the plasma channel formation by the laser pulse propagates in air results in the emission of THz radiation but transverse to the axis of the filament. This is because of radiation pressure exerted by the laser pulse that indues nonlinear plasma oscillations in the longitudinal direction with frequency same as that of plasma frequency. Electron density in filaments is of the order of $n_e \sim 10^{16}$ cm^{-3}. The ponderomotive force is responsible for the THz generation in the system. It is due to this non-linear force that

charge separation is produced and wake is neutral as a whole. Out of many significant properties of filaments, one of them is their potential to produce weak plasmas in the presence of propagating laser pulse. It is also observed that filaments can be used to enlarge the plasma strings

Hourad *et al.* [47] proposed a theory in which the magnitude of terahertz radiation is enhanced by three folds when femtosecond pulse undergoing the action of filamentation in the air was considered, in the influence of the applied electric field. The nonlinear ponderomotive force excites the plasma oscillations. In this theoretical model, it was observed that THz radiation shows sensitive behavior towards the external static electric field.

Pathak *et al.* [48] provided a novel theory for the THz generation by interacting relativistic electron beam with a rippled density plasma with finite transverse ripple factor, When the relativistic beam of electrons incident on the plasma with density ripple making an angle with the direction of the beam, then THz signal provides finite oscillatory velocity to the plasma electrons. These oscillatory electrons make coupling with the density ripple to produce transverse current density which drives the THz signal and amplitude of THz signal increases and so on

Bhasin and Tripathi [49] examined the effect of optical rectification of a picoseconds laser pulse in rippled density magnetized plasma for the enhancement in the THz generation. When D. C. magnetic field is acting perpendicular to the direction of propagation of the laser beam, a nonlinear ponderomotive force will comes into action to provide drift velocity to plasma electrons. This drift velocity of electrons results in density ripple to produce an oscillatory current and this current is responsible for the THz generation. Due to the azimuthal magnetic field, there occurs an increase in the conversion efficiency.

Sharma *et al.* [50] observed the enhancement in the THz generation, when circularly polarized laser beam interacts with density ripple in the collisionless magnetized plasma. The ponderomotive force between high power laser beam and density ripple results in a nonlinear current at some frequency difference. In this system, the magnetic field is applied in the

direction of the circularly polarized beam. There occurs a coupling with density ripple already present to produce nonlinear current density and this generates the THz radiation.

Bhasin and Tripathi [51] used the filamentation action for the generation of THz radiation under the effect of the external static electric field. When two femtosecond laser pulses with filamentation action interact with plasma under the applied electric field perpendicular to the direction of propagation, then laser exerts ponderomotive force as well as static ponderomotive force on the plasma electrons, out of which static ponderomotive force cancels out with pressure gradient force and results in transverse density ripple at zero frequency. The beat frequency ponderomotive force is responsible for velocity oscillations as well as density oscillations. These density oscillations produce a transverse current and this current is suitable for the THz generation.

Malik *et al.* [52] put forward a new approach in which two spatial-Gaussian laser beams with different frequencies and wavenumbers but with the same electric fields interacts in a spatially periodic density plasma under the effect of the static magnetic field applied in the direction perpendicular to the propagation of laser beams to increase the efficiency of THz radiation generation. Due to applied magnetic field, ponderomotive force is resolved in to its components and these components result in the non-linear oscillatory currents. These currents at resonance excites the THz radiation. By optimizing the values of magnetic field amplitude tuning of THz radiation is also possible.

Kumar and Tripathi [53] investigated the non-linear absorption and anharmonic generation, when a short-pulse laser interacts with a gas embedded with anharmonic clusters. The interaction of laser results in the excursions in cluster electrons and these excursions are comparable to the cluster radius. These electron excursions are not linearly proportional to the restoration force, as a result, plasma resonance is widened and there is a broadband absorption and due to this harmonic generations are produced. This theory can be extended for the efficient THz generation.

9

Singh *et al.* [54] proposed a scheme for the effective generation of terahertz radiation by beating two *cosh*-Gaussian laser beams in spatially periodic density plasma. Here *cosh*-Gaussian lasers are preferred because of their high efficiency as compared to Gaussian laser. These lasers exert a non-linear force known as ponderomotive force along the direction perpendicular in which oscillatory velocity is provided to the electrons and couples with density ripple to produce a transient transverse current which further drives the terahertz radiation. In this, they also discussed the importance of laser beam width parameters in providing a notable increase in the magnitude of the THz field and its generation efficiency.

Liu *et al.* [55] investigated that high-intensity laser when interacting with non-uniform density clusters, there occurs broad surface Plasmon resonance due to excursions produced in clusters. As the clusters get heated, there occurs expansion in clusters hydro-dynamically and resulting in enhanced X-ray emission. If we increase the non-uniformity of clusters then yield will decrease. If we increase the intensity of the laser, the non-linearity in laser cluster interactions may arise even before the electron heating. This theory can be applied for the efficient THz generation.

Bakhtiari *et al.* [56] presented a theory in which two flat-topped laser beams with different frequencies and wavenumbers and the same electric field amplitudes undergo beating in spatially periodic density plasma for the THz generation. Here flat-topped laser beams are preferred because of the steep gradient in the distribution of laser intensities and wider cross-section as compared to others. Due to these features stronger ponderomotive force originates to produce a stronger non-linear current and as a result stronger terahertz radiation field. If the flatness of the beams is increased, it results in enhancement of the terahertz radiation field. It was also observed that an increase in beat frequency can have a negative effect on the efficiency of the THz generation but this can be neutralized by making suitable changes in the density ripple magnitudes. Therefore it was clear that terahertz radiations show a high sensitiveness nature towards the flatness of beams and the efficiency of terahertz generation can be increased effectively by optimizing the values of laser and plasma parameters

Kumar and Kumar [57] formulated a new scheme for the THz generation by passing an ultra-short electron bunch over a planner array of carbon nanotubes across their lengths. When an ultra-short electron beam is incident on carbon nanotubes, the repulsive force will act on the free-electron cylinder of each nanotube to displace them with respect to the ion cylinder. When Pulse Pass through, electron cylinders start oscillating at their natural frequency and behave as a dipole antenna to emit THz radiation of suitable frequency.

Ahmad *et al.* [58] proposed a theory in which two laser beams with fundamental frequency ω_1 and close to second harmonic $2\omega_1$ propagating along the same axis and direction undergo self-focusing in multi-ion species of plasma to make efficient THz generation. The ponderomotive force acting on electrons will result in non-linear effects. Due to space charge field effects, ions of higher charged state get strong depletion from the axis, and electrons are surrounded by the ions of lower charge state. During the self-focusing action, the power of the laser beam becomes equal to its critical value. At the same instant, the plasma generates the oscillatory waveguide for the weak beam, as a result, the weak beam shrinks and retraces its path when its frequency is lower than that of its counterpart. Also, it retraces its path when its frequency is more than its counterpart. The non-linear effects will be produced when both beams are equally strong. The cross-coupling of the beams will result in a nonlinear current resulting in the generation of terahertz radiation at $\omega = \omega_{1-}\omega_2$. The Phase matching is provided with an axial density ripple to provide better conversion efficiency in the generation of terahertz radiation.

Sharma and Vijay [59] formulated a theory for the THz generation by using an anharmonic CNTs matrix well embedded in the silica surface. When two collinear laser beams interact with the CNTs matrix, there occur large diplacements by the electrons of CNTs to produce non-linear force at beat frequency $\omega = (\omega_1 - \omega_2)$. This non-linear force is responsible for the non-linear current and hence this non-linear current generates the THz radiation.

Sharma and Vijay [60] formulated a theory for the THz generation by using CNTs embedded on the metal surface. When two laser beams incident on the metal surface at some

angle, due to the non-linear mixing of lasers, a ponderomotive force comes into action on the various electrons of CNTs (arranged in the array) at the beat frequency $\omega = \omega_{1-} \omega_2$. It further results in nonlinear current as a result CNTs will behave as an array on antennae generating THz radiation at the beat frequency. The THz field is resonantly enhanced at plasmon resonance. The collisions are not significant in this theory.

Vij *et al.* [61] proposed a theory in which vertically aligned CNTs can behave as emitters for the THz radiations .when they beat two laser beams and incident on the VA-CNTs under the influence of the applied magnetic field, then the power of THz radiation is enhanced. The normalized power of the THz radiation dpends on the dimensions of the CNTs.

Afanas'ev *et al.* [62] studied that CNTs can behave as dipole antennae which can emit THz radiations in the phase when one or two counter-propagating laser beams incident on an array of CNTs, phase matching condition is obtained. Due to this condition Plasmon waves of THz range can be generated along the CNTs.

Singh *et al.* [63] explained THz generation in density ripple plasma by using Cosh-Gaussian laser beams. These incident laser beams exert ponderomotive force on the free electrons of the plasma and impart finite oscillatory velocity. The coupling with density ripple results in a stronger nonlinear transient current.

Thakur *et al.* [64] provided a theoretical analysis of harmonic generation by interacting laser beam with anharmonic CNTs grown over the silica surface. The laser beam displaces the electrons of CNTs and results in the restoration force. The restoration force of the electrons of CNTs does not vary linearly with the corresponding displacement. As a result, there occurs broad resonance peak to enhance the power conversion efficiency of harmonic generation.

Gurjar *et al.* [65] explained the THz generation by copropagating two laser pulses through the electron-hole plasma. These laser pulses exert a nonlinear ponderomotive force on electrons and holes of the plasma to provide finite oscillatory velocities at the laser beat frequency. The laser beat wave makes interaction with the plasma density perturbation to

produce a nonlinear transverse current density, which is further responsible for the coherent THz radiation.

1.4. Laser plasma Intereaction

Plasma (the fourth state of matter) is defined as the ionized gas, consisting of approximately equals number of electrons an ions and exhibits collective behavior. The plasma was discovered by William Crooks in 1879, with the help of an electrical discharge tube known as 'Crooks tube'. The name 'plasma' was later provided by the Nobel Laureate Irving Langmuir, in 1928. The plasma is known as the conducting medium due to the presence of free electrons and ions. The properties of plasma are not affected by propagation of low intensity electromagnetic waves. However, the interaction of intense laser pulses with plasma attracts great attention since nonlinear effects lead to several interesting phenomena(66, 67). In order to understand nonlinear laser-plasma interaction, consider the electric and magnetic fields of an intense linearly polarized laser field,

$$\vec{E} = \hat{x} E_0(r, z, t) \cos(kz - \omega t), \tag{1.4.1}$$

$$\vec{E} = \hat{y} \frac{ck}{\omega} E_0(r, z, t) \cos(kz - \omega t) \tag{1.4.2}$$

where, E_0, k and ω are known as the amplitude of electric field, wave number and angular frequency of the incident laser beam respectively. The beam is propagating along the z-direction in pre-ionized plasma having ambient electron density $n_0 \, cm^{-3}$. As the ions of the plasma are massive as compared to the electrons of the plasma therefore, ions form immobile background. The propagation of laser beam through the plasma can be explained by the equation given as

$$\left(\nabla^2 - \frac{1}{c^2} \frac{\partial^2}{\partial t^2} \right) \vec{E} = \frac{4\pi}{c^2} \frac{\partial \vec{J}}{\partial t}, \tag{1.4.3}$$

where $\vec{J}$ is known as the current density vector and given by the relation $\vec{J} = n_0 e \vec{v}$, here $\vec{v}$ is the velocity of the plasma electrons. This velocity can be derived by using the basic relations of

Lorentz force and continuity equations. If the plasma frequency is lesser than the frequency of electromagnetic field of incident laser beam then the plasma is known as underdense plasma otherwise it is known as overdense. The electromagnetic fields can not propagate though the overdense plasma because in this case propagation constant becomes imaginary. The critical plasma density condition determines whether the electromagnetic fields can propagate in the plasma or not. One can obtain the refractive index of the medium by using linear dispersion equation and it is given as $\epsilon = \sqrt{1 - \left(\omega_{\mathrm{p}}/\omega\right)^2}$, where ω_{p} is known as plasma frequency. From this relation it is clear that for underdense plasma is always lesser than one.

1.5. Unique Schemes for THz generation

From the beginning of the 21st century, researchers are making efforts to produce efficient THz sources. Numerous schemes have been proposed and devised to achieve highly energetic and efficient THz sources. The common methods to generate THz radiations include lasers, nonlinear optics, and electronics. These common methods can be further divided into some familiar schemes like quantum cascade lasers (QCL), gas lasers (GL), and high-frequency oscillators (HFO). These are furthermore based on electron accelerators, laser-plasma interaction, optical rectification, optical THz generation, and solid-state electronic devices. By using these schemes, THz radiations of various frequencies can be generated. Moreover, these generated THz radiations may be in the pulse form or continuous waveform. The material breakdown, large size, and low conversion efficiency are the unwanted features associated with these familiar methods. To achieve high efficiency, laser-plasma interaction can be used because plasma doesn't have any damage limit. CNTs are used to achieve compactness in the THz sources. Overall, there are two basic schemes to generate THz waves based on the nonlinear laser-plasma interaction [68, 69]. These schemes are known as wakefield and beat wave THz schemes.

1.5.1. Wakefield THz Schemes

In this scheme of THz generation, there occurs interaction between intense laser beam with

plasma and accelerator used is known as laser wakefield accelerator (LWFA). The wakefield excitation has been explained by several research workers by employing different means, where the enhanced amplitude of THz radiation is required in the applications. The wakefield can be explained as a conical emission in the forward direction by laser pulse induced oscillating electrons. The configuration for this scheme was first of all provided by Tajima and Dawson. The incident laser exerts ponderomotive force and the tip of the laser pulse knocks away the electrons of the plasma. As a result, there occurs charge separation in the plasma and this further results in the density oscillation of electrons. This charge oscillation results in the formation of wake or plasma wave. In the most basic scheme, the electron bunch is produced through self-trapping of background plasma electrons in the wake.

1.5.2. Beat Wave Scheme

In Recent few years, numerous experiments based on laser beating in a corrugated plasma have been reported with efficient THz generation. Out of these numerous schemes based on laser plasma interaction, THz generation by beating of two laser beams of nearly same frequencies and wave numbers in plasmas has shown tremendous potential in terms of making enhancement in the amplitude, intensity, and efficiency of THz wave. For particular applications, THz sources based on beating scheme mechanism can be used to enhance the peak power of emitted THz wave. The fundamental mechanism to generate THz radiation by beating of two co-propagating laser beams can be explained in the following manner. In this scheme, THz radiations are generated by beating of two laser beams of slightly different angular frequencies (ω_1, ω_2) and wavenumbers (k_1, k_2) in the plasma such that the difference in the angular frequencies lies in the THz region. Most of the experimental work performed by this scheme reported efficient generation of THz radiations [70-77]. The researchers have used various laser profiles to enhance the amplitude, power, and efficiency of THz radiation in beat wave schemes. In the present research work, we have preferred this scheme in the plasma (in the form of CNTs) to achieve our research objectives by using

various laser profiles. We have also used the anharmonic behavior of the CNTs present in the array.

1.6. Motivation & Objectives of the Research Work

The field of the THz generation has a great impact on the research and development of modern times. It has proved its utilization in almost every field of science and technology. The penetration power of THz radiations is more than the other electromagnetic waves. So, THz technology can be used in the safety-protection and defense sector, This technology provides us the information about concealed weapons and illicit drugs. THz radiations are not harmful to the people because of non-ionizing nature. The rotational and vibrational spectra of explosive materials and banned drugs lie in the THz region. In oral health care, THz technology can bring a medical revolution by taking 3D pictures of the teeth. At present we are using X-rays for this purpose but X-rays can detect oral diseases only at a later stage, when the only remedy left is filling and drilling whereas, with THz technology, we can detect these diseases even at the initial stage. 3D THz imaging and material spectroscopy can be employed to conserve cultural heritage. THz technology can also be used in higher altitude communication systems for example to send a signal from aeroplane to satellite. On the basis of the above explanation, THz generation is the state-of-the-art field of research. However, there are still some obstacles present in the development of THz technology. The main concern and challenging task is to produce compact, efficient, light-weighted, cheap, and powerful THz sources. These are the novel ideas, which require proper research work to familiarize the THz technology. So in the present work, new schemes of THz generation are discussed by using the array of VA-CNTs and HA-CNTs under the combined influence of externally applied static magnetic and electric fields.

1.6.1. Research Objectives of the purposed work

The main motive of the proposed theoretical research work is to step up the level of understanding and control of THz generation sources for their proper development and

appropriate growth. For this, the following objectives have been achieved in the purposed research work by using various improved schemes.

I.   Resonant excitation of Terahertz radiation by the interaction of a filamented laser beam with an array of aligned CNTs in the presence of D.C. electric field.

II. Resonant excitation of terahertz generation in anharmonic CNTs by using the amplitude-modulated laser.

III. To study the effect of external magnetic field on terahertz generation in anharmonic CNTs.

IV. To study the effect of cross focusing on Terahertz generation in anharmonic CNTs.

1.7. Thesis Summary of Research Work

In the present research work, laser-plasma interaction in the array of CNTs, VA-CNTs and HA-CNTs is used for the THz generation. The nonlinear mixing of lasers with anharmonicity plays a key role when external static electric and magnetic fields are applied. In this proposed work, the effects of several phenomena used laser-plasma-CNT parameters and some additional nonlinear processes are discussed. This thesis consists of six chapters

Chapter 1: Introduction

This chapter includes the basic and essential facts about the present research work. The motivation and objectives of the research work by using laser-plasma interactions in CNTs are clearly stated. In this chapter generation of THz radiations by using semiconductors, electro-optic crystals, CNTs, metallic CNTs, semiconductor CNTs etc. is explained in a well-ordered manner. This chapter also throws light on the potential applications of THz technology.

Chapter 2: Research Methodology

In this chapter, we have provided details of the research methodology used in every novel scheme for the THz generation.

Chapter 3: THz generation by the interaction of laser beams with magnetized anharmonic CNTs array

In this chapter, a theoretical analysis of resonant THz generation in the magnetized array of anharmonic CNTs array is presented. Two lasers with frequencies (ω_1, ω_2) and wavenumbers (k_1, k_2) propagate through the array of anharmonic VA-CNTs in the presence of the applied static magnetic field. It provides different displacements to the various electrons of CNTs. Due to this, restoration force varies nonlinearly with the displacements of electrons and hence, results in anharmonicity. This anharmonicity plays a significant role in the enhancement of absorption of lasers by the electrons of CNTs. The nonlinear restoration force produces a current which is responsible for the THz generation.

Chapter 4: THz generation by using laser filaments under the influence of static electric field in magnetized collisional plasma and anharmonic magnetized CNTs

In this, chapter, we have proposed and compared two models for the THz generation. In the first model, we put forward a new scheme of THz generation by employing laser filaments in the plasma under the influence of externally applied static electric and magnetic fields. In this scheme, two femtosecond laser pulses are co-propagating in the magnetized collisional plasma. THz wave is generated due to the nonlinear coupling between nonlinear velocity and electron density in magnetized collisional plasma. We have obtained the expression of a dielectric tensor with anisotropic nature and it is found to be very useful in the study of THz generation. The applied magnetic field also aids to enhance the transverse components of nonlinear current. This nonlinear current is responsible to generate enhanced terahertz waves.

In the second model, we put forward an alternative scheme for THz generation by using the rectangular array of horizontally aligned hollow anharmonic CNTs embedded on the base of the dielectric surface. Two filamented laser beams interact with this array of CNTs under the influence of externally applied static D.C. electric and magnetic fields acting mutually transverse to each other as well as to the propagation direction. The presence of non-uniform

electron density in CNTs, the restoration force on the different electrons is different and this results in anharmonicity. This anharmonicity broadens the resonance peak. The lasers also, exert space periodic ponderomotive force and beat frequency ponderomotive force on the electrons of CNTs. The space periodic ponderomotive force is well neutarlized by the pressure gradient force so that a transverse density ripple can be formed. Nonlinear coupling between D.C. drift velocity of electrons and density of plasma electrons in the array of CNTs results in the enhancement of THz generation.

Chapter 5: THz generation by cross-focusing of Gaussian beams in the array of vertically aligned anharmonic and magnetized CNTs.

In this novel scheme of terahertz (THz) generation, the effect of cross-focusing of Gaussian laser beams in the array of vertically aligned anharmonic carbon nanotubes (CNTs) has been studied. The static magnetic field is applied transverse to the axis of CNTs to magnetize the CNTs. The nonlinearity in the system arises due to the ponderomotive force exerted by the laser beams on the electrons of CNTs. The plasma in the CNTs rearranges itself due to this ponderomotive nonlinearity, which gives rise to the cross-focusing of both laser beams. The nonlinear current at THz frequency appears in the array of CNTs on account of the ponderomotive nonlinearity and anharmonicity of the system. The anharmonicity plays a pivotal role in the enhancement of THz generation. The normalized amplitude of THz radiation shows a notable enhancement with the increase of the externally applied static magnetic field (90 kG to 330 kG), dimensions of CNTs, and inter-tube separation. The cross-focusing of two laser beams in the magnetized collisional plasma makes a significant enhancement in the THz generation with the help of anharmonicity.

Chapter 6: Future scope

This chapter throws light on the futuristic aspects of the present thesis work. With the help of important results and conclusions, we explained the future scope of the presented research work in various fields of science and technology.

References:-

[1] S.S. Dhillon et al., "The 2017 terahertz science and technology roadmap," J. Phys. D: Appl. Phys. **50**(4), 910-928 (2017).

[2] E. Castro-Camus, M. Koch, D.M. Mittleman, " Recent advances in terahertz imaging: 1999 to 2021," Appl. Phys. B **128** (1), 12 (2022)

[3] B. Ferguson and X.C. Zhang, "Materials for terahertz science and technology," Nat. Mater. **1**(1), 26-33 (2002).

[4] K. Sakai and M. Tani, "Introduction to terahertz pulses," Terahertz optoelectronics. **97**(1), 1-30 (2019).

[5] C. Sirtori, "Bridge for terahertz gap," Nature **417**(1), 132-133 (2002).

[6] C. Meng, W. Yingxin, W. Xinke and L. Lianhe, "Advances in Terahertz Detection and Imaging," Front. Phys. **10**(1), 3389 (2022).

[7] W.P. Leemans, "Observation of THz emission from a laser-plasma accelerated electron bunch crossing a plasma-vacuum boundary," Phys. Rev. Lett. **91**(7), 074802 (2003).

[8] D. Dragoman and M. Dragoman, "Terahertz fields and applications," Prog. Quantum Electron. **28**(1), 1-66 (2004).

[9] M.S. Apu and N. Kaabouch, "Characterization of the terahertz sources suitable for biomedical applications," IEEE International Conference on Electro/Information Technology **1**(1), 1-5 (2012).

[10] H.A. Hafez et al., "Intense terahertz radiation and their applications," J. Opt. **18**(9), 093004 (2016).

[11] J.B. Jackson et al., "A survey of terahertz applications in cultural heritage conservation science," Terahertz Sci. Technol. **1**(1), 220-231 (2011).

[12] J. Buldt et al., "Gas-Plasma-Based broad band terahertz radiation with 640 milliwatt average power," **46**(20), 5256-5260 (2022).

[13] C. Baker et al., "Detection of concealed explosives at a distance using terahertz technology," in proceedings of the IEEE. **95**(8), 1559-1565 (2007).

[14] P.H. Siegel, "THz technology," in IEEE Transactions of Microwave Theory and Techniques. **50**(3), 910-928 (2002).

[15] Y.C. Shen et al., "Detection and identification of explosives using terahertz pulsed spectroscopic imaging," Appl. Phys. Lett. **86**(24), 241116 (2005).

[16] J. F. Federici, D. Gary, R. Barat and D. Zimdars, "THz standoff detection and imaging of explosives and weapons," Optics and Photonics in Global Homeland Security **5727**(1), 123-131 (2005).

[17] L. Yu et al., "The medical applications of terahertz technology in non-invasive detection of cells and tissues: Opportunities and Challenges," RSC Advances **9**(17), 9354-9363 (2019).

[18] N. Bourne, R.H. Clothier, M. D'Arienzo, P. Harrison, "The effects of terahertz, radiation on human keratinocytes, primary cultures and neural cell cultures," Altern. Lab. Anim. **36**(6), 667-684 (2008).

[19] H. Tabata, "Applications of terahertz wave technology in the biomedical field," in IEEE Transactions on Terahertz Science and Technology **5**(6), 1146-1153 (2015).

[20] M. Shur and X. Liu,"Biomedical applications of terahertz technology," Proc. SPIE Adavances in Biomedical Imaging and Spectroscopy **11975**(1) 1197502 (2022).

[21] F. Sizov, "Terahertz radiation sensors," Opto Electron. **18**(1), 10-36 (2010).

[22] B.S. William, "Terahertz quantum-cascade lasers," Nat. Photon. **1**(1), 517-525 (2007).

[23] R. Kohler, "Terahertz semiconductor-heterostructure laser," Nature **417**(1), 156-159 (2002).

[24] A. Nahata, A.S. Weling and T.F. Heinz, "A wideband coherent terahertz spectroscopy system using optical rectification and electro-optic sampling," Appl. Phys. Lett., **69**(16), 2321-2323 (1996).

[25] W.P. Leemans, "GeV electron beams from a centimeter-scale accelerator," Nat. Phys. **2**(1), 696-699 (2006)

[26] Q. Wu and X.C. Zhang, "Free-space electro-optic sampling of terahertz beams," Appl. Phys. Lett. **67**(1), 3523-3525 (1995).

[27] L. Xu, X.C. Zhang and D.H. Auston, "Terahertz beam generation by femtosecond optical pulses in electro-optic materials," Appl. Phys. Lett. **61**(15), 1784-1786 (1992).

[28] I.S. Gregory et al., "High resistivity annealed low-temperature GA As with 100 fs lifetimes," Appl. Phys. Lett. **83**(20), 4199-4201 (2003).

[29] S. Iijima, "Helical microtubes of graphitic carbon," Nature **354**(1), 56-58 (1991).

[30] P. Avouris, "Carbon-nanotube photonics and optoelectronics," Nat Photon **2**(1), 341-350 (2008).

[31] S. Kumar, S. Vij, N. Kant and V. Thakur, "Resonant terahertz generation by cross-focusing of Gaussian laser beams in the array of vertically aligned anharmonic and magnetized CNTs," Opt. Commun. **513**(1), 128112 (2022).

[32] Z. Liu, S. Tabakman, K. Welsher and H. Dai, "Carbon nanotubes in biology and medicine: in vitro and in vivo detection, imaging and drug delivery," Nano Res. **2**(1), 85-120 (2009).

[33] O.V. Kibis, M. Rosenau da costa and M.E. Portnoi, "Generation of terahertz radiation by hot electrons in carbon nanotubes," Nano Lett. **7**(11), 3414-3417 (2007).

[34] A. Bachtold, P. Hadley, T. Nakanishi and C. Dekker, "Logic circuits with carbon nanotube transistors," Science **294**(5545), 1317-1320 (2001).

[35] C.L. Kane and E.J. Mele, "Size, shape and low energy electronic structure of carbon nanotubes," Phys. Rev. Lett. **78**(10), 1932-1935 (1997).

[36] F. Lenord, "Metallic carbon nanotubes for current transport," The Physics of Carbon Nanotube Devices, New York, William Andrew 27-50 (2008).

[37] Z. Yao, C.L. Kane and C. Dekker, "High-field electrical transport in single-wall carbon nanotubes," Phys. Rev. Lett. **84**(13), 2941-2944 (2000).

[38] Y. K. Fuh et al., "Terahertz detection in single-wall carbon nanotubes," Appl. Phys. Lett. **92**(3), 033105 (2008).

[39] D. Mann et al., "Electrically driven thermal light emission from individual single-walled carbon nanotubes," Nature Nano. **2**(1), 33-38 (2007).

[40] J.W. Mintmire and C.T. White, "Universal density of states for carbon nanotubes," Phys. Rev. Lett. **81**(12), 2506-2509 (1998).

[41] B.B. Hu and M.C. Nuss, "Imaging with terahertz waves," Opt. Lett. **20**(16), 1716-1718 (1995).

[42] K. Ishigaki et al., "Direct intensity modulation and wireless data transmission characteristics of terahertz oscillating resonant tunneling diodes," Electron. Lett. **48**(10), 582-583 (2012).

[43] H. Hamster et al., "Sub Pico second, electromagnetic pulses from intense laser plasma interaction," Phys. Rev. Lett. **71**(17), 2725-2728 (1993).

[44] H. Hamster, A. Sullivan, S. Gordon and R.W. Falcone, "Short pulse terahertz radiation from high intensity laser produced plasmas," Phys. Rev. E. **49**(1), 671-677 (1994).

[45] A. Braun et al., "Self-channeling of high-peak-power femtosecond laser pulses in air," Opt. Lett. **20**(1), 73-75 (1995).

[46] C.C. Cheng, E.M. Wright and J.V. Moloney, "Generation of electromagnetic pulses from plasma channels induced by femtosecond light strings," Phys. Rev. Lett. **87**(21), 2130011-2130014 (2001).

[47] A. Houard et al., "Strong enhancement of terahertz radiations from laser filaments in air by static electric field," Phys. Rev. Lett. **100**(25), 255006 (2008).

[48] V.B. Pathak, D. Dahiya and V.K. Tripathi, "Coherent terahertz radiation from interaction of electron beam with rippled density plasma," J. Appl. Phys. **105**(1), 013315 (2009).

[49] L. Bhasin and V.K. Tripathi, "Terahertz generation via optical radiation of X-mode laser in a rippled density magnetized plasma," Phys. Plasmas. **16**(10), 103105 (2009).

[50] R.P. Sharma et al., "Interaction of high power laser beam with magnetized plasma and THz generation," Laser Part. Beams. **28**(4), 531-537 (2010).

[51] L. Bhasin and V.K. Tripathi, "Terahertz generation from laser filaments in the presence of a static electric field in plasma," Phys. Plasmas. **18**(12), 123106 (2011).

[52] A.K. Malik, H.K. Malik and U. Stroth, "Terahertz radiation generation by heating of two spatial-Gaussian lasers in the presence of a static magnetic field," Phys. Rev. Lett. E. **85**(1), 016401 (2012).

[53] M. Kumar and V.K. Tripathi, "Non-linear absorption and harmonic generation of laser in a gas with anharmonic electrons," Phys. Plasmas. **20**(2), 023302 (2013).

[54] M. Singh, R.K. Singh and R.P. Sharma, "THz generation by cosh-Gaussian laser in a rippled density plasma," EPL. **104**(3), 35002 (2013).

[55] C.S. Liu, V.K. Tripathi and M. Kumar, "Interaction of high intensity laser with non-uniform clusters and enhanced x-ray emission," Phys. Plasmas. **21**(10), 103101 (2014).

[56] F. Bakhtiari et al., "Generation of THz radiation by heating of two circular flat tapped laser beams in collisional plasma," Laser and Part. Beams **33**(4), 713-722 (2015).

[57] A. Kumar and P. Kumar, "Electron beam induced THz emissions from nanotube array," Phys. Plasmas. **23**(10), 103302 (2016).

[58] N. Ahmad, S. T. Mahmoud, G. Purohit and F. Khan, "Two color laser self-focusing and terahertz generation in multi-ion species plasma," Optik **1589**(1), 1533-1542 (2018).

[59] S. Sharma and A. Vijay, "Terahertz generation via laser coupling to anharmonic carbon nanotube array," Phys. Plasmas. **25**(2), 023114 (2018).

[60] S. Sharma and A. Vijay, "Non-linear mixing of Lasers and terahertz generation on CNT embedded metal surface," Optics **199**(1), 163381 (2019).

[61] S. Vij, N. Kant and V. Thakur, "Resonant enhancement of THz radiation through vertically aligned CNT's array by applying Wiggler magnetic field," Plasmonics **14**(1), 1051–1056 (2019).

[62] S.A. Afanas'ev et al., "Arrays of carbon nanotubes in a field of continuous laser radiation," Russian Microelectronics **49**(1), 16–24 (2020).

[63] E.F. Redish, "Teaching physics with the physics suite," New York: Wiley 16-33 (2003).

[64] V. Thakur, N. Kant and S. Vij, "Harmonic generation by an interaction of laser with an array of anharmonic carbon nanotubes," Chin. J. Phys. **71**(1), 660-668 (2021).

[65] M.C. Gurjar, K. Gopal, D.N. Guptaand and V.V. Kulagin, "Terahertz radiation generation from short-pulse laser interaction with electron-hole plasmas," Europhys. Lett. **133**(1), 14001 (2021).

[66] R. Wilson, M. King, N. M. H. Butler, et al., "Influence of spatial-intensity contrast in ultra-intense laser–plasma interactions," Sci. Rep. **12**(1), 1910 (2022).

[67] P. Varshney, A.P. Singh, M. Kundu *et al.,* "Laser intensity profile based terahertz field enhancement from a mixture of nano-particles embedded in a gas," Opt. Quant. Electron. **54**(1), 222 (2022).

[68] W. Christian and M. Belloni, "Physlet physics: Interactive illustrations, explorations and problems for introductory physics," Upper saddle river, NJ: Pearson education, Inc. 42-54 (2004).

[69] S. Kumar, R.K. Singh and R.P. Sharma, "Strong terahertz generation by beating of two super Gaussian laser beams in axially magnetized plasma," IEEE Trans. Terahertz Sci. Technol. **6**(3), 491 (2016).

[70] I. Dey et al., "Highly efficient broadband terahertz generation from ultra-short laser filamentation in liquids," Nature Commun. **8**(1), 1184 (2017).

[71] C. Meng et al., "Enhancement of terahertz radiation by using circularly polarized two color laser fields," Appl. Phys. Lett. **109**(13), 131105 (2016).

[72] P. Varshney et al., "Strong terahertz radiation generation by beating of two x-mode spatial triangular lasers in magnetized plasma," Laser Part. beams **33**(1), 51-58 (2015).

[73] S. Kumar, N. Kant, S. Vij, A. Mehta and V. Thakur, "Production of terahertz radiations by short pulse lasers," Journal of Phys. Conf. Series **1531**(1), 012011 (2020).

[74] T.M. Antosen Jr, J. Palastro and H.M. Milchberg, "Excitation of terahertz radiation by laser pulses in non-uniform plasma channels," Phys. Plasma **14**(3), 033107 (2007).

[75] R.K. Singh and R.P. Sharma, "Terahertz generation by crossed focused Gaussian laser beams in magnetized plasma," Phys. Plasmas **21**(11), 113109 (2014).

[76] A. Hematizadeh, S.M. Jazayeri and B. Ghafary, "Generation of terahertz radiation by beating of two laser beams in collisional magnetized plasma," Laser Part. Beams **34**(4), 569-575 (2016).

[77] P. Varshney et al., "Tunable terahertz radiation generation by nonlinear photo-mixing of Cosh-Gaussian laser pulses in corrugated magnetized plasma," Laser and Part. beams **35**(2), 279-285 (2017).

Chapter 2
Research Methodology

2.1. Hypothesis Formulation

The main aim of the present theoretical research work is to make advancements in the field of THz science and technology by developing highly efficient and compact sources of THz generation. To achieve this, single-walled CNTs are employed because of their extraordinary electrical and thermal conductivities. The hypothesis is based on the interaction of a high-power laser beam with an array of anharmonic VA-CNTs and HA-CNTs in the presence of the externally applied static magnetic field, electric field, or both. This is in accordance with the experimental, theoretical, and simulation work performed by the researchers in the THz field.

2.2. Numerical Methods

2.2.1. Paraxial Ray Approximation (PRA) Method

The paraxial ray approximation is assumed when intense finite radius pulse propagates in the plasma. The divergence angle of the laser beam is considered to be very small and beam width is much greater than the wave length. Till the beam width remains larger than the radiation wavelength, the wave equation with paraxial approximation gives quite accurate picture of the beam near the axis throughout the propagation. The various nonlinear processes occur during the interaction of laser with the VA-CNTs and HA-CNTs. For the analysis of these nonlinear processes, one can use Paraxial Ray Approximation (PRA), Moment Theory, and Variational Method. Out of these three methods, PRA or 'near axis method' is the simplest and most accurate one. This method was provided by Akhmanov *et al.* [1] in 1968 and shows close agreement with experimental results. Sodha *et al.*[2] also used PRA in their theoretical study of the propagation of electromagnetic waves in various media. Therefore, in the present research work, the PRA approach is preferred to explain the nonlinear processes. The

fundamentals of electrostatic-electromagnetic wave coupling along with ponderomotive force and wave propagation equation are explained below.

2.2.2. Linearization Method

The Linearization is a process to simplify the complexities, which arise due to the presence of nonlinear terms. The system of nonlinear equations is much difficult to solve and not too much mathematical techniques exist to solve and to investigate it qualitatively. So it is difficult to study nonlinear cases in general formulation. The linear case can be studied in general formulation, but is limited by small amplitudes of perturbations (where linear approach is valid). As the plasmas are unstable, therefore different types of instabilities are associated with it. They can be discerned in its initial phase. At this stage it is easily to understand the parameters that govern that instability for example plasma-beam densities and plasma velocity, magnetic field strength, etc. This is possible by linearizing the corresponding equations

The oscillations produced by the electrons of plasma are much faster than the ions because ions are heavier than electrons and assumed as stationary.

$$\vec{\nabla}.\vec{E} = \frac{1}{\epsilon_0}(n_0 - n_e). \tag{2.2.1}$$

$$\frac{\partial n_e}{\partial t} + \vec{\nabla}.(n_e\vec{v}_e) = 0. \tag{2.2.2}$$

$$n_e m_e \frac{\partial \vec{v}_e}{\partial t} + n_e m_e (\vec{v}_e.\vec{\nabla})(\vec{v}_e) = -en_e\vec{E}. \tag{2.2.3}$$

The equation (2.2.2) represents the equation of continuity for the electron density of plasma and equation (2.2.3) is the momentum equation for the electrons of plasma. To simplify these equations one can use linearization method. With this linearization method, we take equilibrium solution $(\partial/\partial t \to 0)$ to the above equations and this equilibrium value is known as zeroth order solution. From there onwards, we assume some perturbation in the equilibrium

solution and this is known as first order quantity. We put this first order quantity in the above equations and neglect the second or higher order terms to get the linearized equations.

2.3. Nonlinear Ponderomotive Force

It is defined as a nonlinear force experienced by the electrons and positive ions in an inhomogeneous oscillating electromagnetic field. In a homogenous electromagnetic field, charged particle makes oscillations around a fixed point whereas, in an inhomogeneous field particle is pushed towards the region of weaker field strength. Consider that a laser beam is propagating along the z-direction in the plasma present in the form of CNTs. The electric field profile of this laser beam is represented by the equation $\vec{E} = E_0 e^{-i(\omega t - kz)}$, where E_0 denotes the amplitude of laser field, ω is the angular frequency and k is the wavenumber of the laser beam. The equation of motion for the plasma electrons of CNTs under the influence of the electric and magnetic fields ($\vec{E}$ and $\vec{B}$) of the wave can be described as

$$m\left[\frac{\partial \vec{v}}{\partial t} + (\vec{v} - \nabla \vec{v})\right] = -e\vec{E} - e\,(\vec{v} \times \vec{B})/c. \qquad (2.3.1)$$

By considering the wave amplitude very small and using the linearization approximation, two nonlinear terms, $m\,(\vec{v}.\nabla\vec{v})$ and $e\,(\vec{v} \times \vec{B})/c$ can be neglected. If wave amplitude is large, then both nonlinear terms become significant and ponderomotive force is given by the relation $\vec{F}_p = -m(\vec{v}.\nabla\vec{v}) - e(\vec{v} \times \vec{B})/c$, where $\vec{v}$ and $\vec{B}$ represents real parts of complex expressions. Hence, one can write the time average ponderomotive force as

$$\vec{F}_p = -R_e\,(m(\vec{v}.\nabla\vec{v}) - R_e\left(e\frac{\vec{v} \times \vec{B}}{c}\right), \qquad (2.3.2)$$

where, R_e represents the real part of each complex expression. By using standard complex number identity, the ponderomotive force can be written as

$$\vec{F}_p = -\frac{m}{2}\,R_e\,[(\vec{v}.\nabla\vec{v} + \vec{v}.\nabla\vec{v}) - \frac{e}{2c}\,R_e[(\vec{v}\,x\,\vec{B} + \vec{v}\,x\,\vec{B})]. \qquad (2.3.3)$$

By neglecting the nonlinear terms from equation (2.3.1) and linearizing it, we get the oscillatory velocity of plasma electrons of CNTs as $e\vec{E}/mi\omega$. By Substituting this value of oscillatory velocity in equation (2.3.3) and using Maxwell's 3rd equation $\vec{\nabla}\times\vec{E} = -\partial\vec{B}/\partial t$, the expression for nonlinear ponderomotive force can be modified as

$$\vec{F}_p = -\frac{e^2}{2m\omega^2} R_e \left[(\vec{E}.\vec{\nabla})\vec{E} + (\vec{E}.\vec{\nabla})\left(\vec{E}^* + \vec{E}^* \times (\vec{v}\times\vec{E}) + \vec{E}\times(\vec{v}\times\vec{E})^*\right]\right. \tag{2.3.4}$$

If we consider un-magnetized plasma, then corresponding ponderomotive force acting on the plasma electrons of CNTs can be expressed by the relation $\vec{F}_p = e\nabla\phi_P$, where ϕ_P is known as ponderomotive potential and given by the relation $\phi_P = -e/4m\omega^2 \nabla |E|^2$. Such expression for the nonlinear ponderomotive force has been interpreted by many researchers, using identical and different approaches [3-6]. This nonlinear force modifies the plasma density of CNTs, which further results in the modification of the refractive index.

2.4. THz wave propagation equation

For the discussion of THz generation through CNTs, the THz wave propagation equation is very useful. This equation can be derived by using Maxwell's four equations of electromagnetic theory.

Maxwell 1st equation: First equation can be yielded from Gauss's law in electrostatics (with due consideration to dielectric polarization). This equation also represents Laplace or Poisson equation

$$\vec{\nabla}.\vec{D} = 4\pi\rho, \tag{2.4.1}$$

where, $\vec{D}$ and ρ are known as electric displacement vector and current density of charge carriers.

Maxwell 2nd equation: Second equation is represented by Gauss's law in magnetism and shows that the divergence of the curl of a vector is always zero.

$$\vec{\nabla} \cdot \vec{B} = 0, \tag{2.4.2}$$

where, $\vec{B}$ is known as the magnetic induction vector

Maxwell 3rd equation: Third equation can be obtained by using Faraday's law and Lenz's law of electromagnetic induction.

$$\vec{\nabla} \times \vec{E} = -\frac{1}{c}\frac{\partial \vec{B}}{\partial t}, \tag{2.4.3}$$

where, the term $\vec{E}$ is known as an electric field vector. The speed of electromagnetic waves in air or vacuum is denoted by c.

Maxwell 4th equation: Fourth equation can be obtained from Ampere's law and Maxwell's modification of displacement current.

$$\vec{\nabla} \times \vec{H} = \frac{4\pi}{c}\vec{J} + \frac{1}{c}\frac{\partial \vec{D}}{\partial t}, \tag{2.4.4}$$

where, $\vec{H}$ is the magnetic vector and $\vec{J}$ is known as current density in the medium. The relation between $\vec{E}$ and $\vec{D}$ is given as $\vec{D} = \epsilon\vec{E}$, here ϵ is known as lattice dielectric constant in semiconductors and dielectric constant in gaseous plasma. The relation between $\vec{H}$ and $\vec{B}$ is given as $\vec{B} = \mu\vec{H}$, here μ is known as magnetic permeability of the medium. By taking curl on both sides of Maxwell's 3rd equation (2.4.3), we can write

$$\text{Curl}(\vec{\nabla} \times \vec{E}) = \text{Curl}\left(-\frac{1}{c}\frac{\partial \vec{B}}{\partial t}\right) \tag{2.4.5}$$

With the help of standard vector identities and Maxwell's 4th equation, the above equation (2.4.5) can be written as

$$\vec{\nabla}(\vec{\nabla} \cdot \vec{E}) - \nabla^2\vec{E} = -\frac{1}{c}\frac{\partial}{\partial t}\left(\frac{4\pi}{c}\vec{J} + \frac{\epsilon}{c}\frac{\partial \vec{E}}{\partial t}\right), \tag{2.4.6}$$

Simplifying the above equation, the THz wave propagation equation can be obtained as

$$\nabla^2 \vec{E} - \vec{\nabla}(\vec{\nabla} \cdot \vec{E}) = \frac{4\pi}{c^2} \frac{\partial \vec{J}}{\partial t} + \frac{4\pi\varepsilon_1}{c^2} \frac{\partial^2 \vec{E}}{\partial t^2}. \tag{2.4.7}$$

2.5. Carbon nanotubes (CNTs)

After the discovery of Carbon Nano Tubes in 1999 [7] by Iijima, CNTs brought a revolution in many areas of science and technology due to their extraordinary electrical and thermal conductivities. The large value of electrical conductivity helps to enhance the nonlinear current density and the large value of thermal conductivity helps to hold the plasma with in the CNTs. CNTs are formed by rolling up the sheets of graphene. A single-walled carbon nanotube (SWCNT) can be formed by rolling a single sheet of graphene into the closed cylinder. The multi-walled carbon nanotube (MWCNT) can be formed by rolling up several graphene sheets concentrically and coaxially.
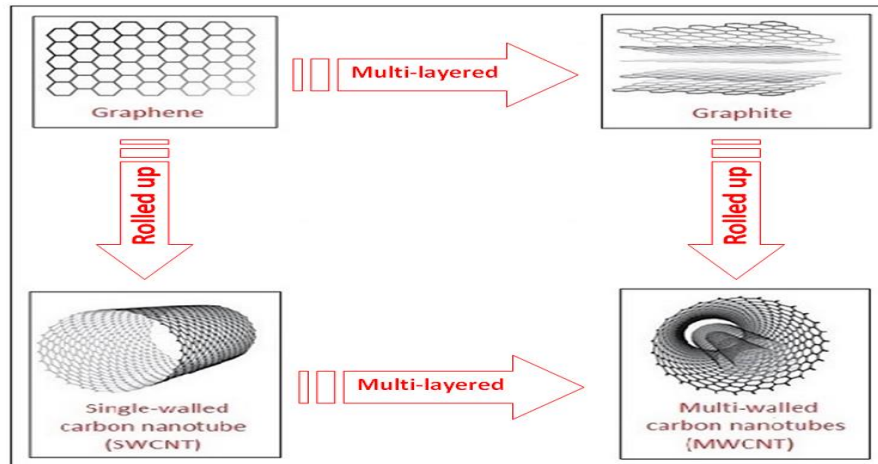
Figure 2.5.1 Representation of SWCNTs and MWCNTs by rolling up the graphene sheets.

Both SWCNT and MWCNT have been shown in figure 2.5.1. In the modern physics world, the Latest trend is due to use the carbon nanotubes for the generation and detection of THz radiation, because of their nano scale dimensions that is compactness (CNTs are cylindrical molecules with 10^{-9} m diameter and 10^{-6} m length) [8] and high efficiency. A metallic nano structure surface was used by welsh and wyne [9] to generate ultrafast THz radiation with the

help of excitation of plasma. More over carbon nano tubes have electron plasma frequencies in the THz range and as a result, CNTs appear as a favorable medium for terahertz radiation generation via nonlinear coupling with lasers. As a result, CNTs are the frontrunners for the next generation THz sources. Several methods have been developed for the synthesis of CNTs like arc methods, laser methods, chemical vapor deposition method (CVD), etc. In our research work, we have preferred the CVD method because it is cost-effective and the dimensions of CNTs can be easily varied according to the requirements

2.6. Anharmonicity

To understand the concept of anharmonicity, we will define the anharmonic oscillator. An anharmonic oscillator is that oscillator which is not oscillating in harmonic motion and the anharmonicity can be calculated by using numerical techniques like perturbation theory. In this, there occurs deviation in the frequency ω from the actual frequency ω_0 of harmonic oscillation. As a result change in frequency will occur and it is given by the relation $\Delta\omega = \omega - \omega_0$. The amplitude of oscillations can be written as

$$A^2 \propto (\omega - \omega_0). \tag{2.6.1}$$

Anharmonicity modifies the energy profile of the resonance curve resulting in super harmonic resonance. In CNTs, anharmonicity comes into action, when laser beam interacts with the array of VA-CNTs or HA-CNTs. Laser beam ionizes the atoms of CNTs by displacing the electrons from the positive ions. The restoration force will act on the electrons of CNTs to bring back the electrons to their original positions. This restoration force is different for different electrons. It means some of the electrons of CNTs will experience weak restoration force, whereas; remaining other electrons will experience strong restoration force. This nonlinearity in the electrons results in the anharmonicity and CNTs behave as anharmonic CNTs. In the present research work, we have used anharmonic CNTs in various schemes. The anharmonicity of CNTs in two of the schemes of the presented work depends on the anharmonicity factor α and characteristic parameter β. The characteristic parameter is given as

$$\beta = \frac{2\log_e(b/a)}{(b/a)^2 - 1}, \qquad\qquad (2.6.2)$$

The anharmonicity factor is given by the relation

$$\alpha = 4/(b+a), \qquad\qquad (2.6.3)$$

where a and b are known as inner and outer radii of CNTs. The numerical values of both β and α (represented by the equations (2.6.2) & (2.6.3)) depend on the dimensions of CNTs. Both β and α plays very significant role in our research work to determine the anharmonicity up to second order. This anharmonicity in the behavior of CNTs has been used to enhance the THz generation.

2.6.1. Derivation of anharmonicity factor α and characteristic parameter β

The incident laser beams interact either with VA-CNTs or HA-CNTs to ionize the atoms of CNTs in the respective array and provide finite oscillatory velocity to the free electrons of CNTs. As a result the electrons of CNTs get knocked out from the ion cylinder to cover a displacement of $\vec{\Delta}$. The space-charge electric field is created with each CNT if the displacement of the electrons $\vec{\Delta}$ is perpendicular to the axis of CNT. This field is represented by the overlapped region of the electron and ion cylinders in figure 2.6.1. The net space charge electric field $\vec{E}_s$ can be calculated as the vector sum of the space-charge electric field due to ion and electron cylinders $\left(\vec{E}_{ele}, \vec{E}_{ion}\right)$ and given as

$$\vec{E}_s = \vec{E}_{ion} + \vec{E}_{ele}. \qquad\qquad (2.6.4)$$

The interior space-charge electric field at a point (r, φ, z) as shown in figure 2.6.1 due to ion cylinder can be calculated as

$$\vec{E}_{ion} = \frac{n_0 e(r^2 - a^2)}{2\epsilon} \frac{\vec{r}}{r^2}, \qquad\qquad (2.6.5)$$

where e is the electronic charge and $\epsilon = \epsilon_0 \epsilon_r$ is known as the electric permittivity of the medium. The interior space-charge electric field at a point (r, φ, z) due to the electron cylinder shifted by displacement $\vec{\Delta}$ with the respect to the ion cylinder is given by the relation
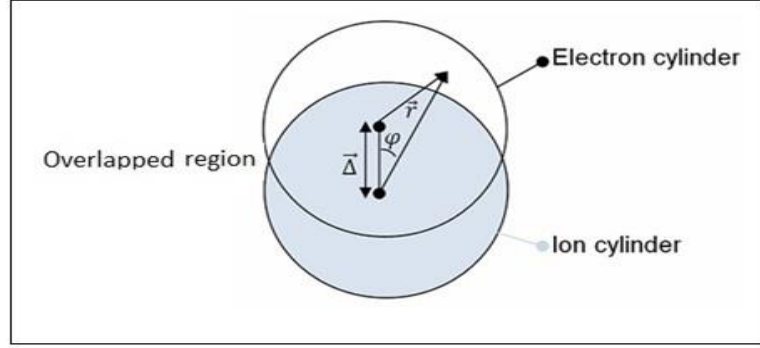
Fig.2.6.1. Shifting of the electron cylinder by distance $\vec{\Delta}$ with respect to the ion cylinder

$$\vec{E}_{ele} = \frac{-n_0 e}{2\epsilon}\left[\left|\vec{r} - \vec{\Delta}\right|^2 - a^2\right]\left[\frac{\vec{r} - \vec{\Delta}}{\left|\vec{r} - \vec{\Delta}\right|^2}\right].$$

(2.6.6)

Substituting Eq. (2.6.4) and (2.6.5) in Eq. (2.6.6), the net space charge electric field at the point (r, φ, z) would be

$$\vec{E}_s = \frac{n_0 e (r^2 - a^2)}{2\epsilon}\frac{\vec{r}}{r^2} - \frac{n_0 e}{2\epsilon_0}\left[\left|\vec{r} - \vec{\Delta}\right|^2 - a^2\right]\left[\frac{\vec{r} - \vec{\Delta}}{\left|\vec{r} - \vec{\Delta}\right|^2}\right].$$

(2.6.7)

It is observed that the displacement of the electrons along the axis of CNTs or parallel to the CNT axis is zero. The displacement of the electrons of CNTs is non-zero along the perpendicular direction (x-axis) and it is represnted in the figure 2.6.1. Therefore, one has to calculate the x-component of space charge electric field and it can be derived from Eq. (2.6.7),

$$E_{sx} = \frac{n_0 e}{2\epsilon}\left[\left(1 + \frac{a^2}{r^2}\right)\Delta_x + \left(\frac{5\cos\varphi}{r} + \frac{4\cos^2\varphi}{r} - \frac{(r^2 - a^2)}{r^3}\cos\varphi\right)\Delta_x^2\right].$$

(2.6.8)

Corresponding to the x-component of space charge electric field, the restoring force for each electron along the x-axis can be obtained by using the relation, $F_{sx} = -eE_{sx}$,

$$F_{sx} = \frac{-n_0 e^2}{2\epsilon}\left[\left(1 + \frac{a^2}{r^2}\right)\Delta_x + \left(\frac{5\cos\varphi}{r} + \frac{4\cos^2\varphi}{r} - \frac{(r^2 - a^2)}{r^3}\cos\varphi\right)\Delta_x^2\right].$$

(2.6.9)

Due to anharmonicity, the restoration force is not the same for all the electrons. Some of the electrons experience a weak restoration force, whereas others experience a strong restoration force. Hence, we need to calculate the φ (average) and the r (average) of restoration force to obtain its linear (F_{Lsx}) and nonlinear components (F_{NLsx}).

$$\langle F_{Lsx} \rangle = -\frac{n_0 e^2}{2\epsilon} \frac{\int_a^b \left(1+\frac{a^2}{r^2}\right) 2\pi r.dr}{\int_a^b 2\pi r.dr} \Delta_x \text{ and } \langle F_{NLsx} \rangle = -\frac{n_0 e^2}{2\epsilon} \left(\frac{1}{2\pi}\right) \int_0^{2\pi} \left(\frac{5\cos\varphi}{r} + \frac{4\cos^2\varphi}{r} - \frac{(r^2-a^2)}{r^3}\cos\varphi\right) d\varphi \, \Delta_x^2.$$

Solving these, net average restoration force is given by

$$\langle F_{Lsx} \rangle + \langle F_{NLsx} \rangle = \frac{-m\omega_P^2}{2\epsilon_r} \Delta_x \left[1 + \left\{2\log_e\left(\frac{b}{a}\right) / (b^2/a^2 - 1)\right\} + \{4/(b+a)\}\Delta_x\right], \quad (2.6.10)$$

where, $\omega_P = [n_0 e^2/m\epsilon_0]^{1/2}$ is the plasma frequency and m is the electronic rest mass and e is the electronic cherge. From the equation (2.6.10), $2\log_e\left(\frac{b}{a}\right) / (b^2/a^2 - 1) = \beta$ and $4/(b+a) = \alpha$ are known as characteristic parameter and anharmonicity factor respectively. Both the terms are responsible for nonlinear mixing in the response. We have calculated anharmonicity up to second order in our neoteric schemes of THz generation.

2.7. Effect of Laser-Plasma Parameters on THz generation

The various laser-plasma parameters affect the THz generation in a very significant manner and it is evident from our research work. The effect of some of the relevant parameters is explained as

2.7.1 Magnetized Plasma

It is the plasma in which the ambient magnetic field is so strong that it can affect the trajectories of the charged particles in a significant manner. It has been used by various researchers in many applications like accelerating charged particles, in generating THz radiations [10, 12]. As magnetized plasmas show different responses to the forces which are parallel, oblique and perpendicular to the applied magnetic field, as a result, magnetized plasmas are anisotropic in nature. If plasma is considered to be in the frame of rest, the electric field will be zero. If magnetized plasma is in the frame of motion, moving with velocity $\vec{v}$ under the influence of the externally applied magnetic field $\vec{B}$, then Lorentz force will come into action and it is given by the relation $\vec{F} = q(\vec{v} \times \vec{B})$. As a result, charged particles will move in circular paths known as gyro-orbits, in the direction perpendicular to $\vec{B}$. The gyro radius of charged particles under the influence of the magnetic field can be written as $r = mv/qB$ and corresponding gyro frequency is $\nu_c = qB/m$. This gyro radius is different

35

for different species, ions, electrons, and neutrals. If the temperature of each species is comparable to each other then one can write $r_e = (m_e/m_i)^2 r_i$. The magnetization parameters can affect the trajectories of charged particles in a significant manner. The external static magnetic field is considered to be very supportive in increasing the amplitude of THz generation. Thus, we have applied static magnetic field in our every research objective.

2.7.2 Rippled density Plasma

For the THz generation, we have considered laser-plasma interaction in the array of VA-CNTs or HA-CNTs. The THz generation cannot be directly excited by the beating of two incident lasers (ω_1, $\vec{k}_1$ and ω_2, $\vec{k}_2$) having frequency difference ($\omega = \omega_1 - \omega_2$) in the THz region because $\vec{k} \neq \vec{k}_1 - \vec{k}_2$; this phase matching condition can be attained by providing some extra momentum to the system. The corrugated plasma with density ripples equal to mismatch in phase may turn the process into a resonant process. There is number of ways in which ripple can be produced in plasma. The best and simplest way to generate ripple is machining.

2.7.3 Laser intensity (Optical power per unit area)

With the advancement in laser technology, we have availability of a broad range of laser intensities (10^{16} Wcm^{-2} to 10^{23} Wcm^{-2}). The intensity of incident beam of the order of 10^{16} Wcm^{-2} is known as the ionization threshold. The laser intensity more than, this ionization threshold is responsible for the ionization of the material. Laser intensity more than 10^{18} Wcm^{-2} is known as the relativistic threshold and results in the relativistic motion of the electrons. In the laser-plasma interactions, the intensity of the incident laser beam plays a very significant role. The highly intense laser beam results in a higher degree of ionization in plasma. It also increases the nonlinearities of the system, which is responsible for the increase in anharmonicity of the system. Because of this, more intense THz radiations are produced. So, the laser intensity of incident beam is directly proportional to the output THz yield.

2.7.4 Laser Polarization

The state of polarization is one of the most significant features of the laser beam and it plays an important role during the laser-plasma interaction in array of anharmonic CNTs. The polarization state of the laser beam identifies the direction, which is always at right angles to the direction of propagation of the incident laser beam, in which the electric field vector is oscillating. This vibration of the electric field vector can be simple, having one direction along the beam propagation. In this case, the laser beam is known as linearly polarized. In the present research work, we have used linearly polarized incident laser beams for the detailed analysis of various THz generation schemes.

2.7.5 Self-focusing and Cross-focusing of laser beams

Both self-focusing and cross-focusing are nonlinear optical phenomenon, which comes into existence due to the interaction of laser beams with plasma [1, 2, 13, &14]. Primarily, three nonlinearities are found to be responsible for these, named as (i) Thermal nonlinearity (ii) Relativistic nonlinearity (iii) Ponderomotive nonlinearity. Thermal nonlinearity is due to collisional heating of the plasma when laser beams incident on it. The collisions between the plasma electrons of CNTs results in the increase of temperature. This rise in temperature induces hydrodynamic expansion in the plasma of CNTs, which further leads to rise in refractive index. Relativistic nonlinearity is due to the increase in the mass of plasma electrons of CNTs, traveling at a speed approaching the speed of light. This results in the rise of the refractive index of the medium. Ponderomotive nonlinearity is caused by ponderomotive force, which knocks the plasma electrons away from the region where the laser beam is more strong and intense. This again results in the rise of the refractive index of the medium. In the cross-focusing phenomenon, there is a simultaneous propagation of two laser beams in such a way that the self-focusing of one beam is affected by the other and vice-versa. The nonlinearity introduced in the medium depends on the intensities of both the laser beams. Both self-focusing and cross-focusing phenomenon are found to be very beneficial in the enhancement of THz generation.

2.7.6 Amplitude Modulation wave

In communication systems, the information message can be transmitted via carrier wave of radio frequency using amplitude modulation technique. In this, the information message can be transmitted to the other end by modulating the strength of the signal. Furthermore, the pulse can be amplitude modulated with the help of THz signal by employing the electro-optic modulator technique. In one of the proposed schemes of the research work, we have used an amplitude-modulated Gaussian laser beam to generate THz radiation.

2.7.7 Gaussian Laser Beam Profile

The Gaussian laser beam is a highly monochromatic electromagnetic radiation whose amplitude envelope is in the transverse plane. The amplitude envelope is represented by the Gaussian function. This Gaussian mode describes the output of most of the lasers because such a beam can be focused into the most concentrated spot. The Gaussian beam remains Gaussian if the paraxial nature of the wave is maintained. As per the requirement in various schemes, one can generate many profiles from Gaussian laser beams by using appropriate methods [13, 15-19]. In the present research work, we have used a Gaussian profile to achieve one of the objectives.

2.7.8 Plasma Density

In the proposed work, the plasma density term plays a major role in the efficient THz generation. It can be defined as the concentration of electrons present in the given volume of plasma. Plasma density determines the plasma state, electron density, and ionized state in fully or ionized gases. The characteristics of plasma can be varied with plasma density. The plasma which has low plasma density is known as cold plasma and the plasma which has high plasma density is known as hot plasma. The other important term in plasma study is the critical density of the plasma. On the basis of the value of critical density, we can make a distinction between underdense and over-dense plasma. The plasma is known as underdense plasma if the electron density of plasma is less than its critical density. The over-dense plasma is that in which the electron density of plasma is more than its critical density. Because of this high electron density, the laser beam cannot propagate through the overdense plasma with

proper ease. In the present research work, we have preferred underdense plasma for the ease of THz wave propagation. The mathematical relation for the plasma density term is given as $\omega_p = (4\pi ne^2/m)^{1/2}$ (in CGS system) and $\omega_p = (ne^2/m\epsilon_0)^{1/2}$ (in SI system), here the terms n, e, and m represent the number density, charge, and mass of electrons respectively.

2.7.9 Filamentation and Filaments

Filamentation is defined as the nonlinear propagation of the laser beam, in a nonlinear medium, when the balance is achieved between optical Kerr effect-induced self-focusing and defocusing effects such as diffraction and plasma defocusing. Laser filament is the propagation zone of the beam, in which there is intensity clamping. Filamentation can be used in various applications like long-distance propagation of ultra-short pulses, generation of harmonics, and THz generation [20-22]. In our present work, we have also employed filamentation in achieving one of the research objectives.

2.8 Research Design

The research design of our proposed research work is based on solving the simple and differential coupled equations by using some standard numerical methods.

2.9 Software used

MATHEMATICA and MATLAB are the software used for analyzing our results, obtained by using standard numerical methods. ORIGIN software is preferred for graphical analysis by plotting the results obtained in various schemes. Origin software is used because of its accuracy in plotting the graphs.

2.10 Tools used

Laptop, printer, and scanner are the tools used in our research work.

2.11 Sources of Data

In our present research work, we have collected the data through various research papers on the related THz generation field. Finally, to obtain the authenticity of our analytical, numerical, and theoretical results, the comparison is made with experimental and simulation work.

References:-

[1]   S.A. Akhmanov, A.P. Sukhorukov and R.V. Khokhlov, "Self-focusing and diffraction of light in a nonlinear medium," Sov. Phys. Uspekhi **10**(5), 609 (1968).

[2]   M.S. Sodha, R.K. Khanna and V.K. Tripathi, "The self-focusing of electromagnetic beams in a strongly ionized magnetoplasma," J. Phys. D: Appl. Phys. **7**(16), 2188 (1974).

[3]   H.A.H. Boot and R.B.R.S. Harvie, "Charged particles in a non-uniform radio-frequency field," Nature **180**, 1187 (1957).

[4]   F.F. Chen and A.W. Trivelpiece, "Introduction to plasma physics," Physics Today **29**(10), 54 (1976).

[5]   W.B. Mori and T. Katsouleas, "Ponderomotive force of a non-uniform electromagnetic wave in a time varying dielectric medium," Phys. Rev. Lett. **69**(24), 3495 (1992).

[6]   W.L. Kruer, "The physics of laser plasma interactions," Edition- Wesley, Redwood city, CA, 41-57 (1988).

[7]   S. Iijima, "Helical microtubes of graphitic carbon," Nature **354**(1), 56-58 (1991).

[8]   R. Saito, G. Dresselhaus and M.S. Dresselhaus, "Physical properties of carbon Nanotubes," Imperial college press **12**(4), 259 (1998).

[9]   G.H. Welsh and K. Wynne, "Generation of ultrafast terahertz radiation pulses on metallic nanostructured surfaces," Opt. Express **17**(4)**,** 2470 (2009).

[10]   R. McLaughlin et al., "Enhanced coherent terahertz emission from indium arsenide in the presence of a magnetic field," Appl. Phys. Lett. **76**(15), 2038 (2000).

[11]   A. Mehta, J. Rajput and N. Kant, "Effect of frequency-chirped laser pulses on terahertz radiation generation in magnetized plasma," Laser Phys. **29**(9), 095405 (2019).

[12] D. Singh and H.K. Malik, "Enhancement of terahertz emission in magnetized collisional plasma," Plasma Sources Sci. Technol. **24**(4), 045001(2015).

[13] M.M.S. Govind and R.P. Sharma, "Cross-focusing of two co-axial Gaussian electromagnetic beams in a magnetoplasma and plasma wave generation," Plasma Phys. **21**(1), 13 (1979).

[14] V. Thakur, N. Kant and S. Vij, "Effect of cross-focusing of two laser beams on THz radiation in graphite nanoparticles with density ripple," Phys. Scr. **95**(4), 045602 (2020).

[15] R.P. Sharma and R.K. Singh, "Terahertz generation by two cross focused laser beams in collisional plasmas," Phys. Plasmas **21**(7), 073101 (2014).

[16] M. Singh, R.K Singh and R.P. Sharma, "THz generation by cosh-Gaussian lasers in a rippled density plasma," EPL **104**(3), 35002 (2013)

[17] P. Varshney et al., "Tunable terahertz radiation generation by nonlinear photo-mixing of cosh-Gaussian laser pulses in corrugated magnetized plasma," Laser and Part. beams **35**(2), 279-285 (2017).

[18] S. Kumar, S. Vij, N. Kant and V. Thakur, "Resonant Terahertz Generation by the Interaction of Laser Beams with Magnetized Anharmonic Carbon Nanotube Array," Plasmonics **17**(1), 381-388 (2022).

[19] S. Kumar, S. Vij, N. Kant and V. Thakur, "Resonant terahertz generation by cross-focusing of Gaussian laser beams in the array of vertically aligned anharmonic and magnetized CNTs," Opt. Commun. **513**(1), 128112 (2022).

[20] A.B. Langdon and B.F. Lasinski, "Filamentation and Subsequent Decay of Laser Light in Plasmas," Phys. Rev. Lett. **34**(15), 934 (1975).

[21] T.J. Wang et al., "Remote generation of high-energy terahertz pulses from two-color femtosecond laser filamentation in air," Phys. Rev. A **83**(5), 053801 (2011).

[22] S. Kumar, S. Vij, N. Kant, A. Mehta and V. Thakur, "Resonant terahertz generation from laser filaments in the presence of static electric field in a magnetized collisional plasma," Euro. Phys. J. Plus **136**(1), 148 (2021).

Chapter 3

THz generation through magnetized anharmonic CNTs array

3.1. Introduction

In this modern world, THz technology has attained great importance due to compact and highly efficient THz sources for various applications in many fields like security–protection [1], medical sciences [2-4], broadband communication [5], etc. The various researchers have proposed a number of schemes for THz wave generation to provide compact, efficient, and reliable THz sources. For this purpose, they have used different mechanisms to enhance the amplitude of THz radiation. Some of these are; by beating of two chirped-pulse lasers in spatially periodic density plasma [6], by the interaction of laser filaments in the presence of a static electric field in a magnetized collisional plasma [7], laser coupling to an anharmonic CNTs array [8], nonlinear mixing of lasers [9], by applying a magnetic field on an array of CNTs [10-12]. The CNTs are considered very reliable and effective sources for THz generation, due to their compact size, large current density, high electrical conductivity, and excellent combination of transverse-longitudinal dimensions. The CNTs are considered a more favorable medium for the efficient generation of terahertz radiation [13]. Moreover, CNTs are also helpful in the strong absorption of the laser beam [14] due to which generated THz amplitude is enhanced. Titova *et al*. [15] have proposed the generation of THz radiation by using single-walled CNTs, excited by femtosecond lasers. Batrakov *et al*. [16] and Portnoi *et al*. [17] have explained and reviewed THz generation processes in CNTs to increase the efficiency of THz generation. Wang and Wu [18] studied the properties of THz radiation experimentally, emitted by CNTs antenna. Dragoman and Dragoman [19] have studied the characteristics of metallic single-walled CNTs as a THz antenna. Dagher *et al*. [20] have studied the amplification of THz radiation in metallic CNTs under the influence of the D.C. magnetic field and observed enhancement in the normalized amplitude of THz radiation.

3.2. Proposed Model for THz generation through anharmonic magnetized CNTs

In the present chapter, we propose a new scheme for THz generation by irradiating two co-propagating lasers of nearly equal frequencies on vertically aligned hollow anharmonic CNTs in the presence of an external static magnetic field. In this, we are using an array of CNTs to ease the propagation of THz radiation. A single-walled carbon nanotube is generally modeled as a hollow cylinder [21] to calculate electrical and optical conductivity. But the response of these nanotubes towards the transverse electric and magnetic fields is assumed as solid cylindrical tubes [22-24]. This assumption is reasonable because the diameter of CNTs is very small and the density of atoms is very high. The array of anharmonic CNTs is grown over the glass dielectric surface. Here restoration force of electrons of CNTs is a non-linear function of electron displacements in CNTs. Consider an array of vertically aligned anharmonic CNTs grown over the dielectric surface of glass ($\epsilon_r = 2.5$). This arrangement of CNTs can be obtained by the chemical vapor deposition (CVD) process. It is because, in the CVD process, radius, length, wall number, and alignment of CNTs can be easily controlled [25, 26]. There are n_c number of CNTs per unit area, given by $n_c = 1/d^2$, where d is known as inter-tube separation. The term n_0 is the number density of free electrons of CNTs. The inner and outer radius of each CNT is denoted by a and b respectively. The length of CNT is represented by L, parallel to the y-axis, and perpendicular to the x-z plane as shown in figure 3.2.1. The external magnetic field $\vec{B}$ is applied along the y-axis, parallel to the axis of CNTs. The lasers with nearly equal angular frequencies (ω_1, ω_2) and wavenumbers (k_1, k_2) propagate through an array of anharmonic CNTs with electric field profiles,

$$\vec{E_j} = \hat{x} A_j e^{-i(\omega_j t - k_j z)}; j = 1,2. \tag{3.2.1}$$

The laser beams ionize the atoms of CNTs and impart finite oscillatory velocity to the free electrons of CNTs. The electrons of CNTs get separated from the ion cylinder with a displacement of $\vec{\Delta}$. When the displacement $\vec{\Delta}$ is perpendicular to the axis of CNT, the space-charge electric field is created. This field is represented by the overlapped region of the electron cylinder and ion cylinder in figure 2.6.1. The net space charge electric field $\vec{E}$ is the vector sum of the space-charge electric field due to ion cylinder $\vec{E}_{ion}$ and electron cylinder $\vec{E}_{ele}$.
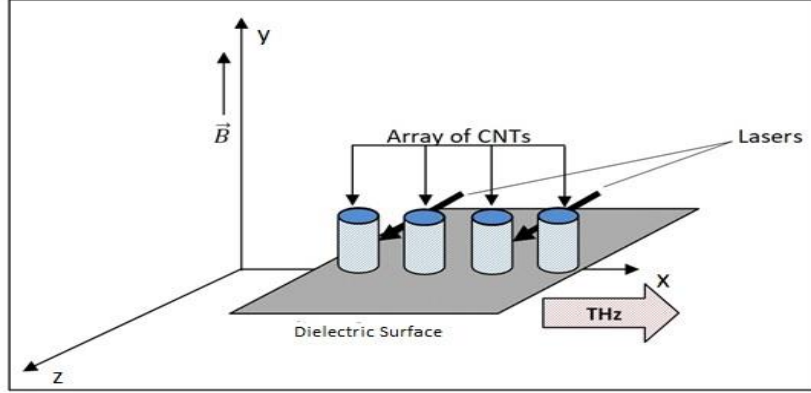
Fig.3.2.1. Schematic of THz generation by the interaction of lasers with vertically aligned anharmonic carbon nanotube array in the presence of an external magnetic field.

$$\vec{E}_s = \vec{E}_{ion} + \vec{E}_{ele}. \tag{3.2.2}$$

By using Eq. (2.6.8) one can write the corresponding x-component of space charge electric field as

$$E_{sx} = \frac{n_0 e}{2\epsilon}\left[\left(1 + \frac{a^2}{r^2}\right)\Delta_x + \left(\frac{5\cos\varphi}{r} + \frac{4\cos^2\varphi}{r} - \frac{(r^2 - a^2)}{r^3}\cos\varphi\right)\Delta_x^2\right]. \tag{3.2.3}$$

Corresponding to the x-component of space charge electric field, the restoring force for each electron along the x-axis can be obtained by using the relation, $F_x = -eE_x$,

$$F_{sx} = \frac{-n_0 e^2}{2\epsilon}\left[\left(1 + \frac{a^2}{r^2}\right)\Delta_x + \left(\frac{5\cos\varphi}{r} + \frac{4\cos^2\varphi}{r} - \frac{(r^2 - a^2)}{r^3}\cos\varphi\right)\Delta_x^2\right]. \tag{3.2.4}$$

Due to anharmonicity, the restoration force is not the same for all the electrons. Some of the electrons experience a weak restoration force, whereas others experience a strong restoration force. Hence, we need to calculate the φ (average) and the r (average) of restoration force to obtain its linear (F_{Lsx}) and nonlinear components(F_{NLsx}). By using Eq. (2.6.10) net average restoration force is given by

$$\langle F_{Lsx}\rangle + \langle F_{NLsx}\rangle = \frac{-m\omega_P^2}{2\epsilon_r}\Delta_x[1 + \beta + \alpha\Delta_x], \tag{3.2.5}$$

where, $\omega_P = [n_0 e^2/m\epsilon_0]^{1/2}$ is the plasma frequency and m is the electronic rest mass. $\beta = 2\log_e(b/a)/(b^2/a^2 - 1)$ and $\alpha = 4/(b + a)$ are known as characteristic parameter and anharmonicity factor respectively. Both the terms are responsible for nonlinear mixing in the

response. The numerical values of both β and α depend upon the inner and outer radii of CNTs. As the static magnetic field $\vec{B}$ is applied along the y-axis, therefore, magnetic force $F_B = e(\vec{v} \times \vec{B})/c$ can be resolved into their x and z components, $F_{Bx} = -ev_zB/c$ and $F_{Bz} = ev_xB/c$ respectively. Under the effect of electric fields of the interacting laser beams, externally applied static magnetic field $\vec{B}$ and space charge electric field, the displacement of electrons in CNTs is directed by the following equations motion

$$\frac{d^2\Delta_x}{dt^2} + \frac{\omega_P^2}{2\epsilon_r}(1 + \beta + \alpha\Delta_x)\Delta_x + \frac{F_{Bx}}{m} + \upsilon\frac{d\Delta_x}{dt} = \frac{-eE_x}{m}, \tag{3.2.6}$$

$$\frac{d^2\Delta_z}{dt^2} + \frac{F_{Bz}}{m} + \upsilon\frac{d\Delta_z}{dt} = \frac{-eE_z}{m}, \tag{3.2.7}$$

where, υ represents electron collision frequency which is lesser than ω.

Simplifying equations (3.2.6) and (3.2.7) we get

$$-\omega^2\Delta_X + \frac{\omega_P^2}{2\epsilon_r}(1 + \beta + \alpha\Delta_x)\Delta_x + i\omega\omega_c\Delta_z - i\omega\upsilon\Delta_x = \frac{-eE_x}{m}, \tag{3.2.8}$$

$$-\omega^2\Delta_z - i\omega\omega_c\Delta_x - i\upsilon\omega\Delta_z = \frac{-eE_z}{m}, \tag{3.2.9}$$

where, $\omega_c = eB/mc$ is known as the cyclotron frequency of plasma electrons.

By solving equations (3.2.8) and (3.2.9) we get

$$\Delta_z = \frac{1}{m}\left[\frac{eE_z - im\omega\omega_c\Delta_x}{\omega^2 + i\upsilon\omega}\right]. \tag{3.2.10}$$

By Substituting Δ_z in equation (3.2.9), and ignoring the anharmonicity, we can calculate Δ_x

$$-\omega^2\Delta_x + \frac{\omega_P^2}{2\epsilon_r}(1 + \beta + \alpha\Delta_x)\Delta_x + \frac{\omega\omega_c}{m}\left[\frac{ieE_z - im\omega\omega_c\Delta_x}{\omega^2 + i\upsilon\omega}\right] - \upsilon\omega\Delta_x = \frac{-eE_x}{m}. \tag{3.2.11}$$

$$\Delta_x = \frac{e\left[E_x + \frac{i\omega\omega_cE_z}{\omega^2 + i\upsilon\omega}\right]}{m\left[\omega^2 - \frac{\omega_P^2}{2\epsilon_r}(1+\beta) - \frac{\omega^2\omega_c^2}{(\omega^2 + i\upsilon\omega)} + i\upsilon\omega\right]}. \tag{3.2.12}$$

As explained above the displacement of electrons in CNTs is finite for the field perpendicular to the CNT axis and zero for the field along the axis. Therefore, the term E_z is taken as zero.

$$\Delta_x = \frac{eE_x}{m\left[\omega^2 - \frac{\omega_P^2}{2\epsilon_r}(1+\beta) - \frac{\omega^2\omega_c^2}{(\omega^2 + i\upsilon\omega)} + i\upsilon\omega\right]}. \tag{3.2.13}$$

The anharmonicity factor α is responsible for nonlinear mixing in the electron response

towards the incident lasers. If we neglect the nonlinear terms, then electron displacement due to lasers is given as,

$$\Delta_j = \frac{eE_j}{m\left[\omega_j^2 - \frac{\omega_P^2}{2\epsilon_r}(1+\beta) - \frac{\omega_j^2 \omega_c^2}{(\omega^2 + iv\omega)} + iv\omega_j\right]}.$$

(3.2.14)

With the help of equations (3.2.6) and (3.2.12), the non-linear term provide electron displacement Δ_x at frequency $\omega = (\omega_1 - \omega_2)$ and becomes responsible for THz generation.

$$\left[\omega^2 - \frac{\omega_P^2}{2\epsilon_r}(1+\beta) - \frac{\omega^2 \omega_c^2}{(\omega^2 + iv\omega)} + iv\omega\right]\Delta_x = -\frac{\alpha\omega_P^2 \Delta_1 \Delta_2^*}{4\epsilon_r},$$

(3.2.15)

$$\Delta_x = \frac{-\alpha\omega_P^2 \Delta_1 \Delta_2^*}{4\epsilon_r\left[-\omega^2 + \frac{\omega_P^2}{2\epsilon_r}(1+\beta) - iv\omega + \frac{\omega^2 \omega_c^2}{(\omega^2 + iv\omega)}\right]}.$$

(3.2.16)

Due to this displacement (Δ_x) of electrons, plasma electrons start oscillating with THz oscillatory velocity given by $v_{\omega x} = -i\omega\Delta_x$. The THz oscillatory velocity is further responsible for the generation of non-linear THz current density $J'^{NL}_{\omega x}$.

$$J'^{NL}_{\omega x} = -en_o v_{\omega x}.$$

(3.2.17)

The nonlinear current density $J'^{NL}_{\omega x}$ is non zero over the cross-section $\pi(b^2 - a^2)$ and zero over the area d^2. Thus, the average nonlinear THz current density due to the array of CNTs is

$$J^{NL}_{\omega x} = -\pi e n_o n_c (b^2 - a^2) v_{\omega x}.$$

(3.2.18)

The standard equation for the generation of THz waves is

$$\nabla^2 E_{\omega x} + k^2 E_{\omega x} = \frac{-4\pi i\omega}{c^2} J^{NL}_{\omega}.$$

(3.2.19)

Along the x-axis above equation, we can write as:

$$\frac{\partial^2 E_{\omega x}}{\partial z^2} + k^2 E_{\omega x} = \frac{-4\pi i\omega}{c^2} J^{NL}_{\omega x},$$

(3.2.20)

where, $k^2 = \frac{\omega^2}{c^2}\left[\epsilon_r - \pi(b^2 - a^2)n_c \frac{\omega_P^2}{\left[\omega^2 - (1+\beta)\frac{\omega_P^2}{2\epsilon_r} - \frac{\omega^2 \omega_c^2}{\omega^2 + iv\omega}\right]}\right]$

On solving Eq. (3.2.20), we get a terahertz electric field $E_{\omega x}$ given below

$$E_{\omega x} = [\pi(b^2 - a^2)n_c]\frac{1}{\epsilon_r}\left[\frac{n_0 e^2}{m \epsilon_0 \omega_1^2}\right]\left[\frac{e A_2 A_1}{m \omega_2 c}\right]\left[\frac{\omega_P^2}{-\omega^2 + (1+\beta)\frac{\omega_P^2}{2\epsilon_r} - iv\omega + \frac{\omega^2 \omega_c^2}{\omega^2 + iv\omega}}\right]\left[\frac{\omega_1^2}{-\omega_1^2 + (1+\beta)\frac{\omega_P^2}{2\epsilon_r} - iv\omega_1 + \frac{\omega_1^2 \omega_c^2}{\omega_1^2 + iv\omega_1}}\right]$$

$$\left[\frac{\omega_2^2}{-\omega_2^2+(1+\beta)\frac{\omega_P^2}{2\epsilon_r}+i\upsilon\omega_2+\frac{\omega_2^2\omega_c^2}{\omega_2^2+i\upsilon\omega_2}}\right]\left[\frac{\omega^2}{[k_\omega^2-(k_1+k_2)^2]c(b+a)\omega_2}\right]. \tag{3.2.21}$$

The normalized THz electric field equation is

$$\frac{E_{\omega x}}{A_1}=[\pi(b^2-a^2)n_c]\frac{1}{\epsilon_r}\left[\frac{n_0e^2}{m\,\epsilon_0\omega_1^2}\right]\left[\frac{e\,A_2}{m\,\omega_2c}\right]\left[-\frac{\omega^2}{\omega_P^2}+\left(\frac{1+\beta}{2\epsilon_r}\right)-i\left(\frac{\omega}{\omega_P}\right)\left(\frac{\upsilon}{\omega_P}\right)+\frac{\omega_c^2/\omega_P^2}{1+i\upsilon/\omega}\right]^{-1}\left[1+i\frac{\upsilon}{\omega_1}-\right.$$

$$\left.\left(\frac{\omega_P^2}{\omega_1^2}\right)\left(\frac{(1+\beta)}{2\epsilon_r}\right)-\frac{\omega_c^2/\omega_1^2}{1+i\upsilon/\omega_1}\right]^{-1}\left[1-i\frac{\upsilon}{\omega_2}-\left(\frac{\omega_P^2}{\omega_2^2}\right)\left(\frac{(1+\beta)}{2\epsilon_r}\right)-\frac{\omega_c^2/\omega_2^2}{1+i\upsilon/\omega_2}\right]^{-1}\left[\frac{\omega^2/\omega_2^2}{[k_\omega^2-(k_1+k_2)^2]c(b+a)/\omega_2}\right]. \tag{3.2.22}$$

3.3. Graphical Analysis and Observations

Numerical simulations are performed with the following set of lasers and CNTs parameters. The carbon dioxide lasers of frequencies $\omega_1 = 2\times10^{14}$ rad/s and $\omega_2 = 1.85\times10^{14}$ rad/s have been chosen in such a way that frequency difference lies in the region of THz. The corresponding wavelengths of lasers are $\lambda_1 = 9.45\,\mu m$ and $\lambda_2 = 10.20\,\mu m$. The intensities of both lasers are $I\sim10^{13}\,W/cm^2$ and $e\,A_2/m\,\omega_2c = e\,A_2/m\,\omega_2c = 0.03$. The length of CNT is $1\,\mu m$ with an inner radius of 20.0 nm, an outer radius of 40.0 nm. Corresponding to these dimensions of CNTs, characteristic parameter $\beta = 0.4622$ and anharmonicity factor $\alpha = 0.06\,nm^{-1}$. The relative permittivity of a dielectric surface is 2.5 and the applied static magnetic field lies in the range 170 kG to 235 kG. In figure 3.3.1., we have plotted the graph between normalized THz amplitude and normalized frequency for different values of external static magnetic field $B = 170\,kG,\ 195\,kG$, and 235 kG. From figure 3.3.1, it is observed that each curve shows an increase in normalized THz amplitude with the increase of normalized THz frequency and attains its maximum value. After attaining the maximum value, normalized THz amplitude shows a decrease with the increase of normalized frequency. The curve shows the maxima at frequency, $\omega = \omega_P\sqrt{(1+\beta)/2\epsilon_r+(\omega_c^2/\omega_P^2)}$. This is the frequency where surface plasmon resonance occurs. At this resonance frequency, absorption of lasers by the electrons of CNT becomes maximum and hence, THz wave of maximum amplitude is produced. Also, the external magnetic field is used to enhance the normalized THz amplitude. It is due to the reason that, the applied magnetic field increases the

nonlinearity of the system. Similar results were shown by Jain *et al.* [11] where they have applied a magnetic field on an array of CNTs embedded on the metal surface. It is further observed from this figure that, with the increase of the external magnetic field, the surface plasmon resonance point gets shifted towards the higher value of normalized frequency. This is due to the dependence of surface plasmon resonance frequency on the external magnetic field. Hence it is observed that surface plasmon resonance condition does not only depend upon dimensions of CNTs but also depends upon the external magnetic field. The inset figure of figure 3.3.1 is plotted in the absence of a static magnetic field; other parameters are the same as in figure 3.3.1. We observe an increase in the normalized THz amplitude, in the presence of a static magnetic field as compared to the absence of a magnetic field. This also shows the significance of a external magnetic field in our proposed theory**.**

To study the effect of dimensions of CNTs on the normalized THz amplitude, we have plotted a graph between normalized THz amplitude with normalized frequency as shown in figure 3.3.2. In the first case, external and internal radii of CNTs are 40.0 nm and 20.0 nm whereas in the second case these are 36.0 nm and 12.0 nm. Corresponding to the first case $b/a = 2.0$, $\beta = 0.4622$, $\alpha = 0.06 \ \text{nm}^{-1}$ whereas, corresponding to second case $b/a = 4.0$, $\beta = 0.1848$, $\alpha = 0.08 \ \text{nm}^{-1}$. The value of normalized THz amplitude is observed to decrease with the increase in the value of b/a. THz amplitude is more for $b/a = 2.0$ (first case) as compared to $b/a = 4.0$ (second case). The physical mechanism of this observation is as follows: with a lesser value of b/a for CNTs, there is more absorption of lasers by CNTs. A similar observation was made by Vij *et al.* [10] where they observed direct dependence of THz amplitude on the radii of CNTs. Watanabe *et al.* [27] have also shown the direct dependence of the THz electric field on the radii of CNTs in their experiment, in which they generated intense THz pulse excitons by using CNTs. Also, a shift in the surface plasmon resonance point is observed towards the lower side of THz frequency at the lower value of b/a. This shift can be well explained from the expression of surface plasmon resonance condition.

In figure 3.3.3, we have shown a variation of normalized THz amplitude with normalized frequency at different values of inter-tube separation $d = 60.0 \ \text{nm}, 75.0 \ \text{nm}, 90.0 \ \text{nm}$. Whereas, other parameters are the same as that of figure 3.3.1.
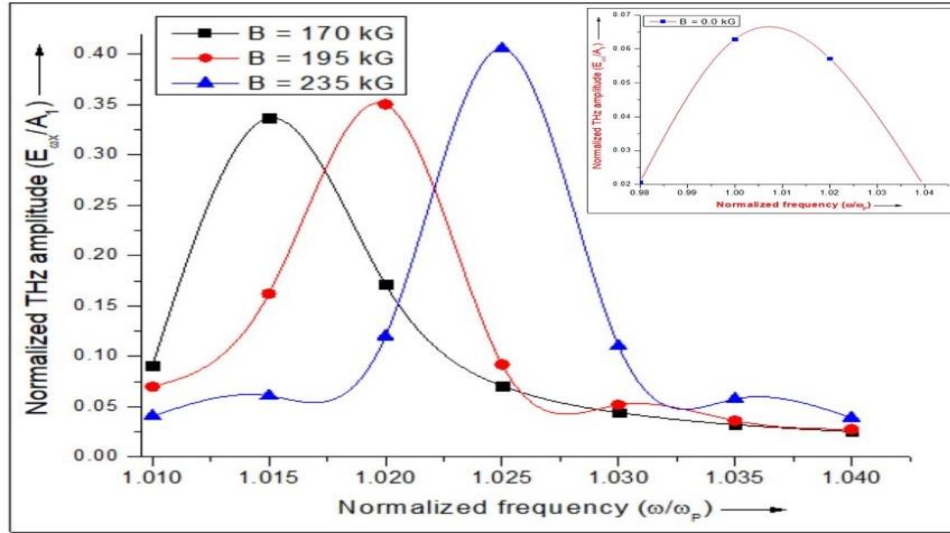
Fig.3.3.1 Variation of normalized terahertz amplitude with normalized THz frequency at different values of external magnetic field B = 170 kG, 195 kG, 235 kG for β = 0.4622 and α = 0.06 nm⁻¹. Inset graph; plot similar to figure, in the absence of static magnetic field.
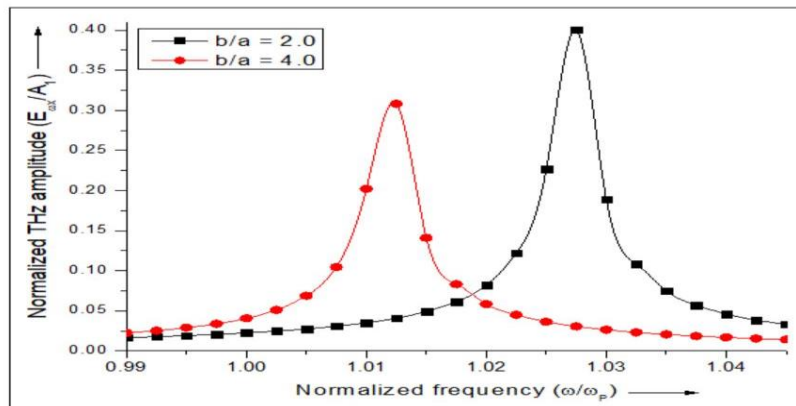
Fig.3.3.2 Variation of normalized terahertz amplitude with normalized THz frequency for different values of characteristic parameter β and anharmonicity factor α at the optimized value of external magnetic field B = 235 kG.

From the three curves of figure 3.3.3, it is observed that the normalized THz amplitude shows maxima at the lower value of inter-tube separation 60.0 nm. This is because at the lower value of inter-tube separation, the number density of CNTs increases, and hence nonlinearity of the

49

array of CNTs behaving as plasma increases. The same observation was made by Kumar *et al.* [28]. From the graph, it is also observed that the surface plasmon resonance shifts towards the left with the decrease in the inter-tube separation. In figure 3.3.4., we have shown the effect on normalized THz amplitude by considering the anharmonicity and without considering the anharmonicity in the CNTs. From the curves, it is clear that by considering the anharmonicity, there is a significant increase in the normalized amplitude of THz radiation. From figure 3.3.4,
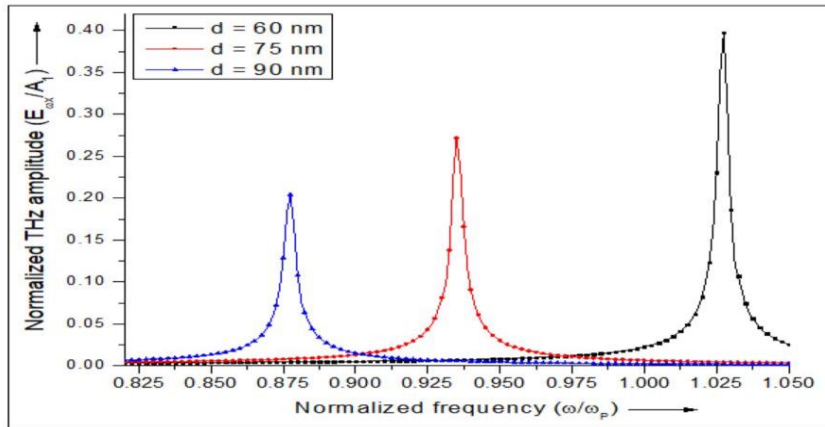
Fig.3.3.3 Variation of normalized terahertz amplitude with normalized THz frequency at different values of inter-tube separation at the optimized value of external magnetic field B = 235 kG for characteristic parameter β = 1.064 and α = 0.06 nm^{-1}.
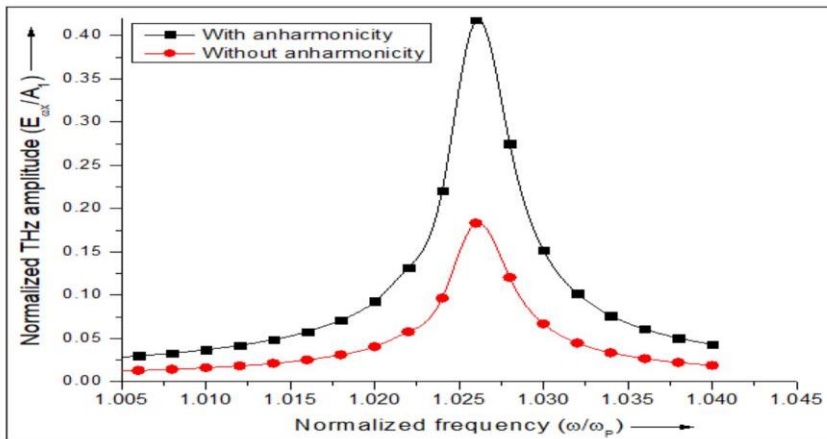
Fig.3.3.4 Variation of normalized terahertz amplitude with normalized THz frequency, with and without anharmonicity at the optimized value of external magnetic field B = 235 kG and other parameters are the same as that of fig.3.3.

it is observed that normalized THz amplitude shows a nearly 2.0 times increase in anharmonic CNTs as compared to the case where anharmonicity is not considered. Hence the THz amplitude is enhanced significantly by considering anharmonicity as compared to considering the ponderomotive nonlinearity only. One more very important observation which we have made from this figure is that the surface plasmon resonance is broadened. It is very useful when we are using this THz source for communication purposes because, with the broadening of surface plasmon resonance frequency, bandwidth is increased.

3.4. Conclusion

The surface plasmon resonance peaks expand and broaden due to the anharmonic behavior of an array of CNTs in the presence of a static magnetic field. It also results in the enhancement of normalized THz amplitude. Under the influence of electric fields exerted by lasers, electrons of CNTs experience restoration force to induce the nonlinear current. This nonlinear current is further responsible for the generation of THz radiations. The normalized THz field gets resonantly enhanced at the surface plasmon resonance frequency. One can tailor this resonance condition $\omega = \omega_P \sqrt{(1 + \beta)/2\epsilon_r + (\omega_c^2/\omega_P^2)}$ for the enhancement of normalized THz amplitude by changing the values of characteristic parameter β and external magnetic field B. It is also observed that the normalized THz amplitude shows a significant variation with the change of values of the applied external magnetic field, inter-tube separation, dimensions, and the density of CNTs, by considering the anharmonicity.

References:-

[1] C. Baker et al., "Detection of concealed explosives at a distance using terahertz technology," Proc. IEEE **95**(8), 1559 (2007).

[2] A.R. Orlando and G.P. Gallerano, "Terahertz Radiation effects and biological applications," J Infrared Millim Terahertz Waves **30**(1), 1308 (2009).

[3] P.H. Siegel, "Terahertz technology," IEEE Transactions on microwave theory and techniques **50**(3), 910 (2002).

[4] D. Dragoman and M. Dragomen, "Terahertz fields and applications," Prog. Quantum Electron. **28**(1) 1-66 (2004).

[5] K. Ishigaki et al., "Direct intensity modulation and wireless data transmission characteristics of terahertz-oscillating resonant tunnelling diodes," Electron. Lett. **48**(1), 582-583 (2012).

[6] A. Mehta, J. Rajput, K. Kang and N. Kant, "Terahertz generation by beating of two chirped pulse lasers in spatially periodic density plasma," Laser Phys. **30**(4), 045402 (2020).

[7] S. Kumar, S. Vij, N. Kant, A. Mehta and V. Thakur, "Resonant terahertz generation from laser filaments in the presence of static electric field in a magnetized collisional plasma," Euro. Phys. J. Plus **136**(1), 148 (2021).

[8] S. Sharma and A. Vijay, "Terahertz generation via laser coupling to anharmonic carbon nanotube array," Phys. Plasmas **25**(2), 023114 (2018).

[9] S. Sharma and A. Vijay, "Nonlinear mixing of lasers and terahertz generation on CNT embedded metal surface," Optik **199**(1), 163381 (2019).

[10] S. Vij, N. Kant and V. Thakur, "Resonant enhancement of THz radiation through vertically aligned carbon Nanotubes Array by applying Wiggler magnetic field," Plasmonics **14**(1), 1051-1056 (2019).

[11] S. Jain, J. Parashar and R. Kurchania, "Effect of magnetic field on terahertz generation via laser interaction with a carbon nanotube array," Int. Nano Lett. **3**(1), 5326 (2013).

[12] A. Mehta and N. Kant, "Terahertz radiation generation driven by the frequency chirped laser pulse in magneto-active plasma," Proc. SPIE **10917**, 109170R (2019).

[13] Q. Zhang et al., "Plasmonic nature of the terahertz conductivity Peak in single-wall carbon nanotubes," Nano Lett. **13**(12), 5991-5996 (2013).

[14] V. Giannini, G. Vecchi and J.G. Rivas, "Lighting up multipolar surface plasmon polaritons by collective resonances in arrays of nanoantennas," Phys. Rev. Lett. **105**(26), 266801 (2010).

[15] L.V. Titova et al., "Generation of terahertz radiation by optical excitation of aligned carbon nanotubes," Nano Lett. **15**(5), 3267-3272 (2015).

[16] K.G. Batrakov et al., "Terahertz processes in carbon nanotubes," J. Nanophotonics **4**(1), 041665 (2010).

[17] M.E. Portnoi, O.V. Kibis and M.R. Da Costa, "Terahertz applications of carbon nanotubes," Superlattices Microstruct **43**(5), 399-407 (2008).

[18] Y. Wang and Q. Wu, "Properties of terahertz wave generated by the metallic carbon nanotube antenna," Chin. Opt. Lett. **6**(10), 770 (2008).

[19] D. Dragoman and M. Dragoman, "Terahertz oscillations in semiconducting carbon nanotube resonant-tunneling diodes," Physics E **24**(3), 282-289 (2004).

[20] M. Dagher et al., "Theoretical investigation of traveling-wave amplification in metallic carbon nanotubes biased by a DC field," IEEE Trans. Nanotech. **11**(3), 463-471 (2012).

[21] S. Reich, C. Thomson and J. Maultzsch, "Carbon Nanotubes: Basic concepts and physical properties," Wiley VCH 54-78 (2004).

[22] W. Lu, D. Wang and L. Chen, "Near-static dielectric polarization of individual carbon nanotubes," Nano Lett. **7**(9), 2729-2733 (2007).

[23] C.S. Liu and V.K. Tripathi, "Observational consequences of parametrically driven vibrations of carbon nanotubes," Phys. Rev. B **70**(11), 115414 (2004).

[24] M. Kumar and V.K. Tripathi, "Nonlinear absorption and harmonic generation of laser in a gas with anharmonic clusters," Phys. Plasmas. **20**(2), 023302 (2013).

[25] H. Dai, "Carbon nanotubes: opportunities and challenges," Surf. Sci. **500**(1), 218-241 (2002).

[26] E. Muñoz et al., "Single-walled carbon nanotubes produced by cw CO2-laser ablation: study of parameters important for their formation," Appl. Phys. A **70**(1), 145-151 (2000).

[27] S. Watanabe, N. Minami and R. Shimano, "Intense terahertz pulse induced exciton generation in carbon nanotubes," Opt. Express **19**(2), 1528-1538 (2011).

[28] A. Kumar and P. Kumar, "Electron beam induced THz emissions from nanotube array," Phys. Plasmas **23**(10), 103302 (2016).

Chapter 4

Terahertz generation by using laser filaments under the influence of static electric field in magnetized collisional plasma and magnetized anharmonic CNTs

4.1. Introduction

In modern days compact and efficient THz sources have great importance in the field of science and technology because of their numerous applications in industrial manufacturing and packaging units [1], security and safety [2], broad band communication [3], biological and pharmaceutical sciences [4-6], remote sensing [7]. Due to this, various researchers have studied the schemes of THz wave generation by using different mechanisms to enhance the normalized THz amplitude like optical rectification [8], cross-focusing [9], optical mixing [10], and filamentation [11,13], etc. Among them, the mechanism of THz generation by laser filamentation produces THz pulses of very high-order energy. Femtosecond laser filamentation is a distinctive, dynamical, and unique phenomenon in which laser beam breaks up in transverse direction by maintaining the balance between an optical Kerr effect induced self-focusing and plasma de-focusing. In this laser, intensity is stabilized along the propagation distance and this is known as intensity clamping. The filamentary propagation of laser pulses in the air was observed in 1995 [14] which led to a lot of research in the emission of electromagnetic waves. Houard *et al*. [15] noticed three orders of magnitude enhancement of the terahertz energy beamed by a femtosecond pulse undergoing filamentation through the air in the presence of the static electric field. Loffler *et al*. [16] observed enhancement in the efficiency of THz radiation generation by using a static electric field. Bhasin *et al*. [17] proposed 30 times increase in the magnitude of normalized terahertz amplitude by applying a D.C. electric field in plasma 50kV/cm. Mclaughlin *et al*. [18] have shown an enhancement in THz field energy by applying an external magnetic field up to 8T in plasma.

In the present work, we develop a comprehensive theoretical model for the generation of terahertz waves by using two filamented femtosecond laser pulses in the presence of an applied static electric field in the magnetized collisional plasma. In this analysis, we have taken two femtosecond lasers of slightly different frequencies so that their difference in frequency may lie in the terahertz region. Also for two lasers of nearly equal frequencies, the symmetry of +ve and –ve half cycles of fundamental laser are broken. As a result, the ionization causes drift currents in the same direction in every cycle. Therefore terahertz generation becomes more efficient [19].

To explain and understand the basic theory of THz generation by using filamented laser beams we have provided two analytical models in this chapter. In the first model, we have generated THz radiations by using laser filaments under the effect of externally applied static electric field in the magnetized collisional plasma whereas, in second theoretical model same has been explained with anharmonic magnetized CNTs. The externally applied both static electric and magnetic fields play vital roles in the enhancement of the normalized THz amplitude and power. In the second model, we have also considered the anharmonicity in the CNTs. The HA-CNTs helps to form compact and highly efficient sources of THz generation.

4.2. Proposed Model for THz generation by using laser filaments under the influence of static electric field in a magnetized collisional plasma

In this, we have considered two transversely amplitude-modulated femtosecond laser beams having electric fields, $\vec{E}_1(\omega_1, k_1)$ and $\vec{E}_2(\omega_2, k_2)$. These laser beams are propagating along Z-direction, polarizing along Y-direction, and amplitude modulated along the x-direction. To produce magnetized plasma, a static magnetic field is applied over the plasma along the y-direction. This static magnetic field can be applied by using a current-carrying coil having a finite number of turns and a magnetic core with an air gap. The static D.C. electric field is applied along X- direction. This D.C. electric field can be applied with the help of two metallic plates, keeping one plate at positive potential and the other at negative potential as shown in figure 4.2.1. The applied electric and magnetic fields aid in the enhancement of the

normalized amplitude of the terahertz wave. The laser fields impart oscillatory velocity to the plasma electrons. Whereas, externally applied static D.C. electric field is responsible for the D.C. drift to electrons in the opposite direction. The lasers also exert a beat ponderomotive force $\vec{F}_{PM\omega}^{NL}$ as well as static ponderomotive force $\vec{F}_{PM\beta}^{NL}$ on the electrons of magnetized collisional plasma. In steady-state, the static ponderomotive force is well poised by pressure gradient force. It results in transverse density ripple at zero frequency and wave number β which can be represented by $n_{0\beta}$. The ponderomotive force gives rise to velocity oscillations $\vec{v}_{\omega,k}^{NL}$ and density oscillations $n_{\omega,k}^{NL}$. The density oscillation beats with D.C. drift to produce a transverse current density $\vec{J}_{\omega,k}^{NL}$ which is responsible for THz generation. In most of the research works on THz generation, collisions have been ignored because of the extraction of energy from the electrons of plasma. In reality, these collisions are the inherent part of every nonlinear system hence, it becomes important to consider the effect of collisions in our analysis to get more accurate results.

We irradiate two transversely amplitude-modulated femtosecond laser pulses in the magnetized collisional plasma with density n_0. The field profile of lasers can be given as

$$\vec{E}_j = \hat{y}\left[1 + \mu_j \cos\beta_0 x\right] D_{j0} e^{-i(\omega_j t - k_j z)}, \tag{4.2.1}$$

Where $j = 1, 2$, μ_j is the modulation depth of the beam and β_0 is the periodicity parameter. The frequency difference of femtosecond lasers ($\omega = \omega_1 - \omega_2$) lies in THz range. The significant gain in the oscillatory velocities of plasma electrons is observed due to the laser filaments and are provided as

$$\vec{v}_j = \frac{-e\,\vec{E}_j}{m_e(i\omega_j - \nu_e)}. \tag{4.2.2}$$

Due to externally applied static D.C. electric field along X-axis, plasma electrons will get D.C. drift and is given as

$$\vec{v}_{D.C} = \frac{-e\vec{E}_{D.C}}{m_e \nu_e}, \tag{4.2.3}$$

Where $-e$, m_e, υ_e represent the electronic charge, mass, and collisional frequency respectively. The term $\vec{E}_{D.C}$ represents the applied D.C. electric field. The plasma electrons drift in the opposite direction of D.C. electric field and get accumulated near the edge of the filament. It results in the complete screening of D.C. electric field in the plasma but at the same time, there occurs a transient process of redistribution of charges. It is due to instantaneous ionization in the plasma. Now electric current is directed along the direction of the external D.C. electric field and it exhibits oscillations at plasma frequency. These oscillations decay due to collisions between the electrons of plasma. The temporal electric current directed along the external D.C. electric field and perpendicular to the laser filament plays a significant role in the generation of THz waves.

The femtosecond lasers beat together in the presence of D.C. electric field and static applied magnetic field to exert a ponderomotive force $\vec{F}_{PM}^{NL}$, which is equivalent to the vector sum of static ponderomotive force $\vec{F}_{PM\beta}^{NL}$ and beat frequency ponderomotive force $\vec{F}_{PM\omega}^{NL}$.

$$\vec{F}_{PM}^{NL} = \vec{F}_{PM\beta_0}^{NL} + \vec{F}_{PM\omega}^{NL} , \tag{4.2.4}$$

where, $\vec{F}_{PM\omega}^{NL} = e \vec{\nabla}\phi_{PM\omega}$ and $\vec{F}_{PM\beta_0}^{NL} = e \vec{\nabla}\phi_{PM\beta_0}$. The beat frequency ponderomotive potential is provided as

$$\phi_{PM\omega} = \frac{-m_e}{2e}\vec{v}_1\vec{v}_2^* , \tag{4.2.5}$$

where, $\vec{v}_1$ & $\vec{v}_2$ represent the velocity of plasma electrons. By putting the value of $\vec{v}_1$ and $\vec{v}_2^*$ and using the standard relation $\cos\beta_0 x = \left(e^{i\beta_0 x} + e^{-i\beta_0 x}\right)/2$, we can calculate the ponderomotive potential. In the expression, we have two terms $e^{-i\beta_0 x}$ and $e^{i\beta_0 x}$. Out of these two terms one term $e^{i\beta_0 x}$ is responsible for exciting THz radiation at resonance condition. We can neglect the second term $e^{-i\beta_0 x}$, because it moves out of resonance.

$$\phi_{PM\omega} = \frac{e}{2\,m_e(i\omega_1 - \nu_e)(i\omega_2 - \nu_e)}\left\{1 + \left(\frac{\mu_1 + \mu_2}{2}\right)e^{i\beta x}\right\}D_{10}D_{20}e^{-i(\omega t - kz)}. \qquad (4.2.6)$$

The static ponderomotive potential is given by

$$\phi_{PM\beta_0} = \frac{e}{4m_e}\left\{\frac{\mu_1 D_{10}^2}{(i\omega_1 - \nu_e)} + \frac{\mu_2 D_{20}^2}{(i\omega_2 - \nu_e)^2}\right\}e^{i\beta_0 x}. \qquad (4.2.7)$$
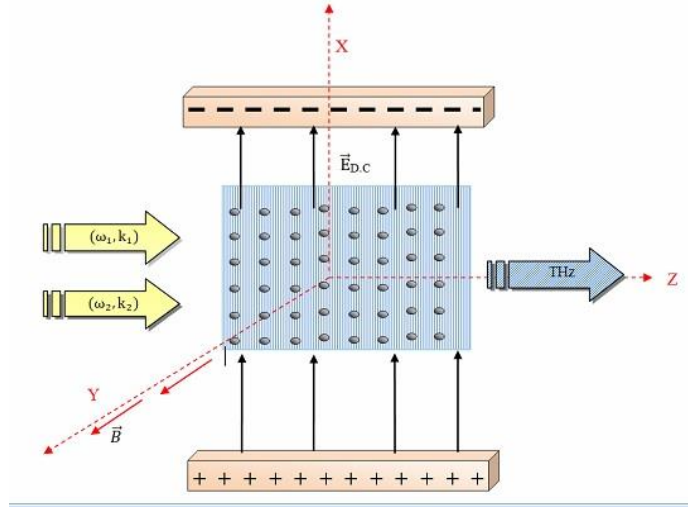
Figure 4.2.1: Schematic of THz generation by irradiating amplitude-modulated lasers in magnetized collisional plasma in the presence of D.C. electric field.

The static ponderomotive force is responsible for ambipolar diffusion of plasma along the direction of the applied D.C. electric field. To obtain the sustainability and balancing condition within the plasma the static ponderomotive force is neutralized by pressure gradient force and results in the zero frequency transverse density ripples in the plasma. By using the equation of motion for electrons in the steady-state, we can obtain the relation between the density of the transverse ripple and the equilibrium temperature of electrons. One can write $n_{0\beta_0} = en_0\,\phi_{PM\beta_0}/T_e$ [18], where T_e is the equilibrium temperature of electrons in the plasma $n_{0\beta_0}$ is the density of the ripple. By using the static ponderomotive potential, $n_{0\beta}$ attains the following form

$$n_{0\beta_0} = \frac{e^2 n_0}{4m_e T_e}\left(\frac{\mu_1 D_{10}^2}{(i\omega_1 - \nu_e)^2} + \frac{\mu_2 D_{20}^2}{(i\omega_2 - \nu_e)^2}\right)e^{i\beta_0 x}. \tag{4.2.8}$$

The beat frequency ponderomotive force and magnetic field force will provide oscillatory velocity to plasma electrons. By using the equations of motion, the oscillatory velocity of electrons can be calculated as

$$m\frac{d\vec{v}_{PM}^{NL}}{dx} = \vec{F}_{PM}^{NL} - e\left(\vec{v}_{PM}^{NL} \times \vec{B}\right), \tag{4.2.9}$$

$$\vec{v}_{PM}^{NL} = \frac{1}{m(\nu - i\omega)}\left[\vec{F}_{PM}^{NL} - e\left(\vec{v}_{PM}^{NL} \times \vec{B}\right)\right], \tag{4.2.10}$$

$$\vec{v}_{PM}^{NL} \times \vec{B} = \frac{1}{m(\nu - i\omega)}\left[\vec{F}_{PM}^{NL} \times \vec{B} - e\left(\vec{v}_{PM}^{NL} \times \vec{B}\right) \times \vec{B}\right], \tag{4.2.11}$$

$$= \frac{1}{m(\nu - i\omega)}\left[\vec{F}_{PM}^{NL} \times \vec{B} + e\,\vec{v}_{PM}^{NL}\,B^2\right], \tag{4.2.12}$$

$$\vec{v}_{PM}^{NL} = \frac{1}{m(\nu - i\omega)}\left[\vec{F}_{PM}^{NL} - \frac{e}{m(\nu - i\omega)}\left(\vec{F}_{PM}^{NL} \times \vec{B} + e\,\vec{v}_{PM}^{NL}\,B^2\right)\right], \tag{4.2.13}$$

$$\vec{v}_{PM}^{NL} = \frac{\vec{F}_{PM}^{NL}}{m_e(\nu_e - i\omega)} - \frac{\vec{F}_{PM}^{NL} \times \vec{\omega}_c}{m_e(\nu_e - i\omega)^2} - \frac{\omega_c^2}{(\nu_e - i\omega)^2}\vec{v}_{PM}^{NL}, \tag{4.2.14}$$

here $\omega_c = eB/m$ is cyclotron frequency of electrons. Due to the applied magnetic field along y-axis, we resolve the velocity of electrons along the x-axis and z-axis as

$$v_{PMx}^{NL} = \frac{e^2 D_{10}D_{20}}{4m_e^2 \omega_\alpha^2 (i\omega_1 - \nu_e)(i\omega_2 + \nu_e)}\left[\{(\nu_e - i\omega)\beta_0 + \omega_c k\}i(\mu_1 + \mu_2)e^{-i(\omega t - kz - \beta_0 x)} + 2\iota\omega_c k\,e^{-i(\omega t - kz)}\right], \tag{4.2.15}$$

$$v_{PMz}^{NL} = \frac{e^2 D_{10}D_{20}}{4m_e^2 \omega_\alpha^2 (i\omega_1 - \nu_e)(i\omega_2 + \nu_e)}\left[\{(\nu_e - i\omega)k - \omega_c\beta_0\}i(\mu_1 + \mu_2)\,e^{-i(\omega t - kz - \beta_0 x)} + 2i(\nu_e - i\omega)k\,e^{-i(\omega t - kz)}\right]. \tag{4.2.16}$$

where $[(\nu_e - i\omega)^2 + \omega_c^2] = \omega_\alpha^2$. With the help of velocity perturbations provided by Eq. (4.2.15) and (4.2.16), density perturbations $n_{\omega,k}^{NL}$, $n_{\omega,k+\beta_0}^{NL}$ in the presence of static electric and magnetic fields can be calculated by using the equation of continuity as

$$n_{\omega,k}^{NL} = \frac{n_0 e^2 D_{10} D_{20} \left[ik^2\right] (\omega_c + \upsilon_e - i\omega)}{2m_e^2 \omega \omega_\alpha^2 (i\omega_1 - \upsilon_e)(i\omega_2 + \upsilon_e)} e^{-i(\omega t - kz)}, \tag{4.2.17}$$

$$n_{\omega,k+\beta_0}^{NL} = \frac{n_0 e^2 (\mu_1 + \mu_2)(D_{10} D_{20})}{4m_e^2 (i\omega_1 - \upsilon_e)(i\omega_2 + \upsilon_e)} \frac{i\left[(\upsilon_e - i\omega)^2 (k^2 + \beta_0^2) - \omega_c^2 \beta_0^2 + \omega_c k^2\right]}{\omega \omega_\alpha^2} e^{-i(\omega t - kz - \beta_0 x)}. \tag{4.2.18}$$

One can write nonlinear current density as the vector sum of three terms $\vec{J}_1, \vec{J}_2$ and $\vec{J}_3$, where the first term $\vec{J}_1$ arises due to coupling between equilibrium plasma density n_0 and nonlinear velocity $\vec{v}_{\omega,k}^{NL}$, the second term $\vec{J}_2$ arises due to coupling between nonlinear density perturbation $n_{\omega,k}^{NL}$ and D.C. drift of electrons $\vec{v}_{D.C}$. The third term $\vec{J}_3$ arises due to coupling between zero frequency transverse density ripple $n_{0\beta}$ and nonlinear velocity $\vec{v}_{\omega,k}^{NL}$. Therefore, the total nonlinear current density $\vec{J}_{\omega,k}^{NL} = \vec{J}_1 + \vec{J}_2 + \vec{J}_3$,

$$\vec{J}_{\omega,k}^{NL} = -n_0 \, e \, \vec{v}_{\omega,k}^{NL} - n_{\omega,k}^{NL} \, e \, \vec{v}_{D.C} - n_{o,\beta}^* \, e \, \vec{v}_{\omega,k+\beta}^{NL}. \tag{4.2.19}$$

On resolving the total current density in its x and z components, we get $J_{x\,\omega,k}^{NL}$ and $J_{z\,\omega,k}^{NL}$ as

$$J_{x\,\omega,k}^{NL} = \frac{-n_0 e^4 D_{10} D_{20}[i]}{2m_e^3 \omega_\alpha^2 (i\omega_1 - \upsilon_e)(i\omega_2 + \upsilon_e)} \left\{ \frac{k^2 E_{D.C}[(\upsilon_e - i\omega + \omega_c)]}{\omega \upsilon_e} - \frac{e\beta_0(\mu_1 + \mu_2)}{8T_e} \left(\frac{\mu_1 D_{10}^2}{(i\omega_1 - \upsilon_e)^2} + \frac{\mu_2 D_{20}^2}{(i\omega_1 + \upsilon_e)^2} \right)(\upsilon_e - i\omega - \right.$$

$$\left. \omega_c) \right\} e^{-i(\omega t - kx)}, \tag{4.2.20}$$

$$J_{z\,\omega,k}^{NL} =$$

$$\frac{-n_0 e^4 D_{10} D_{20}[i]}{2m_e^3 \omega_\alpha^2 (i\omega_1 - \upsilon_e)(i\omega_2 + \upsilon_e)} \left\{ \frac{ek(\mu_1 - \mu_2)}{8T_e} \left(\frac{\mu_1 D_{10}^2}{(i\omega_1 - \upsilon_e)^2} + \frac{\mu_2 D_{20}^2}{(i\omega_1 + \upsilon_e)^2} \right)(\upsilon_e - i\omega + \omega_c) + \right.$$

$$\left. \frac{m_e k(\upsilon_e - i\omega + \omega_c)}{e} \right\} e^{-i(\omega t - kz)}. \tag{4.2.21}$$

Due to the presence of an external magnetic field along the Y-direction in collisional plasma, the dielectric constant will behave as an anisotropic tensor

$$\epsilon = \begin{vmatrix} \epsilon_{XX} & \epsilon_{XY} & \epsilon_{XZ} \\ \epsilon_{YX} & \epsilon_{YY} & \epsilon_{YZ} \\ \epsilon_{ZX} & \epsilon_{ZY} & \epsilon_{ZZ} \end{vmatrix},$$

(4.2.22)

The components of the dielectric anisotropic tensor are

$\epsilon_{YZ} = \epsilon_{ZY} = \epsilon_{YX} = \epsilon_{XY} = 0$, $\epsilon_{YY} = 1 - \omega_p^2/i\omega(\upsilon_e - \iota\omega)$, $\epsilon_{XX} = 1 -$

$\omega_p^2(\upsilon_e - i\omega)/i\omega[(\upsilon_e - i\omega)^2 + \omega_c^2] = \epsilon_{ZZ}$, $\epsilon_{ZX} = -i\omega_c\omega_p^2/\omega[(\upsilon_e - i\omega)^2 + \omega_c^2] = -\epsilon_{XZ}$.

Due to collisions some of the components of dielectric tensor become imaginary which are responsible for the resistivity in plasma. The wave equation for the generation of THz radiation is given by

$$-\nabla^2\vec{E} + \nabla.\left(\nabla.\vec{E}\right) = \frac{4\pi\iota\omega}{c^2}\vec{J}^{NL} + \frac{\omega^2}{c^2}\epsilon\vec{E} \ .$$

(4.2.23)

With the use of components of dielectric constant, Eq. (4.2.23) is modified as

$$-\frac{\omega^2}{c^2}\epsilon_{zz}E_z - \frac{\omega^2}{c^2}\epsilon_{zx}E_x = \frac{+4\pi\iota\omega}{c^2}J_Z^{NL},$$

(4.2.24)

$$-2ik'\frac{\partial E_x}{\partial z} + \left(k'^2 - \frac{\omega^2}{c^2}\left(\epsilon_{xx} + \frac{\epsilon_{zx}^2}{\epsilon_{zz}}\right)\right)E_x = \frac{+4\pi\iota\omega}{c^2}\left(J_x^{NL} + \frac{\epsilon_{zx}}{\epsilon_{zz}}J_z^{NL}\right) \ .$$

(4.2.25)

Where $k' = k_1 - k_2 + \beta_0$ is the wave number with which current density oscillates at frequency ω. The wave number β of transverse density ripple is responsible for phase matching condition by providing extra momentum. By using phase matching condition

$$k'^2 - \frac{\omega^2}{c^2}\left(\epsilon_{xx} + \frac{\epsilon_{zx}^2}{\epsilon_{zz}}\right) = 0,$$

(4.2.26)

$$k_1 - k_2 + \beta_0 = \frac{\omega}{c}\left\{1 - \frac{\omega_p^2}{\iota\omega\omega_\alpha^2}\left((\upsilon_e - i\omega) - \frac{\omega_c^2\omega_p^2}{i\omega\omega_\alpha^2 - \omega_p^2(\upsilon_e - i\omega)}\right)\right\}^{1/2}.$$

(4.2.27)

By using the above condition, Eq. (4.2.25) provides the electric field of THz radiation.

$$E_{\omega x} = \frac{-2\pi\omega}{k'c^2}\left\{J_{x\,\omega,k}^{NL} + \frac{\epsilon_{zx}}{\epsilon_{zz}}J_{z\omega,k}^{NL}\right\}z.$$

(4.2.28)

Using $J_{x\,\omega,k}^{NL}$ and $J_{z\,\omega,k}^{NL}$, the THz electric field can be derived as

$$E_{\omega x} = \frac{-2\pi\omega z}{k'c^2}\left(\frac{-n_0 e^4 D_{10}D_{20}i}{2m_e^3\omega_\alpha^3(i\omega_1-\nu_e)(i\omega_2+\nu_e)}\right)\left(\frac{k^2 E_{D.C}(\nu_e-i\omega+\omega_c)}{\omega\nu_e} - \frac{e\beta_0(\mu_1+\mu_2)}{8T_e}\frac{\mu_1 D_{10}^2}{(i\omega_1-\nu_e)^2} + \frac{\mu_2 D_{20}^2}{(i\omega_2+\nu_e)^2}\right)(\nu_e - i\omega + \omega_c) +$$

$$\frac{\omega_c\omega_P^2}{i\omega\omega_\alpha^2-\omega_P^2(\nu_e-i\omega)}\left\{\frac{ek(\mu_1+\mu_2)}{8T_e}\left(\frac{\mu_1 D_{10}^2}{(i\omega_1-\nu_e)^2} + \frac{\mu_2 D_{20}^2}{(i\omega_2+\nu_e)^2}\right)\right\}(\nu_e - i\omega + \omega_c) + \frac{m_e K}{e}(\nu_e - i\omega + \omega_c). \qquad (4.2.29)$$

Using the above equation, the normalized amplitude of the electric field component of THz radiations can be written as

$$\frac{eE_{\omega x}}{m_e\omega_P c} = \frac{\omega' z' D_{10}' D_{20}' i}{4k'' \omega_0^2(i\omega_{P1}-\nu_e')(i\omega_{P2}+\nu_e')}\left[\frac{k_0^2 E_{D.C}'(\nu_e'-i\omega'+\omega_c')}{\omega'\nu_e'} + \left(\nu_e' - i\omega' - \omega_c'\right)\left\{\frac{k_0}{8}\left(\frac{\omega_c'}{i\omega'\omega'^2-\left(\nu_e'-i\omega'\right)}\right) - \right.\right.$$

$$\left.\left.\frac{\beta'}{8}\right\}\frac{(\mu_1+\mu_2)}{V_{th}'}\left(\frac{\mu_1 D_{10}'^2}{\left(i\omega_{P1}-\nu_e'\right)^2} + \frac{\mu_2 D_{20}'^2}{\left(i\omega_{P2}+\nu_e'\right)^2}\right) + \left(\frac{\omega_c'}{i\omega'\omega'^2-\left(\nu_e'-i\omega'\right)}\right)\right]. \qquad (4.2.30)$$

The different parameters are normalized as,

$D_{10}' = eD_{10}/m\omega_p c$, $D_{20}' = eD_{20}/m\omega_p c$, $\omega' = \omega/\omega_p$, $z' = \omega_p z/c$, $\omega_{p1} = \omega_1/\omega_P$, $\omega_{p2} = \omega_2/\omega_p$, $\nu_e' = \nu_e/\omega_p$, $E_{D.C}' = e\,E_{D.C}/m\omega_p c$. $k_0 = ck/\omega_p$, $k'' = ck'/\omega_p$, $\omega_c' = \omega_c/\omega_p$, $q' = c\beta_0/\omega_p$, $v_{th}' = v_{th}/c$

4.3. Graphical Analysis and Observations

In the present research work, we provide numerical treatment and graphical analysis of THz generation in magnetized collisional plasma with the following set of parameters. CO_2 femtosecond lasers with frequencies $\omega_1 = 2 \times 10^{14}$ rad /s and $\omega_2 = 1.85 \times 10^{14}$ rad/s are chosen. The corresponding wavelengths of CO_2 femtosecond lasers are $\lambda_1 = 10.20$ μm & $\lambda_2 = 9.440$ μm with a peak value of intensity of $\sim 10^{14}$ W/cm^2. The graph between normalized THz amplitude and normalized THz frequency is represented in figure 4.3.1, for values of static magnetic field ranging from 10 kG to 50 kG at the optimized value of D.C. electric field of 10 kV/cm. From the graph, it is concluded that normalized THz amplitude increases with the decrease of normalized THz frequency and vice versa. It is observed that the THz amplitude acquires maximum value when ω/ω_p approaches 1. One can notice from Fig.4.3.1 that the normalized THz amplitude is maximum corresponding to the magnetic field of 50 kG. It is due to the fact that the external magnetic field modifies the plasma dielectric anisotropic tensor and excites nonlinear current strongly. It results in the enhancement of the normalized THz amplitude with the external magnetic field. Similar results are observed by Mehta *et al.*

[20] with a magnetic field range from 54 kG to 322 kG but in the present work magnetic field is applied in the range 10 kG to 50 kG which is very much cost-effective feasible.
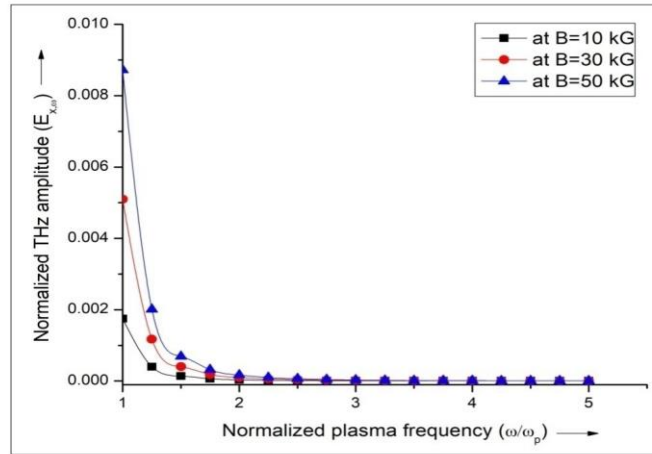
Figure 4.3.1 Plot of the normalized amplitude of THz radiation with normalized THz frequency ω/ω$_p$, at the various value of magnetic fields ranging from 10 kG to 50 kG.

In nonlinear system υ_e is comparable with ω_p. If υ_e is very large as compared to ω_p, then plasma is strongly coupled plasma otherwise plasma is weakly coupled plasma. In most of the expressions υ_e appears together with ω_p and laser frequency ω. The figure 4.3.2 shows an increase of normalized THz amplitude with the decrease of normalized collision frequency υ_e/ω_c. Due to the decrease of collisions in the plasma, the magnitude of the ponderomotive force and hence nonlinear current shows an increase. This increases the normalized THz amplitude. From figure 4.3.2 one can observe clearly that an external magnetic field is useful to decrease the effect of collisions on the normalized THz amplitude
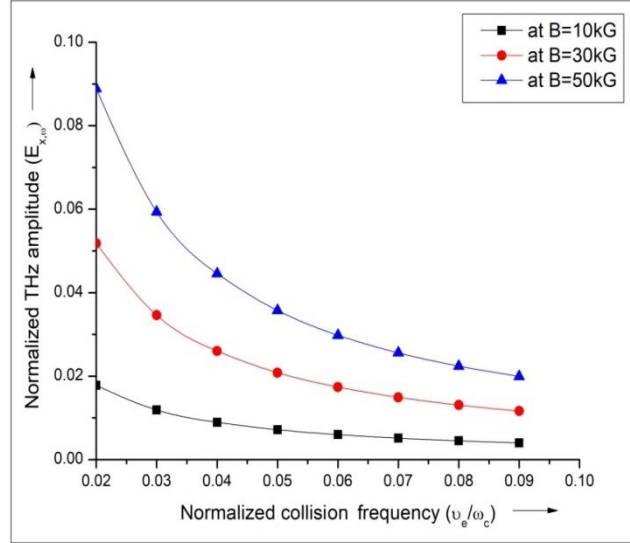
Figure 4.3.2 Plot of the normalized amplitude of THz radiation with normalized collision frequency υ_e/ω_c , at electric field 10 kV/cm.

To check the effect of applied D.C. electric field on the normalized THz amplitude we have drawn a graph between normalized THz amplitude and normalized D.C. electric field at the optimized value of magnetic field B = 30 kG, as shown in figure 4.3.3. Due to the applied D.C. electric field $\vec{E}_{D.C}$ (ranging from $10\,\text{kV/cm}$ to $30\,\text{kV/cm}$, drift force $\left|e\,\vec{E}_{D.C}\right|$ act on the plasma electrons which increases the nonlinearity of the system and hence helps in the enhancement of normalized THz amplitude. Similar results were observed by Bhasin *et al.* [17] when they applied static electric field up to $50\,\text{kV/cm}$ and obtained the maximum value of normalized THz amplitude up to 4.280×10^{-5}. However, In the present work, we have obtained better results by applying D.C. electric and static magnetic field and obtaining the maximum value of normalized THz amplitude up to 0.4650×10^{-3}, for the static electric field of $30\,\text{kV/cm}$.

64
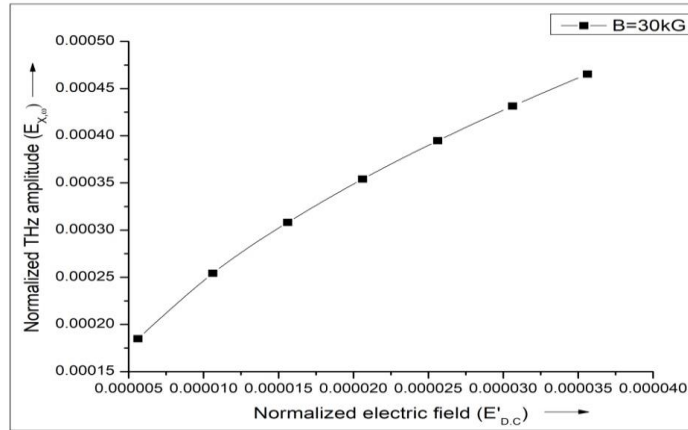
Figure 4.3.3 Plot of the normalized amplitude of THz radiation with the normalized electric field, at the magnetic field of 30kG.s

4.4. Proposed Model for THz Generation by propagating amplitude-modulated lasers through the anharmonic CNTs under the combined influence of D.C. electric and magnetic fields

This is the second theoretical model, in which we proposed a new alternative scheme for the efficient generation of THz radiations by using filamented beams interacting with an array of horizontally aligned anharmonic CNTs (embedded on the base of the dielectric surface) under the influence of externally applied static electric and magnetic fields. Two transversely amplitude-modulated filamented laser beams interact with this array of CNTs in the presence of static D.C. electric and magnetic fields acting mutually perpendicular to each other as well as to the direction of propagation of the laser beam. Due to the non-uniform density of electrons in CNTs, the restoration force on the different electrons is different and this results in anharmonicity. This anharmonicity broadens the resonance peak. The lasers also, exert space periodic ponderomotive force and beat frequency ponderomotive force on the electrons of CNTs. The space periodic ponderomotive force is well balanced by the pressure gradient force to form a transverse density ripple. Nonlinear coupling between D.C. drift velocity of electrons and electron density in the plasma of CNTs results in enhancement in the generation of THz radiation. We have found that the normalized THz amplitude increases significantly

with the increase of applied electric field from 10kV/cm to 30kV/cm and magnetic field from 11.5 kG to 24.5 kG. These optimized values of applied static electric and magnetic fields can easily be attained in any modern laboratory. The terahertz generation is one of the fast-developing areas for the last few decades with a variety of applications in Spectroscopy [21], medical Science [22] photovoltaic manufacturing [23], etc. Creating a Compact, reliable, proper, and efficient source of THz generation is one of the most formidable tasks of modern physics. For this purpose, metallic nano particles and carbon nanotubes are employed to produce THz radiations. The metallic or semiconductor CNTs provide both compactness and efficiency in THz sources [24]. Moreover, CNTs have electron plasma frequencies in the THz range and hence, appear to be a favorable medium for THz generation [25]. Several Schemes for the generation of efficient THz radiations have been proposed by various researchers. Some of which includes THz generation via laser coupling to anharmonic CNTs [26], optical rectification in CNTs to generate THz radiations [27], THz generation from macroscopic arrays of aligned SWCNTs excited by femtosecond optical pulses [28], THz generation through vertical aligned CNTs by using wiggler magnetic field [29]. Dragoman and Dragoman have achieved considerable gain at THz frequencies by using the Gunn effect in semiconductor array biased with D.C. electric field [30]. Welsh and Wyne [31] explained the incoherent rectification in the metallic nanostructure surfaces to generate highly efficient THz radiations with the help of surface plasma excitation. Portnoi et al. [32] have shown that CNTs under the influence of static electric fields can emit THz radiations. They also find that armchair CNTs can be used to form THz detectors and THz emitters. Batrakev et al. [33] have provided a review on THz generation and application of CNTs to the THz optoelectronics. Haurd et al. [15] observed enhancement in the normalized THz amplitude energy due to filamentation of a femtosecond laser pulse in the air in the presence of the static electric field, by using amplitude-modulated laser beams. Kumar et al. [34] also investigated the enhancement in the THz generation by using laser filaments in the presence of a static electric field in magnetized collision plasma. In this chapter, we develop an analytical formulism for the THz generation by the interaction of amplitude-modulated laser beams with the

rectangular array of HA-CNTs in the presence of D.C. electric and magnetic fields as CNTs can support both transverse magnetic and electric plasmon modes with in THz regime [35].

Consider a rectangular array of single-walled CNTs nested in dielectric surface (glass) as shown in Fig. 4.4.1. For this arrangement of CNTs, the microwave plasma-enhanced chemical vapor deposition (MPECVD) technique can be preferred over others [36, 37]. It is because, in CNT structure, wall number, inner radius, outer radius, length, thickness and alignment of CNTs can be easily controlled by the CVD technique [38, 39]. There are n_c CNTs per unit volume, and n_0 is the free electron density of each CNT. Each CNT is characterized by the radius b and length L in the array. As electrons are non-uniformly distributed in each CNT, therefore, the variation of n_0 with r is $n = n_0(1 - b_0\, r/b)$, where b_0 is known as the non-uniformity parameter. Each SWCNT is generally modeled as a hollow cylinder of nanometer thickness and micrometer length to determine the polarization and electrical conductivity [40]. As far as the response of SWCNTs is concerned to the transverse electric and magnetic fields, we assume these nanotubes as solid cylindrical tubes [41, 42]. The amplitude-modulated laser beams co-propagating along the z-axis, polarized along the y-axis, and amplitude modulated along the x-axis. The laser beams impinge on the rectangular array of anharmonic CNTs with the electric and magnetic profile.

$$\vec{E}_j = \hat{y} A_j \left[1 + \mu_j \cos \beta_0 x\right] e^{-i(\omega_j t - k_j z)}; \quad j = 1,2 \tag{4.4.1}$$

and

$$\vec{B}_j = \frac{c \vec{k}_j \times \vec{E}_j}{\omega_j}, \tag{4.4.2}$$

where, μ_j is the modulation depth of laser, β is the periodicity parameter and $k_j^2 = \omega_j^2/c^2\,(1 - \omega_P^2/\omega_j^2)$ represents the dispersion relation of beating lasers. The frequency difference of two laser beams $(\omega_1 - \omega_2)$ lies in the THz region of the spectrum.

The lasers exert ponderomotive force $\vec{F}_{P\omega}$ as well as static ponderomotive force $\vec{F}_{P\beta_0}$ on the electrons of CNTs. In the steady-state, static ponderomotive force is well balanced by pressure gradient force. It results in the formation of transverse density ripple at zero frequency. The beat frequency ponderomotive force is responsible for velocity and density perturbation in CNTs. The laser filaments are also responsible to provide oscillatory velocities to the plasma electrons present in CNTs arranged in the array.

$$\vec{v}_j = \frac{e\vec{E}_j}{m(i\omega_j - \upsilon)},$$

(4.4.3)

where, $-e$, m, and υ represent electronic charge, mass, and collision frequency respectively. The electron collision frequency of plasma electrons in CNTs is υ, which is lesser than ω. The static D.C. electric field $\vec{E}_{D.C.}$ is applied parallel to the x-axis and perpendicular to the applied magnetic field. This D.C. electric field imparts a D.C. drift to electrons of CNTs.

$$\vec{v}_{D.C} = \frac{-e\vec{E}_{D.C.}}{m\upsilon}.$$

(4.4.4)

The plasma electrons present in CNTs drift in the opposite direction of the applied D.C. electric field and get accumulated near the edge of the filament. It results in the complete screening of applied electric field in the plasma but at the same time, there occurs a transient process of redistribution of charges. It is due to instantaneous ionization in the plasma. Now electric current is directed along the direction of the external D.C. electric field and it exhibits oscillations at plasma frequency. These oscillations decay due to collisions between the electrons of plasma present in CNTs. The temporal electric current directed along the external D.C. electric field and perpendicular to the laser filament plays a significant role in the generation of THz wave.
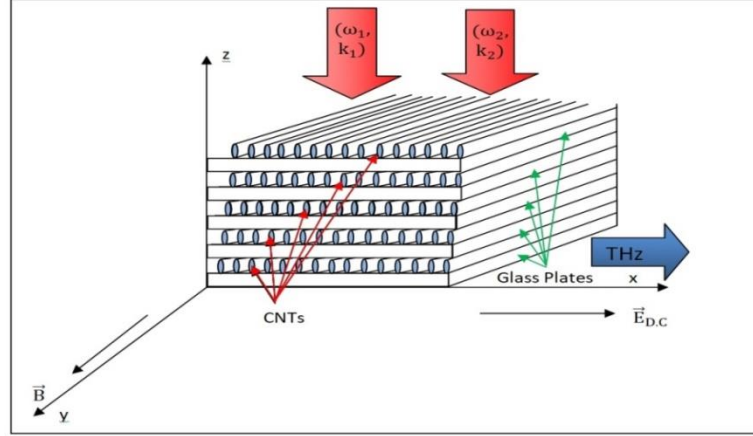
Figure 4.4.1 Schematic representation of THz generation from an array of HA-CNTs nested in the glass plates under the combined influence of magnetic and electric fields.

The amplitude modulated filamented lasers will also exert static ponderomotive force $\vec{F}_{P\beta} = -e\vec{\nabla}\varphi_{P\beta_0}$ and beat frequency ponderomotive force $\vec{F}_{P\omega} = -e\vec{\nabla}\varphi_{P\omega}$ on the electrons of CNTs.

Here, $\varphi_{P\beta_0} = \frac{e}{4m}\left[\frac{A_1^2\mu_1}{(i\omega_1-\upsilon)^2} + \frac{A_2^2\mu_2}{(i\omega_2+\upsilon)^2}\right]e^{i\beta_0 x}$ and $\varphi_{P\omega} = \frac{-eA_1A_2}{2m(i\omega_1-\upsilon)(i\omega_2+\upsilon)}\left[1 + \frac{(\mu_1+\mu_2)}{2}e^{i\beta_0 x}\right]$.

The static ponderomotive force causes ambipolar diffusion of plasma along the x-axis in CNTs. In the steady-state, the static ponderomotive force is balanced by the pressure gradient force. It results in the formation of transverse density ripple in the system.

$$n_{0,\beta_0} = n_0\left(1 - b_0\frac{r}{b}\right)e^{\frac{\varphi_{p\beta_0}}{T_e}} = n_0\left(1 - b_0\frac{r}{b}\right)\frac{e^2}{4mT_e}\left[\frac{A_1^2\mu_1}{(i\omega_1-\upsilon)^2} + \frac{A_2^2\mu_2}{(i\omega_2+\upsilon)^2}\right]e^{i\beta_0 x}, \tag{4.4.5}$$

where, T_e is the equilibrium electron temperature.

The incident amplitude modulated laser beams (co-propagating) interact with the CNTs, to displace electron cylinder from the ion cylinder. As a result, electron cylinder gets separated from the ion cylinder by $\vec{\Delta}$ as shown in Fig.2.6.1. The space charge field in the overlap region is not uniform. Hence, the restoration force on the different electrons is different which results in anharmonicity in the system. The electrons are distributed non-uniformly in CNTs with density profile, $n = n_0(1 - b_0\, r/b)$. The space charge field exerted by the ion cylinder of CNT is given as

69

$$\vec{E}_{ion} = \frac{e \int_0^r n_0 \left(1 - b_0 \frac{r}{b}\right) 2\pi r L \, dr}{2\pi r L \epsilon} \hat{r} \,, \tag{4.4.6}$$

$$= \frac{e \, n_0}{2\epsilon} \left(1 - \frac{2 b_0 r}{3b}\right) \vec{r}. \tag{4.4.7}$$

The space charge field exerted by the electron cylinder of CNT is given as

$$\vec{E}_{ele} = -\frac{e \, n_0}{2\epsilon} \left(1 - \frac{2 b_0}{3b} |\vec{r} - \vec{\Delta}|\right) \left(\vec{r} - \vec{\Delta}\right). \tag{4.4.8}$$

Now, the total space-charge field is calculated as the vector sum of the space charge field due to the electron and ion cylinders $\left(\vec{E}_{ele}, \vec{E}_{ion}\right)$ and is given as

$$\vec{E}_s = \vec{E}_{ion} + \vec{E}_{ele}. \tag{4.4.9}$$

By using Eq. (4.4.7), (4.4.8), and (4.4.9) total space-charge field is,

$$\vec{E}_s = \frac{e \, n_0}{2\epsilon} \left[\left(1 - \frac{2 b_0 r}{3b}\right) \vec{r} - \left(1 - \frac{2 b_0}{3b} |\vec{r} - \vec{\Delta}|\right) \left(\vec{r} - \vec{\Delta}\right)\right]. \tag{4.4.10}$$

As anharmonicity is along the x-axis, therefore x-component of the electric field is,

$$E_{sx} = \frac{e \, n_0}{2\epsilon} \left[\left(1 - \frac{2 b_0 r}{3b} - \frac{2 b_0 r}{3b} \cos^2 \theta\right) \Delta_x + \frac{2 b_0 \Delta^2}{3b} \cos \theta\right]. \tag{4.4.11}$$

The restoration force is different for different electrons with respect to the ion cylinder. We take the average over θ such that the average value of $\cos^2 \theta = 1/2$ and the average value of $\cos\theta = 0$.

$$F_{sx} = -\frac{m \, \omega_P^2}{2 \epsilon_r} \left(1 - \frac{b_0 r}{b}\right), \tag{4.4.12}$$

where, $\omega_P = (n_0 e^2 / m \epsilon_0)^2$, is known as the plasma frequency of CNTs.

The equation of motion executing the shift of the electrons of CNT, under the influence of the electric field of laser, applied magnetic field and space charge restoration force is given as

$$\frac{d^2 \vec{\Delta}}{dt^2} + \frac{\vec{F}_s}{m} + v \frac{d \vec{\Delta}}{dt} + \frac{e}{m} \vec{v} \times \vec{B} = -\frac{\vec{F}_{P\omega}}{m}. \tag{4.4.13}$$

Corresponding to the above equation (4.4.13), one can write the x and z components of the equation of motion as

$$\frac{d^2\Delta_x}{dt^2} + \frac{F_{sx}}{m} + \upsilon\frac{d\Delta_x}{dt} + \frac{e}{m}(-Bv_z) = -\frac{F_{P\omega x}}{m}, \tag{4.4.14}$$

$$\left[\omega^2\Delta_x - \frac{\omega_P^2}{2\epsilon_r}\left(1 - \frac{br}{b}\right) + i\upsilon\omega\Delta_x\right] - i\omega\omega_c\Delta_z = \frac{F_{P\omega x}}{m}, \tag{4.4.15}$$

and

$$\frac{d^2\Delta_z}{dt^2} + \upsilon\frac{d\Delta_z}{dt} + \frac{e}{m}(Bv_x) = 0, \tag{4.4.16}$$

$$\omega^2\Delta_z + i\upsilon\omega\Delta_z + i\omega\omega_c\Delta_x = 0, \tag{4.4.17}$$

where $\omega_c = eB/mc$ represents cyclotron frequency of plasma electrons in CNTs.

On simplifying the equations (4.4.16) and (4.4.17), one can easily obtain the x and z components for the displacement of CNT electrons

$$\Delta_z = \frac{-i\omega_c\Delta_x}{(\omega + i\upsilon)}, \tag{4.4.18}$$

$$\Delta_{x,\omega,k+\beta_0} = \frac{i(\beta_0 + k)(\mu_1 + \mu_2)e^2 A_1 A_2 e^{-i(\omega t - kz - \beta_0 x)}}{4m^2(i\omega_1 - \upsilon)(i\omega_2 + \upsilon)\left[\omega^2 - \frac{\omega_P^2}{2\epsilon_r}\left(1 - \frac{b_0 r}{b}\right) + i\upsilon\omega - \frac{\omega\omega_c^2}{(\omega + i\upsilon)}\right]}, \tag{4.4.19}$$

and

$$\Delta_{x,\omega,k} = \frac{ike^2 A_1 A_2 e^{-i(\omega t - kz)}}{2m^2(i\omega_1 - \upsilon)(i\omega_2 + \upsilon)\left[\omega^2 - \frac{\omega_P^2}{2\epsilon_r}\left(1 - \frac{b_0 r}{b}\right) + i\upsilon\omega - \frac{\omega\omega_c^2}{(\omega + i\upsilon)}\right]}. \tag{4.4.20}$$

The x-component of the displacement $\Delta_{x,\omega,k+\beta}$ and $\Delta_{x,\omega,k}$ has different values for different electrons, depending on their positions with respect to ion cylinder. In the electron cylinder (within a CNT) of radius r, thickness dr, and length L, the number of electrons is $2\pi n_0 r L dr$ and hence, the average value of $\Delta_{x,\omega,k+\beta_0}$ and $\Delta_{x,\omega,k}$ is given as

71

$$\langle \Delta_{x,\omega,k+\beta_0} \rangle = \frac{i(\beta_0+k)(\mu_1+\mu_2)e^2 A_1 A_2 e^{-i(\omega t-kz-\beta_0 x)}}{4m^2(i\omega_1-v)(i\omega_2+v)N} \int_0^R \frac{2\pi r L n_0\left(1-\frac{b_0 r}{b}\right)dr}{\left(\omega^2-\frac{\omega_p^2}{2\epsilon_r}\left(1-\frac{b_0 r}{b}\right)+iv\omega-\frac{\omega\omega_c^2}{(\omega+iv)}\right)}, \tag{4.4.21}$$

and

$$\langle \Delta_{x,\omega,k} \rangle = \frac{ike^2 A_1 A_2 e^{-i(\omega t-kz)}}{2m^2(i\omega_1-v)(i\omega_2+v)N} \int_0^R \frac{2\pi r L n_0\left(1-\frac{b_0 r}{b}\right)dr}{\left(\omega^2-\frac{\omega_p^2}{2\epsilon_r}\left(1-\frac{b_0 r}{b}\right)+iv\omega-\frac{\omega\omega_c^2}{(\omega+iv)}\right)}. \tag{4.4.22}$$

where $N = \int_0^b 2\pi r L n_0(1-b_0\, r/b)dr$.

We can write equations (4.4.21) and (4.4.22) as,

$$\langle \Delta_{x,\omega,k+\beta_0} \rangle = \frac{i(\beta_0+k)(\mu_1+\mu_2)e^2 A_1 A_2 e^{-i(\omega t-kz-\beta_0 x)}}{4m^2(i\omega_1-v)(i\omega_2+v)N} I_1 \text{ and } \langle \Delta_{x,\omega,k} \rangle = \frac{i\beta_0\mu e^2 A_1 A_2 e^{-i(\omega t-kz)}}{2m^2(i\omega_1-v)(i\omega_2+v)N} I_1,$$

where $I_1 = \int_0^b \frac{2\pi r L n_0\left(1-\frac{b_0 r}{b}\right)dr}{\left(\omega^2-\frac{\omega_p^2}{2\epsilon_r}\left(1-\frac{b_0 r}{b}\right)+iv\omega-\frac{\omega\omega_c^2}{(\omega+iv)}\right)}.$

Now average velocity of electrons of CNTs is given by

$$\langle v_{x,\omega,k+\beta_0} \rangle = \frac{\omega(\beta_0+k)(\mu_1+\mu_2)e^2 A_1 A_2 e^{-i(\omega t-kz-\beta_0 x)}}{4m^2(i\omega_1-v)(i\omega_2+v)N} I_1, \tag{4.4.23}$$

and

$$\langle v_{x,\omega,k} \rangle = \frac{\omega k e^2 A_1 A_2 e^{-i(\omega t-kz)}}{2m^2(i\omega_1-v)(i\omega_2+v)N} I_1. \tag{4.4.24}$$

Corresponding to these average velocities of electrons at $(\omega,\ k+\beta_0)$ and (ω, k), average density perturbations of the electrons of CNTs $\left(n_{\omega,k+\beta_0}\right)$ and $\left(n_{\omega,k}\right)$ can be determined with the help of the equation of continuity,

72

$$n_{\omega,k+\beta_0} = \frac{n_0(1-b_0r/b)(\beta_0^2+k^2)(\mu_1+\mu_2)e^2A_1A_2e^{-i(\omega t-kz-\beta_0 x)}}{4m^2(i\omega_1-\upsilon)(i\omega_2+\upsilon)N}I_1, \tag{4.4.25}$$

and

$$n_{\omega,k} = \frac{n_0(1-b_0r/b)k^2\mu e^2A_1A_2e^{-i(\omega t-kz)}}{2m^2(i\omega_1-\upsilon)(i\omega_2+\upsilon)N}I_1. \tag{4.4.26}$$

In our system of CNTs, the corresponding current density at ω, k arises due to coupling between the various nonlinear terms explained as (i) CNTs per unit volume (n_c) with corresponding nonlinear average velocity $\langle v_{x,\omega,k}\rangle$ of the electrons of CNTs (ii) The zero-frequency transverse density ripple n_{0,β_0}^* with corresponding nonlinear average velocity $\langle v_{x,\omega,k+\beta_0}\rangle$ of the electrons of CNTs and (iii) nonlinear density perturbation $n_{\omega,k}$ with D.C. electron drift velocity $\vec{v}_{D.C}$ of the electrons of CNTs

$$J_{x,\omega,k} = -n_cNe\langle v_{x,\omega,k}\rangle - n_{0,\beta_0}^*Ne\langle v_{x,\omega,k+\beta_0}\rangle n_c(\pi b^2L) - n_cNen_{\omega,k}v_{D.C}(\pi b^2L). \tag{4.4.27}$$

$$J_{x,\omega,k} = J_{x1} + J_{x2} + J_{x3}. \tag{4.4.28}$$

Where $J_{x1} = \frac{\omega k n_c e^3 A_1A_2e^{-i(\omega t-kz)}}{2m^2(i\omega-\upsilon)(i\omega+\upsilon)}I_1$, $J_{x2} = \frac{\omega(k+\beta_0)n_c e^5 A_1A_2 n_0^{02}(1-2b_0/3)\pi b^2 L}{8m^3T_e(i\omega-\upsilon)(i\omega+\upsilon)}\left[\frac{A_1^2\mu_1}{(i\omega-\upsilon)} + \frac{A_2^2\mu_2}{(i\omega+\upsilon)}\right]e^{-i(\omega t-kz)}I_1$ and

$$J_{x3} = \frac{-n_0n_c e^4(1-2b_0/3)\pi b^2 Lk^2 A_1A_2 E_{D.C.}}{2m^3(i\omega-\upsilon)(i\omega+\upsilon)\upsilon}e^{-i(\omega t-kz)}I_1.$$

Now, the net nonlinear current density present in the rectangular array of horizontally aligned anharmonic CNTs is given as

$$J_{x,\omega,k} = -\frac{\omega e^3 A_1A_2 n_c}{2m^2(i\omega-\upsilon)(i\omega+\upsilon)}\left[k + n_0(1-2b_0/3)(k+\beta_0)\frac{\pi b^2 Le^2}{16mT_e}\left[\frac{A_1^2\mu_1}{(i\omega-\upsilon)} + \frac{A_2^2\mu_2}{(i\omega+\upsilon)}\right] - \frac{n_0\pi b^2L(1-2b_0/3)k^2 eE_{D.C}}{m\upsilon\omega}\right]e^{-i(\omega t-kz)}I_1. \tag{4.4.29}$$

The standard THz wave propagation equation obtained by using Maxwell's equations can be described as

$$\nabla^2 E_{x,\omega,k} + k_\omega^2\, E_{x,\omega,k} = -\frac{-4\pi i\omega}{c^2} J_{x,\omega,k} \;. \tag{4.4.30}$$

We can write the above equation along the x-axis as

$$\frac{\partial^2 E_{x,\omega,k}}{\partial^2 z} + k_\omega^2 E_{x,\omega,k} = \frac{-i\omega}{c^2\epsilon_0} J_{x,\omega k}. \tag{4.4.31}$$

Simplifying the above equation (4.4.31), we get a terahertz electric field $E_{x,\omega,k}$ as

$$E_{x,\omega,k} = \frac{-i\omega^2 e^3 A_1 A_2 n_c}{2m^2\epsilon_0 c^2 [k_\omega^2 - k^2](i\omega - v)(i\omega + v)}\left[k + n_0(1 - 2b_0/3)\left(k + \beta_0\right)\frac{\pi b^2 Le^2}{16mT_e}\left[\frac{A_1^2\mu_1}{(i\omega_1 - v)} + \frac{A_2^2\mu_2}{(i\omega_2 + v)}\right] - \right.$$
$$\left.\frac{n_0\pi b^2 L(1 - 2b_0/3)k^2 eE_{D.C}}{mv\omega}\right]I_1. \tag{4.4.32}$$

By solving the integral term $I_1 = \displaystyle\int_0^b \frac{2\pi r Ln_0\left(1 - \frac{b_0 r}{b}\right)dr}{\left(\omega^2 - \frac{\omega_P^2}{2\epsilon_r}\left(1 - \frac{b_0 r}{b}\right) + iv\omega - \frac{\omega\omega_c^2}{(\omega + iv)}\right)}$, equation (4.4.32) can be

modified as

$$E_{x,\omega,k} = \frac{-2i\pi b^2 Ln_0^0\omega^2 e^3 A_1 A_2 n_c\epsilon_r}{m^2 b_0\epsilon_0 c^2\omega_P^2[k_\omega^2 - k^2](i\omega - v)(i\omega + v)}\left[k + n_0(1 - 2b_0/3)\left(k + \beta_0\right)\frac{\pi b^2 Le^2}{16mT_e}\left[\frac{A_1^2\mu_1}{(i\omega_1 - v)} + \frac{A_2^2\mu_2}{(i\omega_2 + v)}\right] - \right.$$
$$\left.\frac{n_0^0\pi b^2 L(1 - 2b_0/3)k^2 eE_{D.C}}{mv\omega}\right]\left[\left(1 - \right.\right.$$
$$\left.\left.\frac{b_0}{2}\right)\frac{(1 - \omega_P^2/2\epsilon_r\omega^2 + iv/\omega - \omega_c^2/\omega(\omega + iv))(1 - b_0\omega_P^2/2\epsilon_r\omega^2 + iv/\omega - \omega_c^2/\omega(\omega + iv))}{b_0(\omega_P^2/2\epsilon_r\omega^2)^2}\log\left|\frac{(1 - \omega_P^2/2\epsilon_r\omega^2 + iv/\omega - \omega_c^2/\omega(\omega + iv))}{(1 + (b_0 - 1)\omega_P^2/2\epsilon_r\omega^2 + iv/\omega - \omega_c^2/\omega(\omega + iv))}\right|\right].$$

$$\tag{4.4.33}$$

The normalized THz electric field equation is given as

$$\frac{eE_{x\omega,k}}{m\omega c} = -\frac{2i}{b_0}\left(\pi b^2 Ln_c\right)\epsilon_r\left[\frac{eA_1}{m\omega_1 c}\right]\left[\frac{eA_2}{m\omega_2 c}\right]\left[1 + \frac{iv}{\omega_1}\right]^{-1}\left[1 - \frac{iv}{\omega_2}\right]^{-1}\left[\frac{k_\omega^2}{k^2} - 1\right]^{-1}\left[1 + (\pi b^2 Ln_0)\left(1 - \right.\right.$$
$$\left.\frac{2b_0}{3}\right)\left\{\frac{1}{16}\left(\frac{c}{v_{th}}\right)^{-2}\left(\left(\frac{eA_1}{m\omega_1 c}\right)^2\left(1 + \frac{iv}{\omega_1}\right)^{-2}\mu_1 + \left(\frac{eA_2}{m\omega_2 c}\right)^2\left(1 - \frac{iv}{\omega_2}\right)^{-2}\mu_2\right)\left(1 + \frac{\beta_0}{k}\right) - \left(\frac{eE_{D.C}}{mvc}\right)\right\}\right]\left[\left(1 - \right.$$
$$\left.\left.\frac{b_0}{2}\right)\frac{(1 - \omega_P^2/2\epsilon_r\omega^2 + iv/\omega - \omega_c^2/\omega(\omega + iv))(1 - b\omega_P^2/2\epsilon_r\omega^2 + iv/\omega - \omega_c^2/\omega(\omega + iv))}{b_0(\omega_P^2/\epsilon_r 2\omega^2)^2}\log\left|\frac{(1 - \omega_P^2/2\epsilon_r\omega^2 + iv/\omega - \omega_c^2/\omega(\omega + iv))}{(1 + (b_0 - 1)\omega_P^2/2\epsilon_r\omega^2 + iv/\omega - \omega_c^2/\omega(\omega + iv))}\right|\right].$$

4.5 Graphical Analysis and Observations

We deal with numerical treatment and graphical analysis with the following set of parameters. In our calculations, we have used Nd: YAG lasers with frequencies $\omega_1 = 17.80 \times 10^{14}$ rad/s and $\omega_2 = 17.77 \times 10^{14}$ rad/s, corresponding wavelengths are; $\lambda_1 = 1.058\,\mu m$ and $\lambda_2 = 1.064\,\mu m$. The intensities of beating lasers are $I_1 \sim I_2 \sim 10^{14}$ W/cm^2. The values of $e\,A_1/m\omega_1 c$ and $e\,A_2/m\omega_2 c$ are of the order of 0.02 and 0.03 respectively. Each CNT in the rectangular array is 2μm long with a radius of 15 nm and inter-tube separation is 25nm. The value of relative permittivity of glass, in which CNTs are nested, is 2.5. The non-uniformity parameter b_0 has the values of 0.30, 0.20 and 0.15. The applied static magnetic field lies in the range 11.5 kG to 24.5 kG with applied static D.C. electric field 10 kV/cm to 30 kV/cm. Moreover, these fields are practically feasible and can be achieved in laboratories [40, 43-45].

In fig. 4.5.1, we have shown the variation of normalized THz amplitude with normalized frequency for the above-given parameters corresponding to a magnetic field strength of 11.5 kG to 24.5 kG. The resonant enhancement in normalized THz amplitude is observed when ω approaches towards the resonance; $\omega = \omega_P \sqrt{(1 - b_0)/2\,\epsilon_r + (\omega_c^2/\omega_p^2)}$. At this frequency, surface plasmon resonance occurs. The enhancement in the normalized THz amplitude is due to this plasmon resonance. At the resonance frequency, absorption of lasers by the electrons of CNTs in the array increases, and hence, nonlinearities increase, and hence, the normalized THz amplitude is enhanced. There is a sharp reduction in the normalized THz amplitude, as one moves away from the resonance point on both sides. Similar results have been shown by Jain *et al.* [46] where they have applied a magnetic field of 100 kG on an array of CNTs mounted on a metallic base. In our research work, we have obtained the better results by applying lesser values of the static magnetic field. Vij *et al.* [47] also showed that the THz generation efficiency enhances with the increase of the wiggler magnetic field. Also, according to Yao and Belyanin [48], high order increase of nonlinearities in SWNTs under the

effect of the magnetic field of few kG is observed which shows enhancement in the generation of THz radiation. This also supports our observations.

Fig. 4.5.2 shows the variation of normalized THz amplitude with normalized THz frequency at various values of non-uniformity parameter $b_0 = 0.30, 0.20,$ and 015. The normalized THz amplitude peaks at the surface plasmon resonance frequency. The width of the absorption peak increases with the non-uniformity parameter b_0. The tallness of each peak falls and shifts to a higher frequency side. This shift in the resonance point can be explained by the surface plasmon resonance condition, which depends upon 'b_0'. With the increase of non-uniformity in CNTs, anharmonicity increases which further enhances the
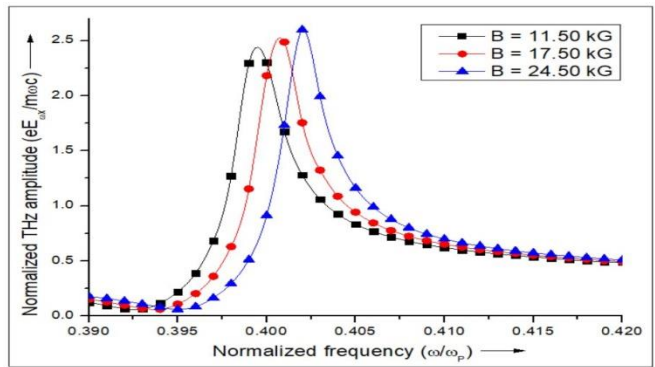
Figure 4.5.1 Variation of normalized THz amplitude with normalized THz frequency at different values of external magnetic field B = 11.5 kG, 17.5 kG, 24.5 kG for b_0 = 0.30, d = 25 nm, b = 15 nm and Static D.C. electric field of 10 kV/cm.
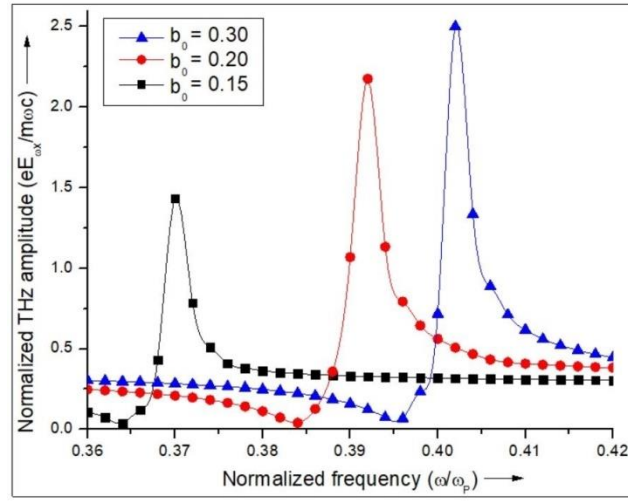
Figure 4.5.2 Variation of normalized THz amplitude with normalized frequency at different values of non-uniformity factor b_0 = 0.30, 0.20, and 0.15 at optimized value of external magnetic field. The other parameters are the same as given in figure 4.5.1.

normalized THz amplitude. Sharma and Vijay [26] have also shown that anharmonicity in CNTs broadens the surface Plasmon resonance peaks. In Fig. 4.5.3, we have plotted the variation of normalized THz amplitude with normalized THz frequency for various values of the radius of CNT, $b = 25$ nm, 30 nm, and 35 nm. The other parameters are kept the same as that of figure 4.5.1. From the curves of figure 4.5.3, it is clear that the normalized THz amplitude attains the peak value at a lower value of CNT radius 15nm. This is because the nonlinearity of the array of CNTs behaving as plasma increases. A similar observation was made by Kumar *et al.* [49]. They found that deccrease in the radius of CNT leads to enhancement of normalized THz amplitude. It is also observed that there is no change in the plasmon resonance point for all three curves.
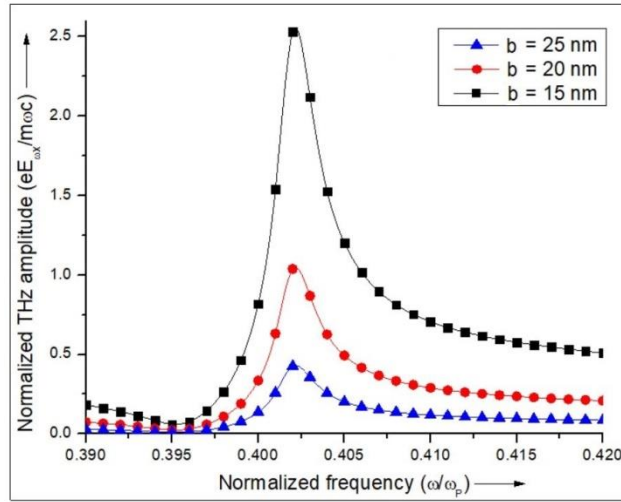
Fig. 4.5.3 Variation of normalized THz amplitude with normalized THz frequency for different values of CNTs radii b = 25 nm, 20 nm, 15 nm at b_0 = 0.30 and optimized value of the external magnetic field. The other parameters are the same as given in figure 4.5.1.
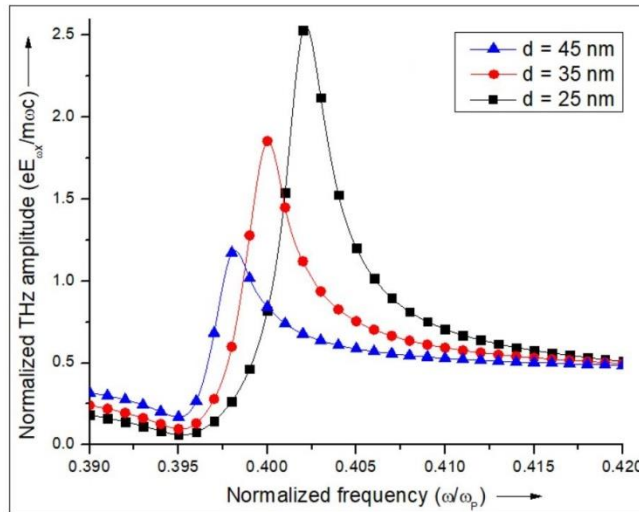
Figure 4.5.4 Variation of normalized THz amplitude with normalized THz frequency at different values of inter-tube separation d = 45 nm, 35 nm, 25 nm for b_0 = 0.30 at the optimized value of the magnetic field. The other parameters are the same as that of figure 4.5.1.

The reason behind this is that the plasmon resonance condition is independent of the radii of CNTs. Vij *et.al* [47] have shown direct dependence of THz power on CNTs radius, under the effect of external magnetic field 200 kG.

In figure 4.5.4, we have shown the variation of normalized THz amplitude with normalized frequency at different values of inter-tube separation between the CNTs $d = 45\,nm, 35\,nm, 25\,nm$. The values of other parameters are kept same as that of figure 4.5.1. It is observed that the normalized THz amplitude increases with the decrease of the inter-tube separation (decreases with the increase of inter-tube separation) and the surface plasmon resonance point shifts towards a higher value of the normalized frequency because more absorption of lasers by the CNTs occurs due to the increase of nonlinearity in CNTs. In figure 4.5.6, we have shown the variation of normalized THz amplitude with normalized THz frequency at various values of static electric field $E = 10\,kV/cm, 20\,kV/cm,$ and $30\,kV/cm$. From the graph, it is observed that normalized THz amplitude increases with the static D.C. electric field. This is because of the increase in
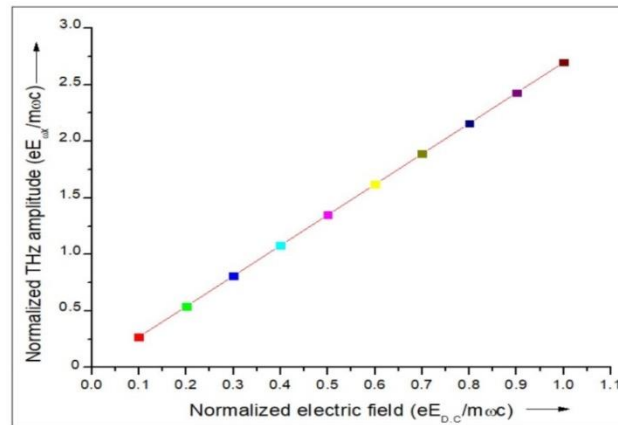
Figure 4.5.5 Variation of normalized THz amplitude with normalized THz frequency at different values of static D.C electric field for $b_0 = 0.30$ at the optimized value of the magnetic field. The other parameters are the same as that in figure 4.5.1.

anharmonicity due to an increase in the mobility of electrons in CNTs. Dragoman *et al.* [50] have shown that the mobility of electrons in CNTs could even attain the value of $1.2 \times 10^9\,cm^2V^{-1}s^{-1}$ at a moderate static electric field of $10\,kV/cm$. Kibis *et al.* [51] have demonstrated that under the applied voltage of 0.16 V, all the SWCNTs will emit THz radiation in a similar fashion. The SWCNTs can be used to create such a THz source, whose frequency is well controlled by the applied voltage. In our case, it can be controlled by a

static D.C. electric field. In figure 4.5.6, we plot normalized THz amplitude as a function of normalized D.C. electric field at the surface plasmon resonance frequency. It shows the increase in normalized THz amplitude with the normalized D.C. electric field and vice versa. This explains the graph shown in figure 4.5.5., is an accurate description of the effect of static D.C. electric field on the normalized THz amplitude
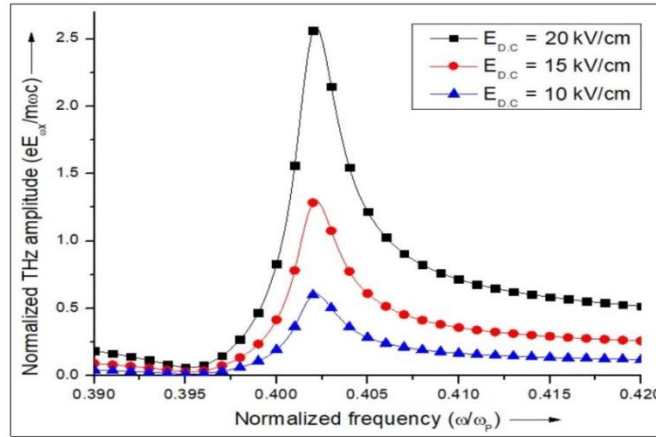
Figure 4.5.6 Variation of normalized THz amplitude with normalized THz frequency at different values of static D.C electric field for $b_0 = 0.30$ at the optimized value of the magnetic field. The other parameters are the same as that of figure 4.5.6.

4.6 Conclusion

In this chapter, we have studied the numerical and graphical analysis of two theoretical models for the efficient THz generation. In the first model, we deal with THz generation by the interaction of filamented laser beams in the collisional plasma under the influence of externally applied static electric and magnetic fields. In the second model, THz radiations are generated by the propagation of filamented laser beams through the array of anharmonic HA-CNTs under the influence of external electric and magnetic fields. The externally applied both static electric and magnetic fields have their own importance and significance in the enhancement of normalized amplitude of emitted THz radiation. The interaction of amplitude-modulated laser beams with the rectangular array of anharmonic CNTs nested in silica glass, under the effect of external static magnetic and electric fields, offers a viable scheme for the

efficient THz generation. The non-uniformity in the density distribution inside the array of CNTs significantly broadens the resonance curve. The height of the resonance peak decreases with the nonuniformity parameter and the width increases. Further, it results in anharmonicity in the response of CNTs. It broadens the resonance peak significantly. The generated THz radiation shows enhancement at surface plasmon resonance. The laser breakdown of the glass dielectric surface is a limiting mechanism for the proposed theory. The Threshold intensity for the dielectric breakdown of the glass surface with Nd: YAG laser is $7 \times 10^{14}\,\text{W/cm}^2$, hence, this theory is applicable for intensity $\leq 7 \times 10^{14}\,\text{W/cm}^2$. By exploiting this condition of resonance $\omega = \omega_P \sqrt{(1 - b_0)/2\epsilon_r + (\omega_c^2/\omega_p^2)}$ for values of non-uniformity parameter and magnetic field, one can enhance the normalized THz amplitude. In our analysis, we have also analyzed the variation of THz amplitude with the inter-tube separation of CNTs, radii of CNTs, density of CNTs, and static D.C. electric field. Thus, our results show that CNTs can be very helpful in providing highly efficient and compact sources of THz generation.

References:-

[1]   B.B. Hu and M.C. Nuss, "Imaging with terahertz waves," Opt. Lett. **20**(16), 1716 (1995).

[2]   C. Baker et al., "Detection of concealed explosives at a distance using terahertz technology," Proceedings of the IEEE **95**(8), 1559-1565 (2007).

[3]   K. Ishigaki et al., "Direct intensity modulation and wireless data transmission characteristics of terahertz-oscillating resonant tunnelling diodes," Electron. Lett. **8**(10), 582 (2012).

[4]   A.R. Orlando and G.P. Gallerano, "Terahertz radiation effects and biological applications," Int. J. Infrared Millimeter Waves **30**(1)**,** 1308-1318 (2009).

[5]   P.H. Siegel, "Terahertz technology," IEEE Trans. Micro. W. Theory Tech **50**(3), 910-928 (2002).

[6]   D. Dragoman and M. Dragoman, "Terahertz fields and applications," Prog. Quantum Electron. **28**(1), 1-66 (2004).

[7]   F. Sizov, "THz radiation sensors," Opt. Electron. Rev. **18**(1), 10-36 (2010).

[8]   R.K. Singh, S. Kumar and R.P. Sharma, "Generation of electromagnetic waves in the terahertz frequency range by optical rectification of a Gaussian laser pulse in a plasma in presence of an externally applied static electric field," Contrib. Plasma Phys. **57**(6), 252-257 (2017).

[9]   V. Thakur, N. Kant and S. Vij, "Effect of cross-focusing of two laser beams on THz radiation in graphite nanoparticles with density ripple," Phys Scr. **95**(4), 045602 (2020).

[10]   M. Kumar and V.K. Tripathi, "Resonant terahertz generation by optical mixing of two laser pulses in rippled density plasma," IEEE J Quantum Elect. **48**(8), 1031-1035 (2012).

[11]   A.B. Langdon and B.F. Lasinski, "Filamentation and subsequent decay of Laser light in plasmas," Phys. Rev. Lett. **34**(15), 934 (1975).

[12]   T.J. Wang et al., "Remote generation of high-energy terahertz pulses from two-color femtosecond laser filamentation in air," Phys. Rev. A **83**(5), 053801 (2011).

[13]   P. Varshney et al., "Effects of transverse static electric field on terahertz radiation generation by beating of two transversely modulated Gaussian laser beams in a plasma," Laser Part. Beams. **32**(3), 375-381 (2014).

[14]   A. Braun et al., "Self-channeling of high-peak-power femtosecond laser pulses in air," Opt. Lett. **20**(1), 73-75 (1995).

[15]   A. Houard et al., "Strong Enhancement of terahertz radiation from laser filaments in air by a static electric field," Phys. Rev. Lett. **100**(25), 255006 (2008).

[16]   T. Löffler, F. Jacob and H.G. Roskos, "Generation of terahertz pulses by photoionization of electrically biased air," Appl. Phys. Lett. **77**(3), 453 (2000).

[17]   L. Bhasin and V.K. Tripathi, "Terahertz generation from laser filaments in the presence of a static electric field in a plasma," Phys. Plasmas **18**(12), 123106 (2011).

[18]   R. McLaughlin et al., "Enhanced coherent terahertz emission from indium arsenide in the presence of a magnetic field," Appl. Phys. Lett. **76**(15), 2038 (2000).

[19]   L. Yu-Tong, W. Wei-Min, L. Chun and S. Zheng-Ming, "High power terahertz pulses generated in intense laser-plasma interactions," Chin. Phys. B **21**(9), 095203 (2012).

[20]   A. Mehta, J. Rajput and N. Kant, "Effect of frequency-chirped laser pulses on terahertz radiation generation in magnetized plasma," Laser Phys. **29**(9), 095405 (2019).

[21]   M.V. Exter, C. Fattinger and D. Grischkowsky, "Terahertz time-domain spectroscopy of water vapor," Opt. Lett. **14**(20), 1128-1130 (1989).

[22]   H.B. Liu, Y. Chen, G.J. Bastiaans and X.C. Zhang, "Detection and identification of explosive RDX by THz diffuse reflection spectroscopy," Opt. Express **14**(1), 415-423 (2006).

[23]   Y.C. Shen et al., "Detection and identification of explosives using terahertz pulsed spectroscopic imaging," Appl. Phys. Lett. **86**(24), 241116 (2005).

[24]   Q. Zhang et al., "Plasmonic nature of the terahertz conductivity peak in single-wall carbon nanotubes," Nano Lett. **13**(12), 5991-5996 (2013).

[25]   P. Avouris, M. Freitag and V. Perebeinos, "Carbon-nanotubes photonics and optoelectronics," Nat. Photonics **2**(1), 341-350 (2008).

[26]   S. Sharma and A. Vijay, "Terahertz generation via laser coupling to anharmonic carbon nanotube array," Phys Plasmas **25**(2), 023114 (2018).

[27]   J. Parashar and H. Sharma, "Optical rectification in a carbon nanotube array and terahertz radiation generation," Physica E. **44**(10), 2069-2071 (2012).

[28]   L.V. Titova et al., "Generation of terahertz radiation by optical excitation of aligned carbon nanotubes," Nano Lett. **15**(5), 3267-3272 (2015).

[29]   S. Vij, N. Kant and V. Thakur, "Cross-focusing of a quadruple Gaussian laser beam in plasma in the relativistic regime," Laser Phys. **29**(9), 095404 (2019).

[30] D. Dragoman and M. Dragoman, **"**Terahertz continuous wave amplification in semiconductor carbon nanotubes," Physica E: Low dimens. Syst. Nanostruct. **25**(4), 492-496 (2005).

[31] G.H. Welsh and K. Wynne, "Generation of ultrafast terahertz radiation pulses on metallic nanostructured surfaces," Opt. Express **17**(4), 2470-2480 (2009).

[32] M.E. Portnoi, O.V. Kibis and M.R. da Costa, "Terahertz applications of carbon nanotubes," Superlattices Microstruct. **43**(5), 399-407 (2008).

[33] K.G. Batrakov et al., "Terahertz processes in carbon nanotubes," J. of Nanophotonics **4**(1), 041665 (2010).

[34] S. Kumar, S. Vij, N. Kant, A. Mehta and V. Thakur, "Resonant terahertz generation from laser filaments in the presence of static electric field in a magnetized collisional plasma," Euro. Phys. J. Plus **136**(1), 148 (2021).

[35] S.A. Mikhailov and K. Ziegler, "New electromagnetic mode in graphene," Phys. Rev. Lett. **99**(1), 016803 (2007).

[36] S. Chang, T. Lin and C. Bai, "Low-temperature process in growing carbon nanotube," Microelectronics J. **38**(6), 657-662 (2007).

[37] Z.F. Ren et al., "Synthesis of large arrays of well-aligned carbon nanotubes on glass," Science **282**(5391), 1105 (1998).

[38] H. Dai, "Carbon nanotubes: opportunities and challenges," Surf. Sci. **500**(1), 218–241 (2002).

[39] E. Munozet et al., "Single-walled carbon nanotubes produced by CW CO2-laser ablation: study of parameters important for their formation," Appl. Phys. A **70**(1), 145-151 (2000).

[40] S. Reich, C. Thomson and J. Maultzsch, "Carbon nanotubes: Basic Concepts and physical properties," Wiley VCH 67-98 (2004).

[41] W. Lu, D. Wang and L. Chen, "Near-static dielectric polarization of individual carbon nanotubes," Nano Lett. **7**(9), 2729 (2007).

[42] C.S. Liu and V.K. Tripathi, "Observational consequences of parametrically driven vibrations of carbon nanotubes," Phys. Rev. B **70**(11), 115414 (2004).

[43] H. Ajiki and T.J. Ando, "Electronic states of carbon nanotubes," Phys. Soc. Jpn. **62**(4), 1255–1266 (1993).

[44] J. Kono and S. Roche, "Magnetic properties carbon nanotubes: Properties and applications," ed O'Connell M J (Boca Raton: CRC Press, Taylor & Francis Group) **5**, 119–151 (2006).

[45] J. Kono, R.J. Nicholas and S. Roche, "High magnetic field phenomena in carbon nanotubes Carbon Nanotubes: Advanced Topics in the Synthesis, Structure, Properties and Applications," Ed. Jorio A, Dresselhaus G and Dresselhaus M S (Berlin: Springer) 393–421 (2008).

[46] S. Jain, J. Parashar and R. Kurchania, "Effect of magnetic field on terahertz generation via laser interaction with a carbon nanotube array," Int. Nano Lett. **3**(1), 5326 (2013).

[47] S. Vij, N. Kant and V. Thakur V, "Resonant enhancement of THz radiation through vertically aligned carbon nanotubes array by applying wiggler magnetic field," Plasmonics. **14**(1), 1051–1056 (2019).

[48] X. Yao and A. Belyanin, "Giant optical nonlinearity of graphene in a strong magnetic field," Phys. Rev. Lett. **108**(25), 255503 (2012)

[49] A. Kumar and P. Kumar, "Electron beam induced THz emissions from nanotube array," Phys. Plasmas **23**(10), 103302 (2016).

[50] M. Dragoman, "Experimental determination of microwave attenuation and electrical permittivity of double-walled carbon," Appl. Phys. Lett. **88**(15), 153108 (2006).

[51] O.V. Kibis, M. Rosenau da Costa and M.E. Portnoi, "Generation of terahertz radiation by hot electrons in carbon nanotubes," Nano Lett. **7**(11), 3414-3417 (2007).

Chapter 5

Resonant THz generation by cross-focusing of Gaussian beams in the array of vertically aligned anharmonic and magnetized CNTs.

5.1. Introduction

In the contemporary technical world, terahertz technology has explored many new research opportunities in various potential fields like imaging [1, 2], medicine [3] biological chemical sensing [4], communication [5], and explosive detection [6]. The numerous schemes for THz generation have been introduced by the researchers to provide packed, compact, highly efficient, and reliable THz sources. To attain this, they have used different mechanisms, techniques, and theories. Some of these are; by applying external static and wiggler magnetic fields on the array of CNTs [7, 8], by nonlinear mixing of lasers [9], by using filamentation under the influence of external magnetic and electric fields applied at the right angle to each other [10], by using laser coupling to anharmonic CNTs array [11] and by using a thin semiconductor slab under the influence of the external magnetic field [12]. The CNTs have extraordinary thermal and electrical conductivity with the advantage of compact size, which makes these nanotubes effective and reliable THz sources. Titova *et al.* [13] have shown the THz generation by using single-walled carbon nanotubes (SWCNTs) with femtosecond lasers. Ahmad *et al.* [14] generated THz radiation from multi-ion plasmas by using two-color laser self-focusing. The study of the cross-focusing in collisional plasma in the presence of a static external electric field has a significant impact on the THz generation [15]. The intense laser beams can undergo cross-focusing in the plasma by the various nonlinear interaction mechanisms. Akhmanov *et al.* [16] and Sodha *et al.* [17] have provided the theoretical models to study the self-focusing of intense laser beams in the plasma by applying an external magnetic field and without applying the magnetic field. Sharma [18] has studied the self-focusing and filamentation of the laser beam in plasma under the effect of the external static magnetic field. The effect of external magnetic field on the cross focusing of two co-

propagating Gaussian laser beams in plasma has been studied and it was observed that the focusing of one beam affects the other and vice versa [19-22].

In this chapter, we have proposed a theoretical model for THz generation by irradiating two cross-focused and co-propagating Gaussian laser beams on vertically aligned hollow anharmonic CNTs in the presence of an external static magnetic field (shown in Fig.5.5.1). The array of CNTs is embedded on the glass dielectric surface, having a refractive index of 2.5. This array is synthesized by using the plasma-enhanced chemical vapor deposition (PECVD) method. The CNTs are coated with non-conductive polymer to suppress the mutual interactions of CNTs and to enhance the THz generation. The mutual interactions between laser beams, THz radiations, and CNTs in the form of plasma can decrease the efficiency of output THz radiations. Therefore THz efficiency has been calculated by using optimized CNT and Gaussian laser beam parameters including the mutual effects. Each CNT is characterized by inner radius a, outer radius b, length L, and free-electron density n_0 corresponding to the plasma frequency $\omega_P = (n_0 e^2/m\varepsilon_0)^{1/2}$, where e and m represent electronic charge and rest mass respectively. In the array, there are n_c number of CNTs per unit area given by $n_c = 1/d^2$, where d is the inter-tube distance. A single-walled CNT is used as a hollow cylinder in most of the experimental works [23] but as far as the response of this CNT towards the electric and magnetic fields of laser is concerned, it behaves like a solid cylindrical tube [24]. The static magnetic field is applied mutually perpendicular to the direction of co-propagation and polarization of laser beams. The ponderomotive force acts on the electrons of CNTs to produce nonlinearity and the plasma of CNTs gets rearranged along the direction of the applied static magnetic field. This nonlinearity carries the main responsibility to produce the cross-focusing of laser beams in the magnetized collisional plasma.

5.2. Proposed Model for THz generation by cross-focusing of Gaussian beams in the array of vertically aligned anharmonic and magnetized CNTs.

In the proposed scheme, we consider two Gaussian laser beams with slightly different frequencies (ω_1, ω_2) and wavenumbers (k_1, k_2), polarized along x-direction and co-propagating along z-direction. The static magnetic field B is applied along the y-direction that

is mutually perpendicular to the direction of propagation of lasers and the axis of CNTs. The electric field profiles of laser beams are provided as

$$\vec{E}_j = \hat{x} E_{jx0} e^{-i(k_j z - \omega_j t)}; \quad j = 1, 2. \tag{5.2.1}$$

where, E_{jx0} represent the amplitude of the electric fields of the laser beams. $k_j = \omega_j \sqrt{\epsilon_j}/c$ is the wavenumber of each beam, ϵ_j is the dielectric function of plasma and c is the speed of light in free space. $\hat{x}$ is the unit vector along the x-axis. j represents the running index of the Gaussian laser beam. One can easily describe the propagation of Gaussian laser beam in the CNTs (in the form of plasma) by the dielectric function given as $\epsilon_j = \epsilon - (\omega_p/\omega_j)^2$, here ϵ is known as the relative permittivity of the lattice. The oscillatory velocities induced by the Gaussian laser beams in the electrons of CNTs can be written as

$$v_{jx} = \frac{e\left[i(\omega_j + iv)E_{jx} - \omega_c E_{jz}\right]}{m\left[(\omega_j + iv)^2 - \omega_c^2\right]} \quad \text{and} \quad v_{jz} = \frac{e\left[i(\omega_j + iv)E_{jz} + \omega_c E_{jx}\right]}{m\left[(\omega_j + iv)^2 - \omega_c^2\right]},$$

where, $\omega_c = eB/m$ and v represent the cyclotron frequency and collision frequency respectively. The collision frequency v of electrons is lesser than ω_j and ω_c. $\vec{E}_{jx}$ and $\vec{E}_{jz}$ are the electric field components of laser beams along the x-axis and z-axis.

The electric permittivity shows anisotropic behavior under the dominion of static magnetic field and hence, acts as an anisotropic tensor. It can be represented by the following equation

$$\epsilon_j = \begin{vmatrix} \epsilon_{jxx} & \epsilon_{jxy} & \epsilon_{jxz} \\ \epsilon_{jyx} & \epsilon_{jyy} & \epsilon_{jyz} \\ \epsilon_{jzx} & \epsilon_{jzy} & \epsilon_{jzz} \end{vmatrix}. \tag{5.2.2}$$

The various components of this anisotropic tensor are as:

$\epsilon_{jzy} = \epsilon_{jyz} = \epsilon_{jxy} = \epsilon_{jyy} = \epsilon_{jyx} = 0$, $\epsilon_{jxx} = \epsilon_{jzz} = 1 - \omega_P^2(\omega_j + iv)/\omega_j\left[(\omega_j + iv)^2 - \omega_c^2\right]$ and $\epsilon_{jxz} = -\epsilon_{jzx} = -i\omega_c\omega_P^2/\omega_j\left[(\omega_j + iv)^2 - \omega_c^2\right]$.

Both the Gaussian lasers exert static ponderomotive force as well as beat frequency ponderomotive force on the electrons of CNTs. The beat frequency ponderomotive force carries the responsibility to generate THz radiation. The static ponderomotive force acting on the electrons of CNTs along the direction of the static magnetic field (y-direction) can be written as

$$F_{Py} = \sum_{j=1,2} \frac{-e^2}{4m\left[(\omega_j+i\nu)^2-\omega_c^2\right]} \frac{\partial}{\partial y}\left(E_{jx}E_{jx}^* + E_{jz}E_{jz}^* + \frac{i\omega_c}{\omega_j}\left(E_{jx}E_{jz}^* - E_{jz}E_{jx}^*\right)\right). \tag{5.2.3}$$

To obtain the equilibrium in the system, the pressure gradient force and static ponderomotive force cancels out each other's effect. Hence, there occurs change in the electron density of the plasma present in the form of CNTs. This change in the electron density is given by the relation $n = n_0 e^{-\sum_{j=1,2} q_j E_{jx}E_{jx}^*}$. The term q_j can be obtained by using the relation $E_{jz} = -\left(\epsilon_{jxz}/\epsilon_{jzz}\right)E_{jx}$ for extraordinary mode and can be written as:

$$q_j = \frac{e^2}{4mK_B(T_e+T_i)\left[(\omega_j+i\nu)^2-\omega_c^2\right]}\left[1+\left(\frac{\omega_c}{\omega_j}\right)^2 \frac{\omega_P^4+2\omega_P^2\left[(\omega_j+i\nu)^2-\omega_c^2-\omega_P^2(1+i\nu/\omega_j)\right]}{\left[(\omega_j+i\nu)^2-\omega_c^2-\omega_P^2(1+i\nu/\omega_j)\right]^2}\right], \tag{5.2.4}$$

where, T_e and T_i are the equilibrium electronic and ionic temperatures respectively. K_B is known as the Boltzmann constant. By using Ampere's and Faraday's law for non-absorbing and non-conducting medium, the wave propagation equation in magnetized collisional plasma can be written as

$$\nabla^2\vec{E}_j - \nabla\left(\nabla\vec{E}_j\right) + \frac{\omega_j^2}{c^2}\left(\epsilon_j\vec{E}_j\right) = 0. \tag{5.2.5}$$

One can make expansion in the dielectric tensor ε_j with in the PRA regime and this expansion is given as $\epsilon_j = \epsilon_{0j} - \epsilon_{2j}x^2$, where ϵ_{0j} and ϵ_{2j} represent the linear and nonlinear parts of the dielectric function. By considering the x-component of equation (5) one can write

$$\frac{\partial^2 E_{jx}}{\partial z^2} + 2\delta_j \frac{\partial^2 E_{jx}}{\partial x^2} + \frac{\epsilon_{jxz0}}{\epsilon_{jzz0}} \frac{\partial^2 E_{jx}}{\partial x\,\partial z} + \frac{\omega_j^2}{c^2}\left(\epsilon_{0j} - \epsilon_{2j}x^2\right)E_{jx} = 0, \tag{5.2.6}$$

where, $\epsilon_{jxx0} = \epsilon_{jzz0} = 1 - \omega_P^2(\omega_j + iv)/\omega_j\left[\left(\omega_j + iv\right)^2 - \omega_c^2\right]$, $\qquad \epsilon_{jxz0} = -\epsilon_{jzx0} =$

$-i\omega_c\omega_P^2/\omega_j\left[\left(\omega_j + iv\right)^2 - \omega_c^2\right]$, $\quad \epsilon_{jzz0} \mp \epsilon_{jxz0} = \epsilon_{j0\pm}$, and $\quad \epsilon_{0+}\epsilon_{0-}/(\epsilon_{0+} + \epsilon_{0-})^2 = \delta_j.$ In these

relations, $+$ and $-$ signs used in the subscripts have their significance. The $+$ sign in the subscript represents the extraordinary mode of the laser beams whereas, $-$ sign in the subscript represents ordinary mode of laser beams. By assuming the solution of equation (5.2.6) as $E_{jx} = A_j(x, z)e^{-ik_jz}$ and neglecting the term $\partial^2 A_{jz}/\partial z^2$ (as A_j varies slowly) one can reduce the wave propagation equation as

$$2ik_j \frac{\partial A_j}{\partial z} = 2\delta_j \frac{\partial^2 A_j}{\partial x^2} - \frac{\omega_j^2}{c^2}\epsilon_{2j}x^2 A_j. \tag{5.2.7}$$

One can solve the above equation (5.2.7) by using the Akhmanov *et al.* [16] approach as extended by Sodha *et al.* [17] and expressing the complex amplitude $A_j(x, z)$ as $A_j(x, z) = A_j e^{-ik_j S_j(x,z)}$. Where $A_j(x, z)$ and $S_j(x, z)$ are the real function of space. By replacing the expression for A_j in equation (5.2.7) and separating the real and imaginary parts, one can write

$$2\left(\frac{\partial S_j}{\partial z}\right) + 2\delta_j\left(\frac{\partial S_j}{\partial x}\right)^2 = \frac{S_j}{k_j^2 A_{j0}} \frac{\partial^2 A_{j0}}{\partial x^2} - \frac{\omega_j^2 \epsilon_{2j}}{k_j^2 c^2}. \tag{5.2.8}$$

$$\frac{\partial A_{j0}^2}{\partial z} + 2\delta_j\left(\frac{\partial S_j}{\partial x}\right)\left(\frac{\partial A_{j0}^2}{\partial x}\right) + \frac{\partial^2 S_j}{\partial x^2} A_{j0}^2 = 0, \tag{5.2.9}$$

By using Gaussian ansatz for A_{j0}^2, one can write the intensity profile of Gaussian laser beams as

$$A_{j0}^2 = \frac{E_{jx00}^2}{f_j} e^{-\left(x^2/r_{j0}^2 f_j^2\right)}, \tag{5.2.10}$$

where, f_j is known as the normalized dimensionless beam width parameter as a function of the distance of propagation z in the paraxial regime. It is used to determine the beam width profile

90

and spot size of laser beams when propagating through the plasma of CNTs. The term r_{j0} represents the radii of Gaussian laser beams. The electric field amplitude is represented as E_{jx00}^2 and the amplitude of eikonal S_j (in paraxial ray approximation) is given as $S_j = (x^2/2)\beta_j(z) + \phi_j(z)$, where $\phi_j(z)$ is the phase factor and $\beta_j(z)$ is known as the wavefront of the laser beam. The value of $\beta_j(z)$ is represented by the relations $\beta_j(z) = (1/2\delta_j\, f_j)\,\partial f_j/\partial z$. One can obtain the following equation for the dimensionless beam width parameter f_j by substituting the values of A_{j0}^2 and S_j in equation (5.2.9).

$$\frac{d^2 f_j}{d\zeta^2} = 4\delta_j^2 \frac{1}{f_j^3} - k_j^2 r_{j0}^4 f_j \epsilon_{2j}, \tag{5.2.11}$$

where, $\zeta = z/k_j\, r_{j0}^2$ is known as normalized distance. Equation (5.2.11) represents the convergence or divergence character of laser beams in the collisional plasma of CNTs when the magnetic field is applied along the y-direction. The values of ϵ_{0j} and ϵ_{2j} can be obtained by using the relation $\epsilon_j = \epsilon_{0j} - \epsilon_{2j}x^2$.

$$\epsilon_{0j} = 2\delta_j\left(\epsilon_{j0+} + \epsilon_{j0-}\right) + 2\left(\frac{\epsilon_{j0+}}{\epsilon_{j0+}+\epsilon_{j0-}}\right)^2 \left(\frac{\omega_P^2}{\omega_j\left((\omega_j+i\nu)+\omega_c\right)}\right)\left(1 + \frac{((\omega_j+i\nu)+\omega_c)\varepsilon_{j0-}^2}{((\omega_j+i\nu)-\omega_c)\varepsilon_{j0+}^2}\right)\left(1 - e^{-q_1 E_{1x00}^2/f_1 - q_2 E_{2x00}^2/f_2}\right). \tag{5.2.12}$$

$$\epsilon_{2j} = 2\left(\frac{\epsilon_{j0+}}{\epsilon_{j0+}+\epsilon_{j0-}}\right)^2 \left(\frac{\omega_P^2}{\omega_j\left((\omega_j+i\nu)+\omega_c\right)}\right)\left(1 + \frac{((\omega_j+i\nu)+\omega_c)\varepsilon_{j0-}^2}{((\omega_j+i\nu)-\omega_c)\varepsilon_{j0+}^2}\right)\left(\frac{q_1 E_{1x00}^2}{r_{10}^2 f_1^3} + \frac{q_2 E_{2x00}^2}{r_{20}^2 f_2^3}\right)e^{-q_1 E_{1x00}^2/f_1 - q_2 E_{2x00}^2/f_2}. \tag{5.2.13}$$

The electrons of CNTs in the presence of static magnetic field experience a non-linear ponderomotive force at beat frequency $\omega = \omega_1 - \omega_2$ and corresponding wave number $k = k_1 - k_2$. One can calculate the ponderomotive force at this beat wave frequency and it is given as

$$\vec{F}_{PM} = -\frac{e^2 \nabla\left(\vec{E}_1\vec{E}_2^*\right)}{2m(i\omega_1+\nu)(-i\omega_2+\nu)}; \quad E_1 E_2^* = \left(1 - \frac{\epsilon_{1xz0}\epsilon_{2xz0}^*}{\epsilon_{1zz0}\epsilon_{2zz0}^*}\right) E_{1x0} E_{2x0}^* e^{-i(kz-\omega t)}. \tag{5.2.14}$$

As the static magnetic field is applied along the y-axis, therefore x and z component of the beat frequency ponderomotive force (F_{PMx} and F_{PMz}) can be expressed as:

$$F_{PMx} = \frac{e^2 E_{1x00} E_{2x00}}{2m(i\omega_1+\nu)(-i\omega_2+\nu)\sqrt{f_1 f_2}} \left(1 - \frac{\epsilon_{1xz0}\epsilon^*_{2xz0}}{\epsilon_{1zz0}\epsilon^*_{2zz0}}\right) \left(\frac{x}{r_{10}^2 f_1^2} + \frac{x}{r_{20}^2 f_2^2}\right) e^{\frac{-x^2}{2}\left(\frac{1}{r_{10}^2 f_1^2}+\frac{1}{r_{20}^2 f_2^2}\right)-i(kz-\omega t)}. \qquad (5.2.15)$$

$$F_{PMz} = \frac{e^2 E_{1x00} E_{2x00}}{2m(i\omega_1+\nu)(-i\omega_2+\nu)\sqrt{f_1 f_2}} \left(1 - \frac{\epsilon_{1xz0}\epsilon^*_{2xz0}}{\epsilon_{1zz0}\epsilon^*_{2zz0}}\right) \left\{ \left(\frac{1}{2f_1}\frac{df_1}{dz} + \frac{1}{2f_2}\frac{df_2}{dz}\right) - x^2 \left(\frac{1}{r_{10}^2 f_1^3}\frac{df_1}{\partial z} + \frac{1}{r_{20}^2 f_2^3}\frac{df_2}{dz}\right) + $$

$$ik\right\} e^{-\frac{x^2}{2}\left(\frac{1}{r_{10}^2 f_1^2}+\frac{1}{r_{20}^2 f_2^2}\right)-i(kz-\omega t)}. \qquad (5.2.16)$$
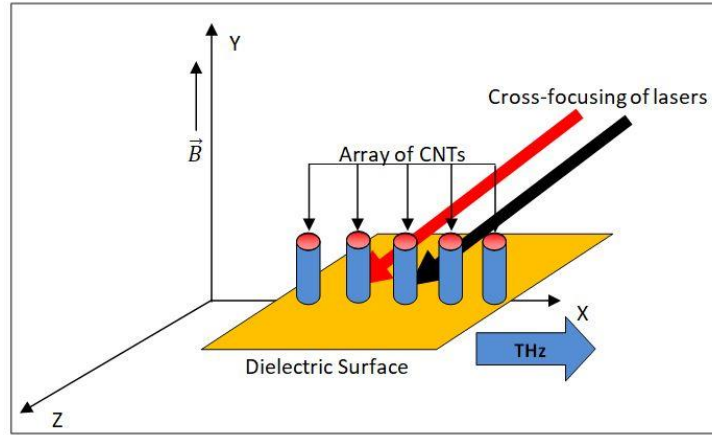
Fig.5.2.1 Schematic of THz generation by the interaction of Gaussian laser beams with vertically aligned anharmonic carbon nanotube array in the presence of an external static magnetic field.

These incident lasers (cross-focusing) interact with the array to ionize the atoms of CNTs and provide oscillatory velocities to the free electrons of CNTs. The electrons of the plasma (in the form of CNTs) get shifted away from the ion cylinder with a displacement of $\vec{\Delta}$. When the displacement of the electrons is perpendicular to the axis of CNTs, there is a creation of space charge electric field. The upper cross-sectional view of this field is shown in figure 2.6.1, as the overlapped region of the electron and ion cylinders. The net space charge electric field $\vec{E}_s$ is calculated as the vector sum of the space charge electric field due to ion and electron cylinders $\left(\vec{E}_{ion} \text{ and } \vec{E}_{ele}\right)$ and given by the relation $\vec{E}_s = \vec{E}_{ion} + \vec{E}_{ele}$. Following Kumar *et al.* [25] one can calculate this net space charge electric field at the point (r, φ, z) as

$$\vec{E}_s = \frac{n_0 e (r^2 - a^2)}{2\epsilon} \frac{\vec{r}}{r^2} - \frac{n_0 e}{2\epsilon_0} \left[\left| \vec{r} - \vec{\Delta} \right|^2 - a^2 \right] \left[\frac{\vec{r} - \vec{\Delta}}{\left| \vec{r} - \vec{\Delta} \right|^2} \right], \qquad (5.2.17)$$

where ϵ is the electric permittivity of the lattice. The displacement of the electrons parallel to the CNT axis is zero but non-zero along the perpendicular direction (x-axis). Therefore, the expression of x-component of space charge electric field can be derived from Eq. (5.2.17),

$$E_{sx} = \frac{n_0 e}{2\epsilon} \left[\left(1 + \frac{a^2}{r^2} \right) \Delta_x + \left(\frac{5\cos\varphi}{r} + \frac{4\cos^2\varphi}{r} - \frac{(r^2 - a^2)}{r^3} \cos\varphi \right) \Delta_x^2 \right]. \qquad (5.2.18)$$

Corresponding to the x-component of space charge electric field, the restoring force for the electrons of the CNTs along the x-axis can be written as

$$F_{sx} = \frac{-n_0 e^2}{2\epsilon} \left[\left(1 + \frac{a^2}{r^2} \right) \Delta_x + \left(\frac{5\cos\varphi}{r} + \frac{4\cos^2\varphi}{r} - \frac{(r^2 - a^2)}{r^3} \cos\varphi \right) \Delta_x^2 \right]. \qquad (5.2.19)$$

Due to the presence of anharmonicity in the CNTs, the restoration force for the electrons of CNTs is not equal. Some of the electrons of CNTs experience a weak restoration force, whereas others experience a strong restoration force. Hence, by using standard integration procedure one can easily calculate the average value of restoration force for various electrons over φ and r to obtain its corresponding linear (F_{Lsx}) and nonlinear components (F_{NLsx}). With the help of equation (2.6.10) the net average restoration force of the electrons of CNTs is given by

$$\langle F_{Lsx} \rangle + \langle F_{NLsx} \rangle = \frac{-m\omega_p^2}{2\epsilon_r} \Delta_x [1 + \beta + \alpha\Delta_x], \qquad (5.2.20)$$

where, $\beta = 2\log_e \left(\frac{b}{a} \right) / \left(b^2/a^2 - 1 \right)$ is known as a characteristic parameter and $\alpha = 4/(b + a)$ is known as anharmonicity factor. Both the α and β are responsible for nonlinear mixing in the response of electrons of CNTs. The numerical values of both α and β depend upon the chosen dimensions of CNTs. The equations governing the displacement of the electrons of CNTs in the presence of space charge restoration force, Ponderomotive force, and the magnetic force is given as

$$\frac{d^2\Delta_x}{dt^2} + \frac{\omega_p^2}{2\epsilon_r} (1 + \beta + \alpha\Delta_x)\Delta_x + \nu \frac{d\Delta_z}{dt} - \frac{eB}{m} \frac{d\Delta_z}{dt} = -\frac{F_{PMx}}{m}. \qquad (5.2.21)$$

$$\frac{d^2\Delta_z}{dt^2} + \nu \frac{d\Delta_z}{dt} + \frac{eB}{m} \frac{d\Delta_x}{dt} = -\frac{F_{PMz}}{m}. \qquad (5.2.22)$$

On solving equations (5.2.23) and (5.2.24), one can find the value of Δ_z and Δ_x as

$$\Delta_z = \frac{\left(\omega^2 - \frac{\omega_p^2}{2\epsilon_r}(1+\beta)+i\upsilon\omega\right)F_{PMz}-\omega\omega_c\,F_{PMx}}{m(\omega^2+i\upsilon\omega)\left(\omega^2-\frac{\omega_p^2}{2\epsilon_r}(1+\beta)+i\upsilon\omega-\frac{\omega^2\omega_c^2}{(\omega^2+i\upsilon\omega)}\right)} \qquad (5.2.23)$$

$$\Delta_x = \frac{(\omega^2+i\upsilon\omega)F_{PMx}+i\omega\omega_c\,F_{PMz}}{m(\omega^2+i\upsilon\omega)\left(\omega^2-\frac{\omega_p^2}{2\epsilon_r}(1+\beta)+i\upsilon\omega-\frac{\omega^2\omega_c^2}{(\omega^2+i\upsilon\omega)}\right)}. \qquad (5.2.24)$$

As the plasma electrons of the CNTs show displacements along the x-direction and z-direction (Δ_x and Δ_z), therefore they start oscillating with THz oscillatory velocity, $v_x = -i\omega\Delta_x$ and $v_z = -i\omega\Delta_z$.

$$v_x = -i\omega\frac{(\omega^2+i\upsilon\omega)F_{PMx}+i\omega\omega_c\,F_{PMz}}{m(\omega^2+i\upsilon\omega)\left(\omega^2-\frac{\omega_p^2}{2\epsilon_r}(1+\beta)+i\upsilon\omega-\frac{\omega^2\omega_c^2}{(\omega^2+i\upsilon\omega)}\right)}. \qquad (5.2.25)$$

$$v_z = -i\omega\frac{\left(\omega^2-\frac{\omega_p^2}{2\epsilon_r}(1+\beta)+i\upsilon\omega\right)F_{PMz}-\omega\omega_c\,F_{PMx}}{m(\omega^2+i\upsilon\omega)\left(\omega^2-\frac{\omega_p^2}{2\epsilon_r}(1+\beta)+i\upsilon\omega-\frac{\omega^2\omega_c^2}{(\omega^2+i\upsilon\omega)}\right)}. \qquad (5.2.26)$$

The nonlinear current density corresponding to the oscillatory velocity of CNT electrons can be expressed by using the relation $J^{NL} = -en_q v$, where $n_q = n_{q0}e^{-iqz}$, n_{q0} is known as the amplitude and q as the wavenumber of the ripple density. This current density has a finite value over the CNT cross-section $\pi(b^2 - a^2)$ whereas, over the area d^2 (d is known as the intertube-separation distance between the consective CNTs arranged in the array) nonlinear current density becomes zero. Therefore, one has to calculate the average value of THz nonlinear current density over the array. This average nonlinear current density is given by the relation

$$J^{NL} = -\pi e n_{q0} n_c (b^2 - a^2) v. \qquad (5.2.27)$$

By using the above relation (5.2.27), x and z components of nonlinear current density are,

$$J_x^{NL} = i\omega\pi\left(b^2 - a^2\right)n_c en_{q0} \frac{\left(\omega^2 + iv\omega\right)F_{PMx} + i\omega\omega_c\, F_{PMz}}{m(\omega^2 + iv\omega)\left(\omega^2 - \frac{\omega_P^2}{2\epsilon_r}(1+\beta) + iv\omega - \frac{\omega^2\omega_c^2}{(\omega^2 + iv\omega)}\right)}. \tag{5.2.28}$$

$$J_z^{NL} = i\omega\pi\left(b^2 - a^2\right)n_c en_{q0} \frac{\left(\omega^2 - \frac{\omega_P^2}{2\epsilon_r}(1+\beta) + iv\omega\right)F_{PMz} - \omega\omega_c\, F_{PMx}}{m(\omega^2 + iv\omega)\left(\omega^2 - \frac{\omega_P^2}{2\epsilon_r}(1+\beta) + iv\omega - \frac{\omega^2\omega_c^2}{(\omega^2 + iv\omega)}\right)}. \tag{5.2.29}$$

The above calculated nonlinear current density J_x^{NL} provides its contribution to the THz generation. It is obvious from the following standard wave propagation equation (derived from Maxwell's equations)

$$\nabla^2\vec{E}_{TH} - \nabla\left(\nabla.\vec{E}_{TH}\right) = \frac{4\pi}{c^2}\frac{\partial}{\partial t}\left(\vec{j}^{NL}\right) + \frac{1}{c^2}\frac{\partial^2\vec{E}_{TH}}{\partial t^2}, \tag{5.2.30}$$

where, $\vec{E}_{TH}$ is the THz field produced by the THz radiations. It varies as

$$\vec{E}_{TH} = \hat{x}\vec{E}_{TH0}(x,t)e^{-i(kz - \omega t)}. \tag{5.2.31}$$

On solving the above equation (5.2.30), by neglecting the term $\nabla\left(\nabla.\vec{E}_{TH}\right)$, one can write the following equation of THz electric field

$$-2ik\frac{\partial E_{THx0}}{\partial z} - \left[k - \frac{\omega^2}{c^2}\left\{1 - \frac{\omega_P^2}{\omega^2}\left(\frac{\omega\left(\omega(\omega + iv) - \omega_P^2\right)}{(\omega + iv)(\omega(\omega + iv) - \omega_P^2) - \omega\omega_c^2}\right)\right\}\right] =$$

$$\left(\frac{n_{q0}}{n_0}\right)\left(\frac{\omega}{\omega + iv}\right)\frac{(\pi(b^2 - a^2)n_c)}{ec^2}\left(\frac{\omega_P^2}{\omega^2}\right)\left(1 - \frac{\omega_P^2}{2\omega^2\epsilon_r}(1+\beta) + \frac{iv}{\omega} - \frac{\omega_c^2}{(\omega^2 + iv\omega)}\right)^{-1} \times$$

$$\left[\frac{\left\{\omega^2(\omega + iv)((\omega + iv)^2 - \omega_c^2) - \omega\omega_P^2\left((\omega + iv)^2 - i\omega_c^2\right)\right\}F_{PMx} + \left[i\omega^2\omega_c((\omega + iv)^2 - \omega_c^2) - \omega_c\omega_P^2\left\{\omega(\omega + iv) + \left(\omega^2 - \frac{\omega_P^2}{2\epsilon_r}(1+\beta) + iv\omega\right)\right\}\right]F_{PMz}}{\omega((\omega + iv)^2 - \omega_c^2) - \omega_P^2(\omega + iv)}\right].$$

$$\tag{5.2.32}$$

The phase-matching condition demands that

$$k = \sqrt{\frac{\omega}{c}\left\{1 - \frac{\omega_P^2}{\omega^2}\left(\frac{\omega\left(\omega(\omega + iv) - \omega_P^2\right)}{(\omega + iv)\left(\omega(\omega + iv) - \omega_P^2\right) - \omega\omega_c^2}\right)\right\}}. \tag{5.2.33}$$

Finally, the normalized equation for the electric field amplitude of THz radiation is obtained as

$$\frac{\partial}{\partial \zeta}\left(\frac{E_{THx0}}{E_{2x00}}\right) + \frac{1}{2i}\left(\frac{k_1}{k}\right)r_{10}^2\left[k^2 - \frac{\omega^2}{c^2}\left\{1 - \frac{\omega_P^2}{\omega^2}\left(\frac{\left((1+iv/\omega)-\omega_P^2/\omega^2\right)}{(1+iv/\omega)\left((1+iv/\omega)-\omega_P^2/\omega^2\right)-\omega_c^2/\omega^2}\right)\right\}\right] = \frac{1}{4i}(\pi(b^2-a^2)n_c)(1+$$

$$iv/\omega)^{-1}\left(\frac{n_{q0}}{n_0}\right)\left(\frac{\omega_P^2}{\omega^2}\right)\left(1 - \frac{\omega_P^2}{2\omega^2\epsilon_r}(1+\beta) + \frac{iv}{\omega} - \frac{\omega_c^2/\omega^2}{(1+iv/\omega)}\right)^{-1}\left(\frac{eE_{2x00}}{m\omega c}\right)\left(\frac{\omega}{\omega_1}\right)\left(\frac{\omega}{\omega_2}\right)\frac{1}{(1-iv/\omega_1)(1+iv/\omega_2)\sqrt{f_1 f_2}}\left(1 - \right.$$

$$\frac{\epsilon_{1xz0}\epsilon_{2xz0}^*}{\epsilon_{1zz0}\epsilon_{2zz0}^*}\right) \times$$

$$\left[\left\{D_1\left(\frac{x_1}{kr_{10}f_1^2} + \frac{x_2}{kr_{20}f_2^2}\right) + D_2\left\{\left(\frac{1}{2(kr_{10})(k_1r_{10})f_1}\frac{df_1}{d\zeta} + \frac{1}{2(kr_{20})(k_1r_{20})f_2}\frac{df_2}{d\zeta}\right) - \left(\frac{x_1^2}{f_1^3(kr_{10})(k_1r_{10})}\frac{df_1}{\partial\zeta} + \frac{x_2^2}{f_2^3(kr_{20})(k_1r_{20})}\frac{df_2}{d\zeta}\right) + i\right\}\right]/D_3\right]$$

, (5.2.34)

where, $D_1 = \left(1 + \frac{iv}{\omega}\right)\left(\left(1 + \frac{iv}{\omega}\right)^2 - \frac{\omega_c^2}{\omega^2}\right) - \frac{\omega_P^2}{\omega^2}\left(\left(1 + \frac{iv}{\omega}\right)^2 - \frac{i\omega_c^2}{\omega^2}\right),$

$$D_2 = \left[\frac{i\omega_c}{\omega}\left\{\left(1 + \frac{iv}{\omega}\right)^2 - \frac{\omega_c^2}{\omega^2}\right\} - \frac{\omega_P^2}{\omega^2}\left(1 + \frac{iv}{\omega}\right)\right] - i\left(\frac{\omega_c}{\omega}\right)\left(\frac{\omega_P^2}{\omega^2}\right)\left[1 - \omega_P^2(1+\beta)/2\omega^2\epsilon_r + \frac{iv}{\omega}\right],$$

$$D_3 = \left[\left(1 + \frac{iv}{\omega}\right)^2 - \frac{\omega_c^2}{\omega^2}\right] - \frac{\omega_P^2}{\omega^2}\left(1 + \frac{iv}{\omega}\right), \ x_1 = x/r_{10}, \text{ and } x_2 = x/r_{20}.$$

As the efficiency of the generated terahertz radiation plays a very significant role in many of the THz applications. So, we have to calculate the efficiency of emitted THz radiation. The efficiency of THz radiation is defined as the ratio of the energy of generated THz radiation (W_{THx}) to the energy of the incident Gaussian laser beams (W_L) . The average energy per unit volume associated with electromagnetic radiations is given as

$$W_{Ei} = \frac{\epsilon}{8\pi}\frac{\partial}{\partial\omega_i}\left[\omega_i\left(1 - \left(\frac{\omega_p}{\omega_i}\right)^2\right)\right]\langle|E_i|^2\rangle. \tag{5.2.35}$$

By using equation (5.2.35) we can calculate the efficiency of THz radiation. The efficiency η of the THz radiation is given by the relation

$$\eta = \frac{W_{THx}}{W_L} = \frac{\epsilon|E_{THx}|^2}{\epsilon_1 E_{1x00}^2 + \epsilon_2 E_{2x00}^2}. \tag{5.2.36}$$

When the energy transferred from the Gaussian laser beams to the THz radiation is of a small order then the above-mentioned equation (5.2.36) is correct. This means equation (5.2.36) is valid for the THz generation with small efficiency ($\eta \ll 1$). Following Bakhtiari *et al*. [26], if the THz generation efficiency is not small, we have to use a self-consistent method by considering the mutual interaction between the incident laser beams, generated THz radiation, and CNTs in the form of plasma. With the help of equation (5.2.36), the energy density of THz radiation emitted in the plasma is given by the relation $W_{THx} = \eta W_L$. This is known as first-order density reduction of Gaussian laser beams due to the THz generation. As a result of this reduction, one can write the energy density of Gaussian laser beams and THz radiation by using first-order correction, and is given as $W_{L1} = (1 - \eta)W_L$ and $W_{THx1} = \eta_1 W_L$ respectively. Here, $\eta_1 = \eta(1 - \eta)$ is known as THz radiation efficiency with first-order correction. Similarly, the energy density of Gaussian laser beams and THz radiation up to second-order corrections are given as $W_{L2} = (1 - \eta_1)W_L$ and $W_{THx2} = \eta_2 W_L$ respectively. Here, $\eta_2 = \eta(1 - \eta_1)$ is the efficiency up to second-order correction. Continuing in this way, we can obtain $W_{THxn} = \eta_n W_L$, here $\eta_n = \eta(1 - \eta_{n-1})$. This recursion formula results in a series, which converges to the given relation $\eta' = \eta/(1 + \eta)$. By using this relation, for the specified parameters of laser-plasma, CNTs, and the optimized value of the normalized density ripple (n_{q0}/n_0)=0.3, the conversion efficiency is of the order of 2.36×10^{-2}. Here, the mutual interactions between lasers, THz radiations, and CNTs in the form of plasma have been included. If we calculate the THz generation efficiency by neglecting these interactions then for the specified parameters of laser-plasma and CNTs, the conversion efficiency increases slightly and becomes of the order of 2.4×10^{-2}. Hamster *et al.* [27] and Kim *et al.* [28] have provided the efficiency of 10^{-5} in their model of THz generation as compared to the efficiency of 0.0236 provided in our case. On the basis of conversion efficiency, we can say that the present analysis of cross-focusing of two Gaussian laser beams in the array VA-CNTs provides a better alternate scheme for the efficient THz generation.

5.3. Graphical Analysis and Observations

One can solve the equation (11) numerically by using Runge-Kutta (RK) method. For this purpose, the following initial conditions are employed (i) $f_1|_{\zeta=0} = f_2|_{\zeta=0} = 1$. (ii) $\frac{df_1}{d\zeta}\Big|_{\zeta=0} = \frac{df_2}{d\zeta}\Big|_{\zeta=0} = 0$. To investigate the quantitative mathematical analysis, we have preferred the following specified parameters of laser-plasma and CNTs: $\omega_1 = 2.40 \times 10^{14} \text{rads}^{-1}$, $\omega_2 = 2.10 \times 10^{14} \text{rads}^{-1}$, $\lambda_1 = 0.800$ μm, $\lambda_2 = 0.700$ μm, the intensity of both laser beams $I_1 \sim I_2 = 10^{14} \, W\text{cm}^{-2}$, radii of both laser beams $r_{10} = 20$ μm and $r_{20} = 40$ μm. The inner and outer radii of CNTs are 40 nm and 80 nm respectively. The inter-tube separation between the CNTs is $d = 60$ nm in the array. The variation of dimensionless beam width parameters f_1 and f_2 of two laser beams (characterized by $q_1 E_{1x00}^2 = 0.4$ and $q_2 E_{2x00}^2 = 0.60$) with normalized distance ζ is depicted in Fig. 3. From the curves, it is observed that at the start of the journey, the laser beams tend to converge. After covering a small distance, in the direction of propagation, laser beams tend to diverge. This is because of the energy attenuation due to the collisions and anharmonicity between the plasma electrons of CNTs. As a result of this energy attenuation, the laser beams are unable to propagate longer distances in the CNTs From fig. 5.3.1, we also observe that both laser beams when propagating through the magnetized CNTs, the focusing of one laser beam is guided by the other and vice versa. Hence, the mutual guidance between the two lasers results in the phenomenon of cross focusing of the lasers. A similar observation was also made by Sodha *et al.* [29] in their work of cross-focusing of Gaussian lasers in the collisional magnetoplasma. It is also observed that the focusing of both the Gaussian laser beams increases with the increase of the static magnetic field. The same behavior has been observed by Singh and Sharma [30] in their study of THz generation by using two cross-focused Gaussian lasers.

The variation of normalized THz field amplitude with normalized distance ζ at the optimized value of static magnetic field 330 kG is shown in Fig. 5.3.2. From the graph, it is quite evident that normalized THz amplitude shows an oscillatory behavior and exhibits maxima and minima with the normalized distance of propagation ζ. The normalized THz amplitude shows maxima at the point where the laser beams are cross-focused. Therefore, a very important role is played by the cross focusing of the lasers in the enhancement of the THz amplitude. The normalized THz field obtained in the present scheme is more as compared to some other schemes [31, 32].
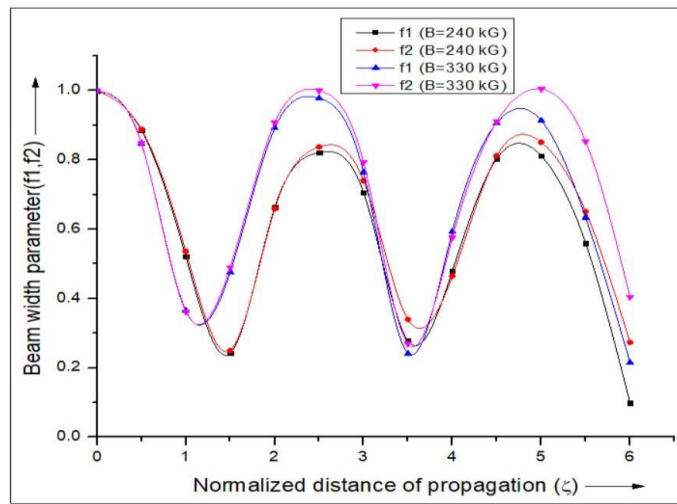
Fig. 5.3.1 Variation of the beam width parameter f_1 and f_2 with normalized distance ζ, when both laser beams are present at the optimized value of static magnetic field 330 kG.

Figure 5.3.2 Variation of normalized THz field amplitude with normalized distance ζ, at the optimized value of the static magnetic field.

Figs**.** 5.3.3(a) and 5.3.3(b) depict the three-dimensional variation of normalized THz field amplitude in the radial x/r_{10} and axial direction ζ, at the optimized value of static magnetic field 330kG, with and without (i.e., $f_1(\zeta) = 1, f_2(\zeta) = 1$) cross focusing respectively. From the plot, it is evident that the normalized THz amplitude attains maximum value along the direction of co-propagating laser beams and decreases along with the radial distance. The normalized THz amplitude shows oscillatory behavior with the normalized distance of propagation ζ. From the Figs. 5.3.3(a) and 5.3.3(b), it is clear that normalized THz amplitude increases by approximately 4.6 times with cross focusing as compared to, without cross focusing. This is because, with the focusing of the beam, the intensity of the beam increases and results in the enhancement of the normalized THz amplitude. A similar result has also been observed by Sharma and Singh [15] due to cross-focusing in collisional plasma. Thakur *et al.* [20] has also shown such amplitude enhancement of THz radiation in carbon nanoparticles, in the presence of cross focusing. In Fig. 5.3.3(a), the peak at $\zeta = 4.7$ is observed to have a maximum normalized amplitude as compared to other peaks. At the normalized distance of propagation $\zeta = 4.7$, both the laser beams are cross-focused, because of which their intensities increase. This results in a significant enhancement in the normalized THz amplitude. A similar result has been

Figure 5.3.3 Variation of normalized THz field amplitude with normalized distance ζ and x/r_{10} at the optimized value of static magnetic field (a) with cross focusing (b) without cross focusing

shown by Singh and Sharma [31] by using the cross-focusing of two laser beams in the THz generation. Figs. 5.3.4(a), 5.3.4(b), and 5.3.4(c) illustrate the variation of normalized THz amplitude with x/r_{10} and ζ, at various values of applied static magnetic field ($B = 330\,\text{kG}, 240\,\text{kG}, \text{and} 140\,\text{kG}$). The variation of normalized THz amplitude has also been shown by the 2D graph in figure 5.3.4(d). The values of other corresponding parameters are kept the same as that of Fig. 5.3.3(a). From these three graphs, it is observed that the normalized THz amplitude increases with the increase of the magnetic field. This is because of the increase in the ponderomotive nonlinearity in the direction of the applied static magnetic field. The normalized THz amplitude attains its peak value in Fig. 5.3.4(a), at the frequency $\omega = \omega_P\sqrt{(1 + \beta)/2\epsilon_r + (\omega_c^2/\omega_P^2)}$. This is known as the resonance point condition. The optimized value of static magnetic field corresponding to this resonance point is $330\,\text{kG}$. It is because of the significant increase in the ponderomotive nonlinearity in the system. Similar results have been shown by Sharma and Singh [33] in their study of THz generation by the cross-focused lasers in magnetized plasma.

101

Fig. 5.3.4 Variation of normalized THz field amplitude with normalized distance ζ and x/r$_{10}$ at various values of static magnetic field (a) 330 kG (b) 240 kG (c) 140 kG and (d) shows 2D variation.
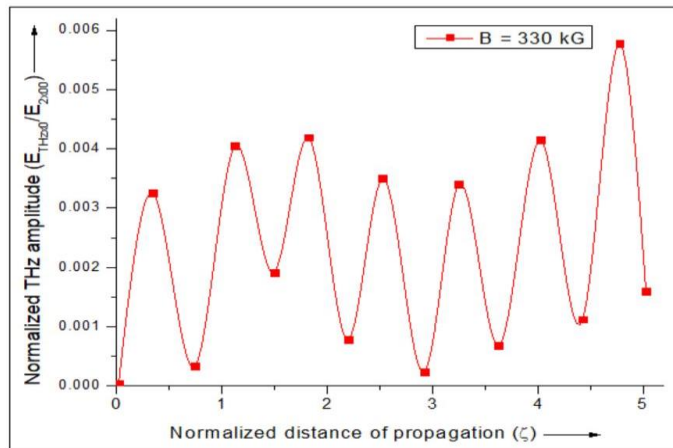
The variation of normalized THz field amplitude with normalized distance ζ and x/r$_{10}$ at the optimized value of applied static magnetic field 330 kG, for various values of CNTs outer radii (b = 60 nm, 70 nm, and 80 nm) has been illustrated in Figs. 5.3.5(a), 5.3.5(b), and 5.3.5(c). The same variation has been shown by the 2D graph in 5.3.5(d). The inner radius of each CNT in the array is kept constant (a = 40 nm). The values of other corresponding parameters are kept the same as that of Fig. 5.3.3(a). Corresponding to these dimensions of CNTs, respective characteristic parameters, and anharmonicity factors are given as: ($\beta = 0.648, \alpha = 0.04$ nm^{-1}), ($\beta = 0.542, \alpha = 0.036$ nm^{-1}), ($\beta = 0.462, \alpha = 0.031$ nm^{-1}) and ($\beta = 0.398, \alpha = 0.0296$ nm^{-1}). From the graphs, it is clear that normalized THz amplitude rises with the increase of the value of the characteristic parameter (α) and anharmonicity factor (β). Therefore, normalized THz amplitude attains maximum value in Fig. 5.3.5(a).
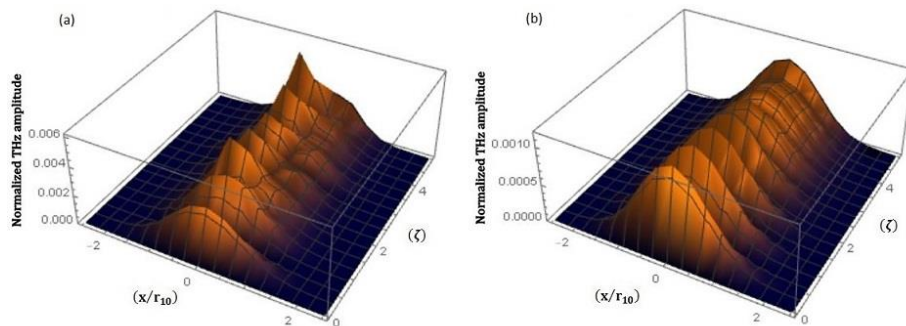

Fig. 5.3.5 Variation of normalized THz field amplitude with normalized distance ζ and x/r$_{10}$ at the optimized value of static magnetic field 330 kG for various values of CNT radii (a) 60 nm (b) 70 nm (c) 80 nm and (d) shows 2D variation.

102

The physics behind this can be explained as with the increase in the value of α and β, there is more absorption of laser beams by the electrons of CNTs and hence, an increase in the nonlinearities of the system. This results in a significant enhancement in the THz amplitude of the radiation. Such dependence of normalized THz amplitude on the dimensions of CNTs has been shown by Vij *et al.* [7] in resonant THz generation through CNTs by applying a wiggler magnetic field. In their experimental work, Watanabe *et al.* [34] has also shown the dependence of the THz electric field on the radii of CNTs. In this experiment, they generated intense THz pulse excitons by using CNTs.

The variation of normalized THz amplitude with normalized distance ζ and x/r_{10} at the optimized value of applied static magnetic field $330 \, \text{kG}$, for various values of inter-tube separation (d = 60 nm, 70 nm, and 80 nm) is illustrated in Figs. 5.3.6(a), 5.3.6(b), and 5.3.6(c).
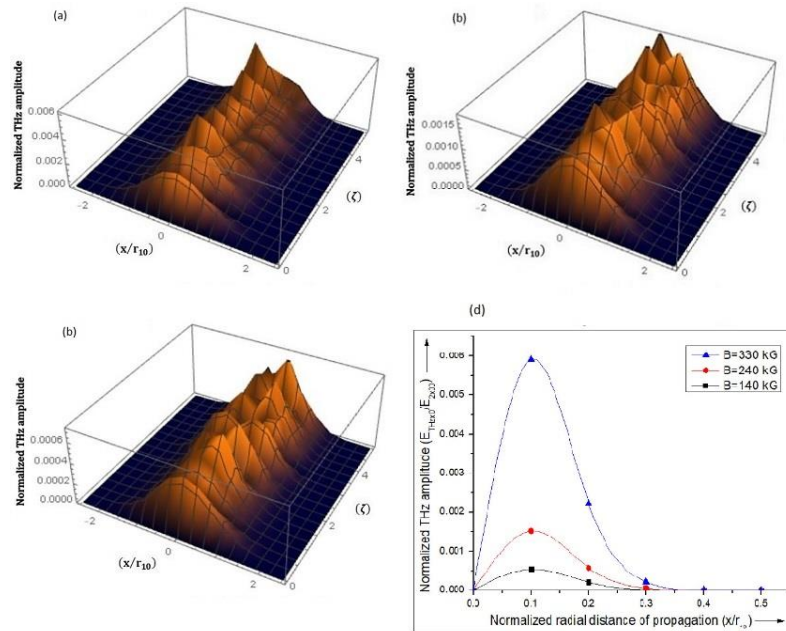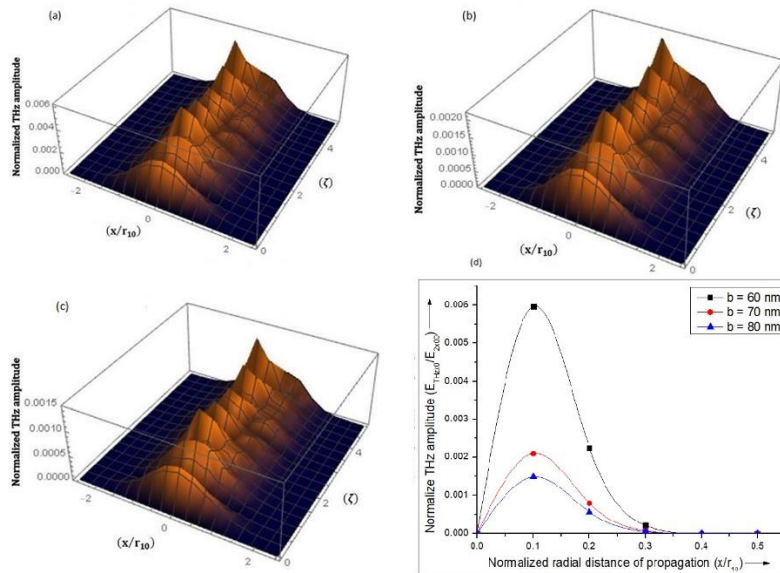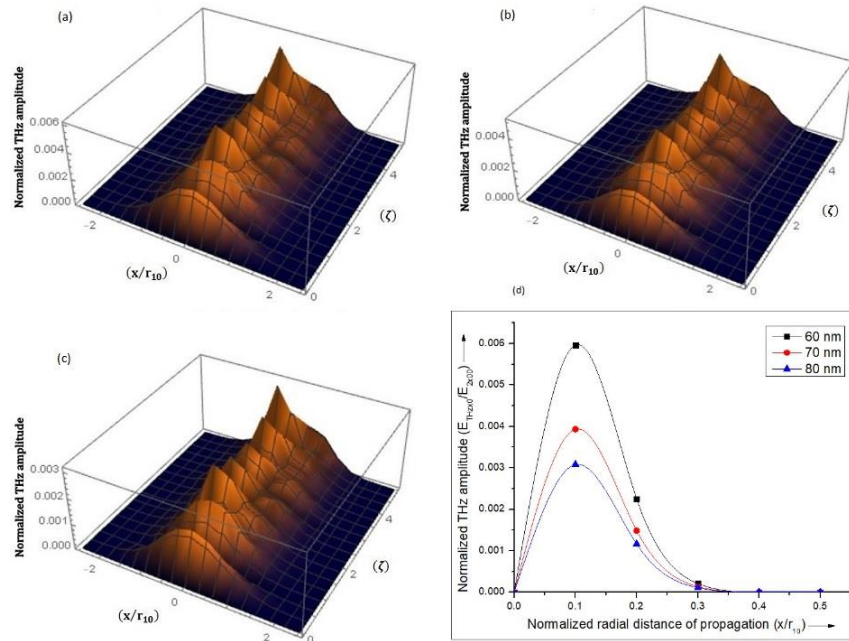

Fig. 5.3.6 Variation of normalized THz field amplitude with normalized distance ζ and x/r_{10} at the optimized value of magnetic field 330 kG for various values of inter-tube separation distance (a) 60 nm (b) 70 nm (c) 80 nm and (d) shows 2D variation.

The same has been shown by the 2D graph in 5.3.6(d). The values of other corresponding parameters are kept the same as that of Fig. 5.3.3(a). From Fig. 5.3.6, it is clear that the normalized THz amplitude shows maxima at the lower value of inter-tube separation. The normalized amplitude attains maximum value in the case of Fig. 5.3.6(a). This is because at the lower value of inter-tube separation, the number density of CNTs increases. This increases the nonlinearities of the array of CNTs behaving as plasma. Parashar and Sharma [35] have shown similar results in their theoretical study of THz generation through CNTs by using optical rectification.

5.4 Conclusion

In this proposed scheme, the THz generation is well enhanced by the cross focusing of two Gaussian laser beams in the vertical array of CNTs, under the influence of the static magnetic field. The nonlinear coupled differential equations have been derived by using PR and WKB approximation, to discuss the beam width parameters of laser beams. The focusing of each beam depends upon the applied static magnetic field and intensity of each laser beam. The normalized THz amplitude shows significant enhancement with the increase of cross-focusing as compare to the case without cross-focusing. It is also observed that the normalized THz amplitude shows significant variation with the change of the values of the magnetic field, radii of CNTs, inter-tube separation, and density of CNTs in the array, by considering the anharmonicity.

References:-

[1]   J.B. Jackson et al., "A survey of terahertz applications in cultural heritage conservation science," IEEE Trans. Terahertz Sci. Technol. **1**(1), 220-231 (2011).

[2]   J.B. Jackson et al., "Terahertz imaging for non-destructive evaluation of mural paintings," Opt. Commun. **281**(4), 527-532 (2008).

[3]   B. Ferguson and X.C. Zhang, "Materials for terahertz science and technology," Nat. Mater. **1**(1), 26-33 (2002).

[4] P.H. Siegel, "Terahertz technology in biology and medicine," IEEE Trans. Micro Theory Tech. **52**(10), 2438-2447 (2004).

[5] J. Federici and L.J. Moeller, "Review of terahertz and subterahertz wireless communications," Appl. Phys. **107**(11), 111101 (2010).

[6] M. Tonouchi, "Cutting-edge terahertz technology," Nat. photon. **1**(1), 97-105 (2007).

[7] S. Vij, N. Kant and V. Thakur, "Resonant enhancement of THz radiation through vertically aligned carbon nanotubes array by applying wiggler magnetic field," Plasmonics. **14**(1), 1051–1056 (2019).

[8] S. Jain, J. Parashar and R. Kurchania, "Effect of magnetic field on terahertz generation via laser interaction with a carbon nanotube array," Int. Nano Lett. **3**(1), 5326 (2013).

[9] S. Sharma and A. Vijay, "Terahertz generation via laser coupling to anharmonic carbon nanotube array," Phys. Plasmas. **25**(2), 023114 (2018).

[10] S. Kumar, S. Vij, N. Kant, A. Mehta and V. Thakur, "Resonant terahertz generation from laser filaments in the presence of static electric field in a magnetized collisional plasma," Euro. Phys. J. Plus **136**(1), 148 (2021).

[11] S. Sharma and A. Vijay, "Nonlinear mixing of lasers and terahertz generation on CNT embedded metal surface," Optik **199**(1), 163381 (2019).

[12] N. Ahmad and A.M. Alshehri, "Terahertz eigenmodes of a magnetized semiconductor slab and their excitation by beating of laser beams," J. Phys. Chem. Solid **130**(1), 270-275 (2019).

[13] L.V. Titova et al., "Generation of terahertz Radiation by optical excitation of aligned carbon nanotubes," Nano Lett. **15**(5), 3267-3272 (2015).

[14] N. Ahmad, T. S. Mahmoud, G. Purohit and F. Khan, "Two color laser self-focusing and terahertz generation in multi-ion species plasma," Optik **158**(1), 1533-1542 (2018)

[15] R.P. Sharma and R.K. Singh, "Terahertz generation by two cross focused laser beams in collisional plasmas," Phys. Plasmas **21**(7), 073101 (2014).

[16] S.A. Akhmanov, A.P. Sukhorukov and R.V. Khokhlov, "Self-focusing and diffraction of light in a nonlinear medium," Sov. Phys. Uspekhi **10**(5), 609 (1968).

[17]   M.S. Sodha, R.K. Khanna and V.K. Tripathi, "The self-focusing of electromagnetic beams in a strongly ionized magnetoplasma," J. Phys. D: Appl. Phys. **7**(16), 2188 (1974).

[18]   A.K. Sharma, "Transverse self-focusing and filamentation of a laser beam in a magnetoplasma," J. Appl. Phys. **49**(4), 2396 (1978).

[19]   M.M.S. Govind and R.P. Sharma, "Cross-focusing of two co-axial Gaussian electromagnetic beams in a magnetoplasma and plasma wave generation," Plasma Phys. **21**(1), 13 (1979).

[20]   V. Thakur, N. Kant and S. Vij, "Effect of cross-focusing of two laser beams on THz radiation in graphite nanoparticles with density ripple," Phys. Scr. **95**(4), 045602 (2020).

[21]   V. Thakur and N. Kant, "Influence of linear absorption and density ramp on self-focusing of the Hermite-Gaussian chirped pulse laser in plasma," Opt. Quantum Electron. **53**(1), 1-10 (2021)

[22]   N. Kant et al., "Relativistic self-focusing of Hermite-cosh-Gaussian laser beam in magnetoplasma with exponential plasma density ramp," Commun. Theor. Phys **71**(12), 1469 (2019).

[23]   S. Reich, C. Thomson and J. Maultzsch, "Carbon Nanotubes: Basic concepts and physical properties," Wiley VCH 54-78 (2004).

[24]   W. Lu, D. Wang and L. Chen, "Near-static dielectric polarization of individual carbon nanotubes," Nano Lett. **7**(9), 2729-2733 (2007).

[25]   S. Kumar, S. Vij, N. Kant and V. Thakur , "Resonant terahertz generation by the interaction of laser beams with magnetized anharmonic carbon nanotube array," Plasmonics **17**(1), 381-388 (2022).

[26]   F. Bakhtiari, M. Esmaeilzadeh and B. Ghafary, "Terahertz radiation with high power and high efficiency in a magnetized plasma," Phys. Plasmas **24**(7), 073112 (2017)

[27]   H. Hamster, A. Sullivan, S. Gordon, W. White and R. W. Facone, "Sub-picosecond, electromagnetic pulses from intense laser-plasma interaction," Phys. Rev. Lett **71**(11), 2725 (1993).

[28]   K. Kim, A. J. Taylor, T. H. Glownia and G. Rodriguez, "Coherent control of terahertz super-continuum generation in ultrafast laser-gas interactions   Nat. Photon **2**(1), 605-609 (2008).

[29]   M.S. Sodha, S.K. Mishra and S.K. Aggarwal, "Self-focusing and cross-focusing of Gaussian electromagnetic beams in fully ionized collisional magnetoplasma," Phys. Plasmas **14**(11), 112302 (2007).

[30]   R. K. Singh and R. P. Sharma, "Terahertz generation by two cross focused Gaussian laser beams in magnetized plasma," Phys. Plasmas **21**(11), 113109 (2014)

[31]   T. Bartel, P. Gaal, K. Reimann, M. Woerner and T. Elsacsser, "Generation of single-cycle THz transients with high electric-field amplitudes," Opt. Lett. **30**(20), 2805-2807 (2005)

[32]   D. You, R. Jones, P. Bucksbaum and. D.R. Dykaar, "Generation of high-power sub-single-cycle 500-fs electromagnetic pulses," Opt. Lett. **18**(4), 290-292 (1993)

[33]   M. Singh and R. P. Sharma, "THz generation by cross-focusing of two laser beams in a rippled density plasma," EPL **101**(2), 25001 (2013).

[34]   S. Watanabe, N. Minami and R. Shimano, "Intense terahertz pulse induced exciton generation in carbon nanotubes," Opt. Express **19**(2), 1528-1538 (2011).

[35]   P. Parashar and H. Sharma, "Optical rectification in a carbon nanotube array and terahertz radiation generation," Physica E **44**(10), 2069 (2012).

Chapter 6
Future Prospective and Scope

6.1. Future prospective and Scope

To enhance the efficiency of terahertz radiation along with its intensity, amplitude, power, directionality, compactness, and tunability, we have provided the various neoteric schemes in the proposed research work analysis. We have introduced anharmonicity in the CNTs along with laser and plasma interactions to obtain an appreciable gain in the THz yield. Also, we have optimized the various parameters of the laser, plasma, and CNTs such as plasma density, polarization, modulation index, beam width parameter, initial laser intensity, the inner radius of CNTs, outer radius of CNTs, number density of CNTs, and inter-tube separation between the consective CNTs in the array, etc. to obtain enhanced efficiency of THz output. THz wave propagation equation, equation of continuity, the ponderomotive force equation has been derived along with nonlinear current density. Also, the role of transverse density ripple, anharmonicity, externally applied static magnetic and electric fields has been elaborated in different schemes of the present thesis. The conclusion of the significant results obtained from the presented schemes has already been explained in the last section of the particular chapter. The results obtained from our present theoretical work provide a mathematical guideline for generating compact, efficient, and cost-effective sources of THz radiation. Thus THz sources developed in our research work will have a significant effect on the wide-ranging potential utilizations in various fields of scientific research and technology. In this way, this research work can be successful in attracting inter-disciplinary and cross-disciplinary researches. With this, THz science and technology can make great advancements in every field. So, the proposed work in the thesis is expected to have significant impacts on the THz high field community, condensed matter researchers, and other multiple research communities that will take advantage of the capabilities of this new source of THz radiations. The proposed novel unprecedented THz source opens up the following new opportunities:-

6.2. THz Community

In the proposed research work, an unconventional and unorthodox scheme is developed by using CNTs to obtain the novel THz source to generate efficient THz radiations. This novel THz source can provide excellent support in upgrading the THz applications. It can also provide a helping hand in making more understanding of nonlinear effects involving THz-matter interactions. This can also open up the doors for many unrevealed nonlinear effects.

6.3. Ultra intense THz-Plasma interactions

The generation of THz radiations from relativistic laser-plasma interactions is one of the emerging research areas of high-energy-density physics. The extreme THz pulses offer a new long-wavelength pump light source capable of driving strong-field physics, opening a door for a new branch of research known as ultra-intense THz-plasma interactions.

6.4. Modern Condensed Matter Physics

It is defined as the branch of physics that deals with the various physical properties of solid and liquid phases. These properties are due to the presence of electromagnetic forces between the atoms of the solid and liquid phases. THz applications in phase transition and spintronics are also the most active research areas of modern material science. The average energy of the THz photon (4.2 meV) is comparable to the energy of excitons, magnons, and phonons in various systems. Thus, THz technology acts as an anchor to control transient states of matter such as photonics, spintronics, etc. The novel THz sources can be used in the research work of previously inaccessible transients in materials.

6.5. Material Science and Strong Field Physics

During the laser-plasma interactions in the array of VA-CNTs or HA-CNTs, the generation of THz radiations is also accompanied by some highly energetic particles and radiations. Most of the time, these highly energetic particles and radiations are electrons, neutrons, positive ions, negative ions, x-rays, γ-rays, etc. By using these additional particles and radiations, we can develop a multipurpose THz pump, x-ray probe, THz probe. These pumps and probes can be further used in many applications of material science and strong-field physics.

6.6. Particle Physics

The highly energetic THz radiations produced by powerful and efficient THz sources can be used to accelerate electrons in accelerators. Such accelerators can be further used in many investigations of particle physics. This can also help reduce the size of high-energy particle accelerators.

6.7. THz Astronomy

THz observations of interstellar atoms, molecules, and dust serve as powerful probes of the conditions within the interstellar medium that spreads all our the galaxy, providing insights into the origins of far away stars, planets, galaxies, and the Universe. By using THz radiation, one can make a cross-disciplinary approach to the subject. THz Astronomy can help in exploring the new rapidly evolving fields.

Researchers from the fields of chemistry and biology are likely to use such a THz source as a unique and powerful research tool to investigate chemo-catalysis and hydration, respectively.

Curriculum Vitae

Personal Details:

Name	:	Sandeep Kumar
Father's Name	:	Sh. Hem Raj Sharma
Mother's Name	:	Mrs. Arun Sharma
D. O. B.	:	29th Nov. 1977
Language Known	:	English, Hindi, Punjabi
Hobbies	:	Reading Books, Listening Music, Gardening, Playing Chess
Mobile No	:	9815429828
E-mail	:	sanphymagic@gmail.com
Correspondence Address	:	1043/12-7, Katra Sher Singh, Near, D. A. V. College Library, PCM Point, Amritsar, Punjab, India.

Career Objective

To achieve the great heights in the field of academia and to gain more of knowledge by making collaborations with people, institutes and others.

Key Skills and Strengths

- ✓ Good performer under pressure
- ✓ Good Listener
- ✓ Always ready to learn

- ✓ High learning ability
- ✓ Hard Working

Academic Growth

Exams Qualified	Year	Board// University	College/School	CGPA/ Percentage
Ph. D	2021	Lovely Professional University, Phagwara.	University Campus.	8.63
M.Sc.	1998	Guru Nanak Dev University, Amritsar.	University Campus.	72%
B.Ed.	1999	Panjab University, Chandigarh.	D.A.V. College of Education, Abohar.	71%
B.Sc.	1996	Guru Nanak Dev University, Amritsar.	D.A.V. College, Amritsar.	67 %

Academics Experience

- ✓ Worked as an assistant professor in the Physics department at D.A.V. College, Amritsar for 2 years.
- ✓ Worked as a Physics teacher in Gyan Ashram Senior Secondary School for 14 years.
- ✓ Worked as Physics teacher in Alexandra school for 6 years.

Area of Interest
- ✓ THz radiation generation
- ✓ Laser-plasma interaction
- ✓ Optics
- ✓ Electronics

Paper Publication

Paper Publication in SCI Journal

1. **Sandeep Kumar**, Shivani Vij, Nitikant, Alka Mehta and Vishal Thakur, "Resonant terahertz generation from laser filaments in the presence of static electric field in a magnetized collisional plasma," Eur. Phys. J. Plus 136, 148 (2021).

2. **Sandeep Kumar**, Shivani Vij, Nitikant and Vishal Thakur, "Resonant terahertz generation by the interaction of laser beams with magnetized anharmonic carbon nanotubes array," Plasmonics 17, 381-388 (2021)

3. **Sandeep Kumar**, Shivani Vij, Nitikant and Vishal Thakur, "Resonant Terahertz generation by cross-focusing of Gaussian beams in the array of vertically aligned anharmonic and magnetized CNTs," Opt. Commun. 513 128112 (2022

4. **Sandeep Kumar**, Shivani Vij, Nitikant and Vishal Thakur, "Combined effect of transverse electric and magnetic fields on THz generation by beating of two amplitude-modulated laser beams in the collisional plasma," J. Astrophys. Astron. **43,** (30)1-5 (2022).

Paper Accepted By SCI Journal

1. **Sandeep Kumar**, Shivani Vij, Nitikant and Vishal Thakur, "Resonant excitation of THz radiations by interaction of amplitude-modulated lasers with an anharmonic CNTs in the presence of static D.C. electric and magnetic fields," Chin. J. Phys (2022).

Paper Communicated to SCI Journal

1. **Sandeep Kumar**, Shivani Vij, Nitikant and Vishal Thakur, "Nonlinear interaction of Gaussian Laser beam with the anharmonic magnetized and rippled CNTs: THz generation" Appl. Phys. B (2022).

2. **Sandeep Kumar**, Shivani Vij, Nitikant and Vishal Thakur, "Beating of dark hollow laser beams in magnetized plasma under the influence of D.C. electric field to generate THz radiation" Appl. Opt. (2022).

3. **Sandeep Kumar**, Shivani Vij, Nitikant and Vishal Thakur, "THz generation by obliquely incident beating lasers on the close-packed array of vertically aligned anharmonic carbon" Waves Random Complex Media (2022).

4. **Sandeep Kumar**, Shivani Vij, Nitikant and Vishal Thakur, "Interaction of spatial-Gaussian Laser's with the magnetized CNTs in the presence of D.C. electric field and enhanced THz emission" Physica Scripta (2022).

5. **Sandeep Kumar**, Shivani Vij, Nitikant and Vishal Thakur, "THz generation by propagating lasers through magnetized SWCNTs." Indian J. Phys. (2022).

6. **Sandeep Kumar**, Shivani Vij, Nitikant and Vishal Thakur, "Enhanced THz generation by using two AM laser beams in a magnetized plasma under the presence of D.C. electric field," Phys. Lett. A (2022).

Paper published in UGC care listed journal

1. **Sandeep Kumar** and Vishal Thakur, "Enhancement in the THz-radiation Generation by fs Laser Pulse" JETIR **6** 377-381 (2019).

2. **Sandeep Kumar** and Vishal Thakur, "Enhancement In Tera Hertz Radiations Produced by Short Pulse Laser" Eur. j. mol. **07** 3466-3470 (2020).

Paper published in International Conference

1. **Sandeep Kumar**, Shivani Vij, Nitikant, Alka Mehta and Vishal Thakur, "Production of Terahertz Radiations by Short Pulse Lasers" journal of physics: conference series **1531** 012011 (2020).

Paper Communicated to International Conference

1. **Sandeep Kumar**, Shivani Vij, Nitikant and Vishal Thakur, "Production of Terahertz Radiations by interacting Gaussian laser beam in CNTs array. Journal of physics : conference series 2021 (Proceedings)

Conferences & Workshops

Conferences Attended

1. Recent Advantage in Fundamental and Applied Sciences (2020)
2. Advances in Plasma Science and Technology (2021)
3. Recent Advantage in Fundamental and Applied Sciences (2021)
4. Chandra's Contribution in Plasma Astrophysics (2021)
5. 36th National Symposium in Plasma Science & Technology (2021)
6. Virtual National Conference on Plasma Science and Applications (2021)
7. 3rd National Conference on Recent Advancement in Physical Sciences (2021)
8. 2nd International Conference on Plasma Theory and Simulation (2022)

Workshop Attended

1. ELI Summer School 2021 Workshop on Dual Color Laser-Plasma Accelerator.

It is certified that the above information given by me is correct and complete to the best of my belief.

Date: 15-July-2022   Sandeep Kumar

**THE EUROPEAN
PHYSICAL JOURNAL PLUS**

Resonant terahertz generation from laser filaments in the presence of static electric field in a magnetized collisional plasma

Sandeep Kumar[1]**, Shivani Vij**[2]**, Niti Kant**[1]**, Alka Mehta**[1]**, Vishal Thakur**[1,a]

[1] Department of Physics, Lovely Professional University, G.T. Road, Phagwara, Punjab 144411, India
[2] Department of Applied Sciences, DAV Institute of Engineering and Technology, Jalandhar 144008, India

Abstract A new scheme of terahertz (THz) generation from laser filaments in plasma in the presence of static electric and magnetic fields is proposed. Two femtosecond laser pulses of different frequencies (ω_1, ω_2) and wave numbers (k_1, k_2) are co-propagating under the action of filamentation in a magnetized collisional plasma. THz wave is generated due to the nonlinear coupling between nonlinear velocity and electron density in magnetized collisional plasma. For suitable laser and plasma parameters, the nonlinear coupling results in enhanced nonlinear current density which leads to resonant THz waves. The external D.C. electric and magnetic fields are applied perpendicular to each other and mutually perpendicular to the direction of co-propagating lasers. We have obtained the expression of a dielectric tensor with anisotropic nature, and it is found very useful in the study of THz generation. The applied magnetic field also aids to enhance the transverse components of nonlinear current. This nonlinear current is responsible to generate enhanced terahertz waves at frequency $(\omega_1 - \omega_2)$. We have found that the normalized THz amplitude increases significantly with the increase in applied D.C. electric field from 10 to 30 kV/cm and magnetic field from 10 to 50kG. Our scheme with numerical analysis may open the door for efficient and cost-effective way to generate THz radiation.

1 Introduction

In modern days, compact and efficient THz sources have great importance in the field of science and technology because of their numerous applications in industrial manufacturing and packaging units [1], security and safety [2], broad band communication [3], biological and pharmaceutical sciences [4–6], remote sensing [7]. Due to this, various researchers have studied the schemes of THz wave generation by using different mechanisms to enhance the normalized THz amplitude like optical rectification [8], cross-focusing [9], optical mixing [10] and filamentation [11–13], etc. Among them, the mechanism of THz generation by laser filamentation produces THz pulses of very high order energy. Femtosecond laser filamentation is a distinctive, dynamical and unique phenomenon in which laser beam breaks up

---

[a] e-mail: vishal20india@yahoo.co.in (corresponding author)

Springer

in transverse direction by maintaining the balance between an optical Kerr effect induced self-focusing and plasma de-focusing. In this laser intensity is stabilized along the propagation distance and this is known as intensity clamping. The filamentary propagation of laser pulses in air was observed in 1995 [14] which led to lot of research in the emission of electromagnetic waves. Houard et al. [15] noticed three orders of magnitude enhancement of the terahertz energy beamed by a femtosecond pulse undergoing filamentation through air in the presence of static electric field. Loffler et al. [16] observed enhancement in the efficiency of THz radiation generation by using static electric field. Bhasin et al. [17] proposed 30 times increase in magnitude of normalized terahertz amplitude by applying a D.C. electric field in plasma 50 kV/cm. Mclaughlin et al. [18] have shown an enhancement in THz field energy by applying external magnetic field up to 8 T in plasma.

In the present work, we develop a comprehensive theoretical model for the generation of terahertz waves by using two filamented femtosecond laser pulses in the presence of applied static electric field in magnetized collisional plasma. In this analysis, we have taken two femtosecond lasers of slightly different frequencies so that their difference in frequency may lie in terahertz region. Also for two lasers of nearly equal frequencies, the symmetry of + ve and –ve half cycles of fundamental laser is broken. As a result, the ionization causes drift currents in the same direction in every cycle. Therefore, terahertz generation becomes more efficient [19].

We have considered two transversely amplitude modulated femtosecond laser beams having electric fields, $\vec{E}_1(\omega_1, k_1)$ and $\vec{E}_2(\omega_2, k_2)$. These laser beams are propagating along Z-direction, polarizing along Y-direction and amplitude modulated along X-direction. To produce magnetized plasma, static magnetic field is applied over the plasma along Y-direction. This static magnetic field can be applied by using current carrying coil having finite number of turns and magnetic core with an air gap. The static D.C. electric field is applied along X-direction. This D.C. electric field can be applied with the help of two metallic plates, keeping one plate at positive potential and the other at negative potential as shown in Fig. 1. The applied electric and magnetic fields aid in the enhancement of the normalized amplitude of terahertz wave. The laser fields impart oscillatory velocity to the plasma electrons. Whereas, externally applied static D.C. electric field is responsible for the D.C. drift to electrons in the opposite direction. The lasers also exert a beat ponderomotive force $\vec{F}_{PM\omega}^{NL}$ as well as static ponderomotive force $\vec{F}_{PM\beta}^{NL}$ on the electrons of magnetized collisional plasma. In steady-state, the static ponderomotive force is well poised by pressure gradient force. It results in transverse density ripple at zero frequency and wave number β which can be represented by $n_{0,\beta}$. The ponderomotive force gives rise to velocity oscillations $\vec{v}_{\omega,k}^{NL}$ and density oscillations $n_{\omega,k}^{NL}$. The density oscillation beats with D.C. drift to produce transverse current density $\vec{J}_{\omega,k}^{NL}$ which is responsible for THz generation. In most of the research works on THz generation, collisions have been ignored because of extraction of energy from the electrons of plasma. In reality, these collisions are the inherent part of every nonlinear system; hence, it becomes important to consider the effect of collisions in our analysis to get more accurate results.

The present paper is organized as, in second segment of the paper we provide calculations for nonlinear velocity components under the effect of D.C. electric and magnetic fields at THz frequency.

$\omega = \omega_1 - \omega_2$ and wave numbers $k = k_1 - k_2$ and $k' = k_1 - k_2 + \beta$. In this segment of the paper, the role of nonlinear coupling factor is discussed and calculations for various components of nonlinear current density are given. In third segment, proper mathematical treatment is given to find out the elements of anisotropic dielectric constant in the presence
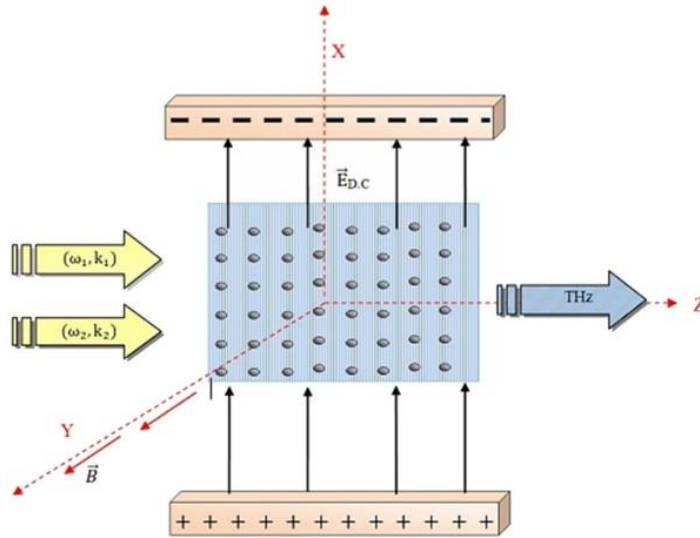
Fig. 1 Schematic of THz generation by irradiating amplitude-modulated lasers in magnetized collisional plasma in the presence of D.C. electric field

of external magnetic field. THz wave generation dynamics is also present in this segment of paper. The graphs and results are provided in last segment of paper with detailed discussions and conclusion. In this segment, whole analysis is included.

2 Analytical formulism for nonlinear velocities and nonlinear current density

We irradiate two transversely amplitude modulated femtosecond laser pulses in the magnetized collisional plasma with density n_p^0. The field profile of lasers can be given as

$$\vec{E}_j = \widehat{y}\big[1 + \mu_j \cos \beta x\big] D_{j0} e^{-\iota(\omega_j t - k_j z)}, \tag{1}$$

where $j = 1, 2$, μ_j is the modulation depth of the beam and β is the periodicity parameter. Frequency difference of femtosecond lasers ($\omega = \omega_1 - \omega_2$) lies in THz range. The significant gain in the oscillatory velocities of plasma electrons is observed due to the laser filaments and are provided as

$$\vec{v}_j = \frac{-e\vec{E}_j}{m_e(\iota\omega_j - \upsilon_e)}. \tag{2}$$

Due to externally applied static D.C. electric field along X-axis, plasma electrons will get D.C. drift and is given as

$$\vec{v}_{D.C} = \frac{-e\vec{E}_{D.C}}{m_e \upsilon_e}, \tag{3}$$

where $-e, m_e, \upsilon_e$ represent the electronic charge, mass and collisional frequency, respectively. The term $\vec{E}_{D.C}$ represents the applied D.C. electric field. The plasma electrons drift in opposite direction of D.C. electric field and get accumulated near the edge of filament.

$$\vec{v}_{PM}^{NL} = \frac{1}{m(\upsilon - \iota\omega)}\left[\vec{F}_{PM}^{NL} - e\left(\vec{v}_{PM}^{NL} \times \vec{B}\right)\right], \tag{10}$$

$$\vec{v}_{PM}^{NL} \times \vec{B} = \frac{1}{m(\upsilon - \iota\omega)}\left[\vec{F}_{PM}^{NL} \times \vec{B} - e\left(\vec{v}_{PM}^{NL} \times \vec{B}\right) \times \vec{B}\right], \tag{11}$$

$$= \frac{1}{m(\upsilon - \iota\omega)}\left[\vec{F}_{PM} \times \vec{B} + e\vec{v}_{PM}^{NL}B^2\right], \tag{12}$$

$$\vec{v}_{PM}^{NL} = \frac{1}{m(\upsilon - \iota\omega)}\left[\vec{F}_{PM}^{NL} - \frac{e}{m(\upsilon - \iota\omega)}\left(\vec{F}_{PM}^{NL} \times \vec{B} + e\vec{v}_{PM}^{NL}B^2\right)\right], \tag{13}$$

$$\vec{v}_{PM}^{NL} = \frac{\vec{F}_{PM}^{NL}}{m_e(\upsilon_e - \iota\omega)} - \frac{\vec{F}_{PM}^{NL} \times \vec{\omega}_c}{m_e(\upsilon_e - \iota\omega)^2} - \frac{\omega_c^2}{(\upsilon_e - \iota\omega)^2}\vec{v}_{PM}^{NL}, \tag{14}$$

here, $\omega_c = eB/m$ is cyclotron frequency of electrons. Due to applied magnetic field along Y-axis, we resolve the velocity of electrons along the X-axis and Z-axis as

$$v_{PMx}^{NL} = \frac{e^2 D_{10} D_{20}}{4m_e^2\omega_\alpha^2(\iota\omega_1 - \upsilon_e)(\iota\omega_2 + \upsilon_e)}$$
$$\times \left[\{(\upsilon_e - \iota\omega)\beta + \omega_c k\}\iota(\mu_1 + \mu_2)e^{-\iota(\omega t - kz - \beta x)} + 2\iota\omega_c ke^{-\iota(\omega t - kz)}\right], \tag{15}$$

$$v_{PMz}^{NL} = \frac{e^2 D_{10} D_{20}}{4m_e^2\omega_\alpha^2(\iota\omega_1 - \upsilon_e)(\iota\omega_2 + \upsilon_e)}$$
$$\times \left[(\mu_1 + \mu_2)ie^{-\iota(\omega t - kz - \beta x)}\{(\upsilon_e - \iota\omega)k - \omega_c\beta\}\iota + 2i(\upsilon_e - \iota\omega)ke^{-\iota(\omega t - kz)}\right], \tag{16}$$

where $\left[(\upsilon_e - \iota\omega)^2 + \omega_c^2\right] = \omega_\alpha^2$. With the help of velocity perturbations provided by Eq. (15) and (16), density perturbations $n_{\omega,k}^{NL}, n_{\omega,k+\beta}^{NL}$ in the presence of static electric and magnetic fields can be calculated by using the equation of continuity as

$$n_{\omega,k}^{NL} = \frac{n_p^0 e^2 D_{10} D_{20}[\iota k^2](\omega_c + \upsilon_e - \iota\omega)}{2m_e^2\omega\omega_\alpha^2(\iota\omega_1 - \upsilon_e)(\iota\omega_2 + \upsilon_e)}e^{-\iota(\omega t - kz)}, \tag{17}$$

$$n_{\omega,k+\beta}^{NL} = \frac{n_p^0 e^2(\mu_1 + \mu_2)(D_{10}D_{20})}{4m_e^2(\iota\omega_1 - \upsilon_e)(\iota\omega_2 + \upsilon_e)}\frac{\iota\left[(\upsilon_e - \iota\omega)^2\left(k^2 + \beta^2\right) - \omega_c^2\beta^2 + \omega_c k^2\right]}{\omega\omega_\alpha^2}e^{-\iota(\omega t - kz - \beta x)}. \tag{18}$$

One can write nonlinear current density as the vector sum of three terms $\vec{J}_1$, $\vec{J}_2$ and $\vec{J}_3$, where the first term $\vec{J}_1$ arises due to coupling between equilibrium plasma density n_p^0 and nonlinear velocity $\vec{v}_{\omega,k}^{NL}$, the second term $\vec{J}_2$ arises due to coupling between nonlinear density perturbation $n_{\omega,k}^{NL}$ and D.C. drift of electrons $\vec{v}_{D.C}$. The third term $\vec{J}_3$ arises due to coupling between zero frequency transverse density ripple $n_{0\beta}$ and nonlinear velocity $\vec{v}_{\omega,k}^{NL}$. Therefore, the total nonlinear current density $\vec{J}_{\omega,k}^{NL} = \vec{J}_1 + \vec{J}_2 + \vec{J}_3$,

$$\vec{J}_{\omega,k}^{NL} = -n_p^0 e\vec{v}_{\omega,k}^{NL} - n_{\omega,k}^{NL}e\vec{v}_{D.C} - n_{0,\beta}^*e\vec{v}_{\omega,k+\beta}^{NL}. \tag{19}$$

On resolving the total current density in its x and z components, we get $J_{x\omega,k}^{NL}$ and $J_{z\omega,k}^{NL}$ as

$$J_{x\omega,k}^{NL} = \frac{-n_p^0 e^4 D_{10} D_{20}[\iota]}{2m_e^3\omega_\alpha^2(\iota\omega_1 - \upsilon_e)(\iota\omega_2 + \upsilon_e)}$$

$$\times \left\{ \frac{k^2 E_{D.C}[(\upsilon_e - \iota\omega + \omega_c)]}{\omega\upsilon_e} - \frac{e\beta(\mu_1 + \mu_2)}{8T_e} \left(\frac{\mu_1 D_{10}^2}{(\iota\omega_1 - \upsilon_e)^2} + \frac{\mu_2 D_{20}^2}{(\iota\omega_1 + \upsilon_e)^2} \right)(\upsilon_e - \iota\omega - \omega_c) \right\} e^{-\iota(\omega t - kx)}, \tag{20}$$

$$J_{z\omega,k}^{NL} = \frac{-n_p^0 e^4 D_{10} D_{20}[\iota]}{2m_e^3 \omega_\alpha^2 (\iota\omega_1 - \upsilon_e)(\iota\omega_2 + \upsilon_e)}$$

$$\times \left\{ \frac{ek(\mu_1 - \mu_2)}{8T_e} \left(\frac{\mu_1 D_{10}^2}{(\iota\omega_1 - \upsilon_e)^2} + \frac{\mu_2 D_{20}^2}{(\iota\omega_1 + \upsilon_e)^2} \right)(\upsilon_e - \iota\omega + \omega_c) + \frac{m_e k(\upsilon_e - \iota\omega + \omega_c)}{e} \right\} e^{-\iota(\omega t - kz)}. \tag{21}$$

3 Anisotropic dielectric constant and THz wave dynamics

Due to the presence of external magnetic field along the Y-direction in collisional plasma, the dielectric constant will behave as anisotropic tensor.

$$\epsilon = \begin{vmatrix} \epsilon_{XX} & \epsilon_{XY} & \epsilon_{XZ} \\ \epsilon_{YX} & \epsilon_{YY} & \epsilon_{YZ} \\ \epsilon_{ZX} & \epsilon_{ZY} & \epsilon_{ZZ} \end{vmatrix}, \tag{22}$$

The components of dielectric anisotropic tensor are $\epsilon_{YZ} = \epsilon_{ZY} = \epsilon_{YX} = \epsilon_{XY} = 0$, $\epsilon_{YY} = 1 - \omega_p^2/\iota\omega(\upsilon_e - \iota\omega)$, $\epsilon_{XX} = 1 - \omega_p^2(\upsilon_e - \iota\omega)/\iota\omega[(\upsilon_e - \iota\omega)^2 + \omega_c^2] = \epsilon_{ZZ}$, $\epsilon_{ZX} = -\iota\omega_c\omega_p^2/\omega[(\upsilon_e - \iota\omega)^2 + \omega_c^2] = -\epsilon_{XZ}$.

Due to collisions, some of the components of dielectric tensor become imaginary which are responsible for the resistivity in plasma.

The wave equation for the generation of THz radiation is given by

$$-\nabla^2 \vec{E} + \nabla \cdot \left(\nabla \cdot \vec{E} \right) = \frac{4\pi\iota\omega}{c^2} \vec{J}_{\omega,k}^{NL} + \frac{\omega^2}{c^2} \epsilon\vec{E} \tag{23}$$

With the use of components of dielectric constant, Eq. (23) is modified in the following form

$$-\frac{\omega^2}{c^2} \epsilon_{zz} E_z - \frac{\omega^2}{c^2} \epsilon_{zx} E_x = \frac{+4\pi\iota\omega}{c^2} J_{Z\omega,k}^{NL}, \tag{24}$$

$$-2\iota k' \frac{\partial E_x}{\partial z} + \left(k'^2 - \frac{\omega^2}{c^2} \left(\epsilon_{xx} + \frac{\epsilon_{zx}^2}{\epsilon_{zz}} \right) \right) E_x = \frac{+4\pi\iota\omega}{c^2} \left(J_{x\omega,k}^{NL} + \frac{\epsilon_{zx}}{\epsilon_{zz}} J_{z\omega,k}^{NL} \right). \tag{25}$$

where $k' = k_1 - k_2 + \beta$ is the wave number with which current density oscillates at frequency ω.

The wave number β of transverse density ripple is responsible for phase matching condition by providing extra momentum. By using phase matching condition

$$k'^2 - \frac{\omega^2}{c^2} \left(\varepsilon_{xx} + \frac{\varepsilon_{zx}^2}{\varepsilon_{zz}} \right) = 0, \tag{26}$$

$$k_1 - k_2 + \beta = \frac{\omega}{c} \left\{ 1 - \frac{\omega_P^2}{\iota\omega\omega_\alpha^2} \left((\upsilon_e - \iota\omega) - \frac{\omega_c^2 \omega_P^2}{\iota\omega\omega_\alpha^2 - \omega_P^2(\upsilon_e - \iota\omega)} \right) \right\}^{1/2}. \tag{27}$$

By using above condition, Eq. (25) provides the electric field of THz radiation.

$$E_x = \frac{-2\pi\omega}{k'c^2} \left\{ J_{x\omega,k}^{NL} + \frac{\varepsilon_{zx}}{\varepsilon_{zz}} J_{z\omega,k}^{NL} \right\} z. \tag{28}$$

120

Using $J_{x\omega,k}^{NL}$ and $J_{z\omega,k}^{NL}$, the THz electric field can be derived as

$$E_x = \frac{-2\pi\omega z}{k'c^2}\left(\frac{-n_p^0 e^4 D_{10} D_{20}\iota}{2m_e^3 \omega_\alpha^3 (\iota\omega_1 - \upsilon_e)(\iota\omega_2 + \upsilon_e)}\right)$$

$$\times \left(\frac{k^2 E_{D.C}(\upsilon_e - \iota\omega + \omega_c)}{\omega\upsilon_e} - \frac{e\beta(\mu_1 + \mu_2)}{8T_e}\frac{\mu_1 D_{10}^2}{(\iota\omega_1 - \upsilon_e)^2} + \frac{\mu_2 D_{20}^2}{(\iota\omega_2 + \upsilon_e)^2}\right)(\upsilon_e - \iota\omega + \omega_c)$$

$$+ \frac{\omega_c \omega_P^2}{\iota\omega_\alpha^2 - \omega_P^2(\upsilon_e - \iota\omega)}\left\{\frac{ek(\mu_1 + \mu_2)}{8T_e}\left(\frac{\mu_1 D_{10}^2}{(\iota\omega_1 - \upsilon_e)^2} + \frac{\mu_2 D_{20}^2}{(\iota\omega_2 + \upsilon_e)^2}\right)\right\}$$

$$\times (\upsilon_e - \iota\omega + \omega_c) + \frac{m_e K}{e}(\upsilon_e - \iota\omega + \omega_c) \qquad (29)$$

Using the above equation, the normalized amplitude of electric field component of THz radiations can be written as

$$\frac{eE_x}{m_e\omega_P c} = \frac{\omega' z' D_{10}' D_{20}' \iota}{4k''\omega_0^2 (\iota\omega_{P1} - \upsilon_e')(\iota\omega_{P2} + \upsilon_e')}$$

$$\cdot \left[\frac{k_0^2 E_{D.C}'(\upsilon_e' - \iota\omega' + \omega_c')}{\omega'\upsilon_e'} + (\upsilon_e' - \iota\omega' - \omega_c')\left\{\frac{k_0}{8}\left(\frac{\omega_c'}{\iota\omega'\omega^2 - (\upsilon_e' - \iota\omega')}\right) - \frac{\beta'}{8}\right\}\right.$$

$$\left. \cdot \frac{(\mu_1 + \mu_2)}{V_{th}'}\left(\frac{\mu_1 D_{10}'^2}{(\iota\omega_{P1} - \upsilon_e')^2} + \frac{\mu_2 D_{20}'^2}{(\iota\omega_{P2} + \upsilon_e')^2}\right) + \left(\frac{\omega_c'}{\iota\omega'\omega^2 - (\upsilon_e' - \iota\omega')}\right)\right] \qquad (30)$$

The different parameters are normalized as,

$$D_{10}' = eD_{10}/m\omega_p c, \ D_{20}' = eD_{20}/m\omega_p c, \ \omega' = \omega/\omega_p, \ z' = \omega_p z/c, \ \omega_{p1} = \omega_1/\omega_P,$$
$$\omega_{p2} = \omega_2/\omega_p, \ \upsilon_e' = \upsilon_e/\omega_p, \ E_{D.C}' = eE_{D.C}/m\omega_p c, \ k_0 = ck/\omega_p, \ k'' = ck'/\omega_p,$$
$$\omega_c' = \omega_c/\omega_p, \ q' = c\beta/\omega_p, \ V_{th}' = V_{th}/c.$$

4 Results and discussion

In the present work, we provide numerical treatment and graphical analysis of THz generation in magnetized collisional plasma with the following set of parameters. CO_2 femtosecond lasers with frequencies $\omega_1 = 2 \times 10^{14}$ rad /s and $\omega_2 = 1.85 \times 10^{14}$ rad/s are chosen. The corresponding wavelengths of lasers are $\lambda_1 = 10.2$ μm and $\lambda_2 = 9.44$ μm with peak intensity of 10^{14} W/cm^2. The graph between normalized THz amplitude and normalized THz frequency is represented in figure 2, for values of static magnetic field ranging from 10 to 50 kG at optimized value of D.C. electric field of 10 kV/cm. From the graph, it is concluded that normalized THz amplitude increases with the decrease in normalized THz frequency and vice versa. It is observed that the THz amplitude acquires maximum value when ω/ω_p approaches 1. One can notice from Fig. 2 that the normalized THz amplitude is maximum corresponding to the magnetic field of 50 kG. It is due to the fact that the external magnetic field modifies the plasma dielectric anisotropic tensor and excites nonlinear current strongly. It results in the enhancement of the normalized THz amplitude with the external magnetic field. Similar results are observed by Mehta et al. [20] with magnetic field range from 54 to 322 kG, but in the present work magnetic field is applied in the range 10 kG to 50 kG which is very much cost-effective feasible.
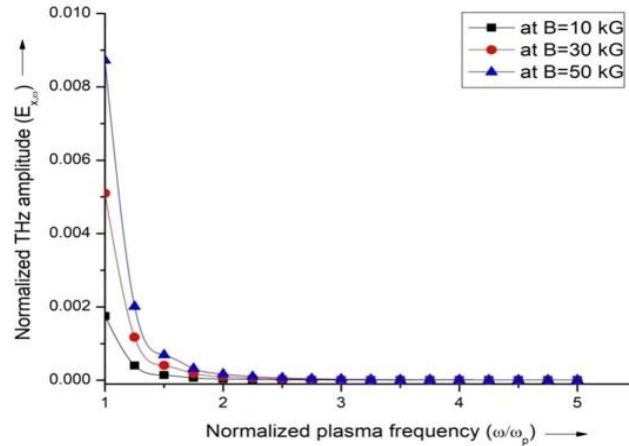
Fig. 2 Plot of normalized amplitude of THz radiation with normalized THz frequency ω/ω_p, at various value of magnetic field ranging from 10 to 50kG
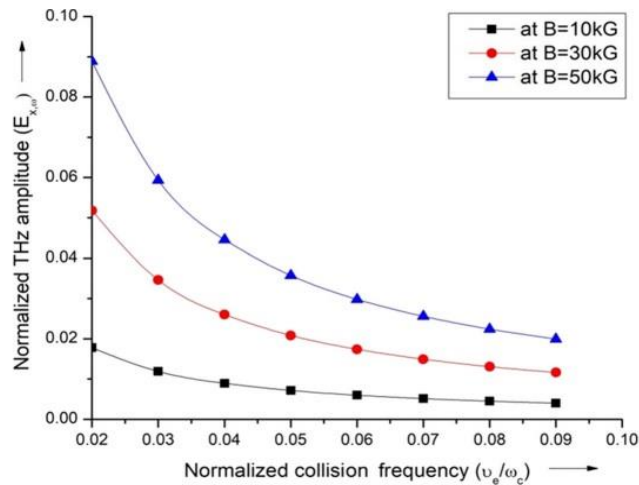
Fig. 3 Plot of normalized amplitude of THz radiation with normalized collision frequency υ_e/ω_c, at electric field 10 kV/cm

In nonlinear system, υ_e is comparable with ω_p. If υ_e is very large as compared to ω_p, then plasma is strongly coupled plasma; otherwise, plasma is weakly coupled plasma. In most of the expressions, υ_e appears together with ω_p and laser frequency ω. Figure 3 shows increase in normalized THz amplitude with the decrease in normalized collision frequency υ_e/ω_c. Due to decrease in collisions in the plasma, the magnitude of the ponderomotive force and hence nonlinear current shows increase. This results in the increase in the normalized THz amplitude. From Fig. 3, one can observe clearly that external magnetic field is useful to decrease the effect of collisions on the normalized THz amplitude.

Fig. 4 Plot of normalized amplitude of THz radiation with normalized electric field, at magnetic field of 30kG
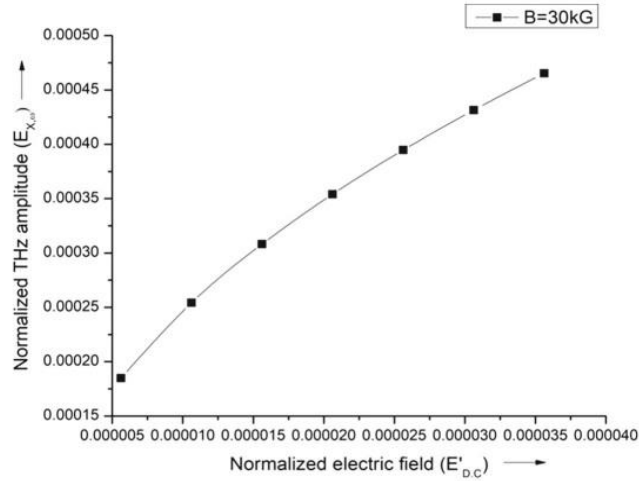
To check the effect of applied D.C. electric field on the normalized THz amplitude, we have drawn graph between normalized THz amplitude and normalized D.C. electric field at optimized value of magnetic field B = 30 kG, as shown in Fig. 4. Due to the applied D.C. electric field $\vec{E}_{D.C}$ (ranging from 10 KV/cm to 30 KV/cm), drift force $|e\,\vec{E}_{D.C}|$ acts on the plasma electrons which increases the nonlinearity of the system and hence helps in the enhancement of normalized THz amplitude. The similar results were observed by Bhasin et al. [17], when they applied static electric field up to 50 kV/cm and obtained the maximum value of normalized THz amplitude up to 4.28×10^{-5}. However, in the present work, we have obtained the better results by applying D.C. electric and static magnetic field and obtain the maximum value of normalized THz amplitude up to 0.465×10^{-3}, for the static electric field of 30 kV/cm.

5 Conclusion

We have proposed a new scheme of THz generation on the basis of filamentation action between the femtosecond laser under the effect of static D.C. electric and magnetic fields in collisional plasma. In this scheme, we have also considered the collisions in magnetized plasma which is important in the nonlinear systems. Due to decrease in the electron-neutral collisions, an increase in the normalized THz amplitude is noticed. The applied D.C. electric field provides drift force to plasma electrons in addition with the ponderomotive force (static and beat frequency type). Both static electric and magnetic fields help to generate THz radiation according to our requirement by varying the values of these fields. On the basis of above results, our scheme provides efficient and cost-effective way to generate THz radiation.

Springer

123

References

1. B.B. Hu, M.C. Nuss, Opt. Lett. **20**, 1716 (1995)
2. Baker C, Lo T, Tribe W.R, Cole B.E, Hogbin M.R and Kemp M.C *Proceedings of the IEEE* 2007 95 1559–1565.
3. K. Ishigaki, M. Shiraishi, S. Suzuki, M. Asada, N. Nishiyama, S. Arai, Electron. Lett. **8**, 582 (2012)
4. A.R. Orlando, G.P. Gallerano, Springers **30**, 1809–1818 (2009)
5. P.H. Siegel, IEEE Trans Microw Theory Tech **50**, 910–928 (2002)
6. D. Dragoman, M. Dragoman, Prog. Quantum. Electron. **28**, 1–66 (2004)
7. F. Sizov, Opto-Electrons Rev **18**, 009–0029 (2010)
8. R.K. Singh, S. Kumar, R.P. Sharma, Contrib. Plasma Phys. **57**, 252–257 (2017)
9. V. Thakur, N. Kant, S. Vij, Phys Scr **95**, 045602 (2020)
10. M. Kumar, V.K. Tripathi, IEEE J Quantum Elect. **48**, 1031–1035 (2012)
11. A.B. Langdon, B.F. Lasinski, Phys. Rev. Lett. **34**, 934 (1975)
12. T.J. Wang, J.F. Daigle, S. Yuan, F. Théberge, M. Châteauneuf, J. Dubois, G. Roy, H. Zeng, S.L. Chin, Phys. Rev. A **83**, 053801 (2011)
13. P. Varshney, V. Sajal, P. Chauhan, R. Kumar, K.N. Sharma, Laser Part. Beams. **32**, 375–381 (2014)
14. A. Braun, G. Korn, X. Liu, D. Du, J. Squier, G. Mourou, Opt Lett. **20**(73), 75 (1995)
15. A. Houard, Y. Liu, B. Prade, V.T. Tikhonchuk, A. Mysyrowicz, Phys. Rev. Lett. **100**, 255006 (2008)
16. T. Löffler, F. Jacob, H.G. Roskos, Appl. Phys. Lett. **77**, 453 (2000)
17. L. Bhasin, V.K. Tripathi, Phys. Plasmas **18**, 123106 (2011)
18. R. McLaughlin, A. Corchia, M.B. Johnston, Q. Chen, C.M. Ciesla, D.D. Arnone, G.A.C. Jones, E.H. Linfield, A.G. Davies, M. Pepper, Appl. Phys. Lett. **76**, 2038 (2000)
19. L. Yu-Tong, W. Wei-Min, L. Chun, S. Zheng-Ming, Chin. Phys. B **21**, 095203 (2012)
20. A. Mehta, J. Rajput, N. Kant, Laser Phys. **29**, 095405 (2019)

124

Production of Terahertz Radiations by Short Pulse Lasers

Sandeep Kumar[1], Niti Kant[1], Shivani Vij[2] , Alka Mehta[1] and Vishal Thakur[1]*

[1].   *Department of Physics, Lovely Professional University, G.T. Road, Phagwara - 144411, Punjab,*

India

[2].   *Department of Applied Sciences, DAV Institute of Engineering and Technology, Jalandhar,*

144008, India

[3].   **E-mail:** vishal20india@yahoo.co.in

Abstract

In this paper, we develop an analytical formalism for THz generation from Laser filaments in the presence of static electric field in the magnetized collisional plasma. Two femtosecond laser pulses with different frequencies undergo filamentation in magnetized collisional plasma to have non-linear coupling in the presence of transverse static electric field. This results in balancing action of static ponderomotive force with pressure gradient force and forms transverse density ripple and non-linear ponderomotive force couple with density ripple to provide strong non-linear transverse current which results in excitation of THz Radiations at resonance. This coupling is further enhanced by electric static field.

Keywords: THz Radiations, magnetized collisional plasma, non-linear ponderomotive force

I. Introduction

In modern era THz radiation has become an important research tool due to its scientific and commercial applications such as Topography, remote sensing [1], medical imaging [2], communication [3], explosives detection [4], spectroscopy [5]. More over THz radiations can also be used to produce second harmonic generation and third harmonic generation[6],which further can be

used in various applications like particle accelerators [7,8] . Out of various schemes proposed in the literature, THz pulse energy achieved from laser filament is very High [9].

Filamentation denotes a peculiar Phenomenon related to propagation of a beam of light through a medium without apparent diffraction. Counter acting the natural spreading of the beam is possible with intense laser pulses owing to optical Kerr effect, which causes a change of refractive index in the medium proportional to the beam intensity. The core of beam is more intense than the wings results in self focusing of beam. One of the main feature of filaments is their ability to generate plasmas in the wave of propagating pulse which in turn modifies narrow band pulse laser into broadband pulse. [10,11] Houard *et al.* [12] studied and observed 3 order of magnitude enhancement of THz energy due to filamentation of femtosecond laser pulse in air in presence of a static Transverse electric field approximate10kv/cm [13,14]. The Laser intensity was approximate 9×10^{13} W/cm^2.

Wu *et al.* [15-17] studied significant enhancement in the efficiency of THz generation, where Transverse magnetic field is applied.

In this paper we provide Theoretical treatment for THz generation from Laser filaments in the presence of static (D.C. biased) electric field in magnetized collisional plasma.

Consider Two Transversely amplitude modulated laser beams with electric fields propagating along z-axis, polarized along y-axis and amplitude modulated along x-axis. To produce magnetized plasma, mag. field is applied along y-axis D.C. electric field is applied across x-axis, which can provide d.c drift to electrons.

The laser exerts a Ponderomotive force F_{qw} as well as ponderomotive static force F_{Pq} on electron. In the steady state, the static Ponderomotive force is balanced by pressure gradient force. It results in Transverse density ripple at zero frequency and wave vector that is $\left(n_{0q}\right)$.

The beat frequency Ponderomotive force is responsible for velocity and density oscillations.

2

126

The density oscillations beats with D.C. drift to produce a Transverse current $J_{\omega,k}$ which is responsible for THz generation. In section II we obtain the expressions for non linear velocity perturbation at THz frequency $\omega = (\omega_1 - \omega_2)$ and wave vectors $k = k1 - k2$, $k + q$ and non linear density perturbation at THz frequency and wave vectors k, $k + q$ by choosing non linear coupling of suitable factors an expression for non linear current density at frequency ω and wave vectors k is obtained. In section III we determine THz wave generation and determine normalized amplitude. In section IV there is a discussion of results. Most of the researchers have not considered the collisions between electrons and neutrals in plasmas but in reality collisions are present in every non linear system. In this paper we will also discuss the resonance condition and the effect of collisions on it.

II. Production of Non-Linear Current

Consider a magnetized collisional plasma of electrons density $n^0{}_0$ having a D.C. electric field applied along X-axis. Due to the $\vec{E}_{d.c}$ electrons will acquire drift velocity

$$\vec{V}_{d.c} = \frac{-e\vec{E}_{d.c}}{m\nu_e}$$

(1)

Where $-e$ = charge of electron
   m = mass of electron
   ν_e = collisional frequency of electron

We incident two transversely amplitude modulated (by filamentation) lasers in to the plasma which is magnetized collisional plasma.
The electric fields of lasers are

$$\vec{E}_j = \hat{y}\, A_{j0}\left[1 + \mu_j cosqx\right] e^{-i(\omega_j t - k_j z)} \ where\ j = 1,2$$

(2)

μj = index of modulation.
Frequency difference of lasers $\omega = \omega_1 - \omega_2$ lies in THz range.

The laser filaments import oscillatory velocities to plasma electrons.

$$\vec{V}_J = \frac{-e\,\vec{E}_J}{m(\iota\omega_j - \ \upsilon)}$$

(3)

3
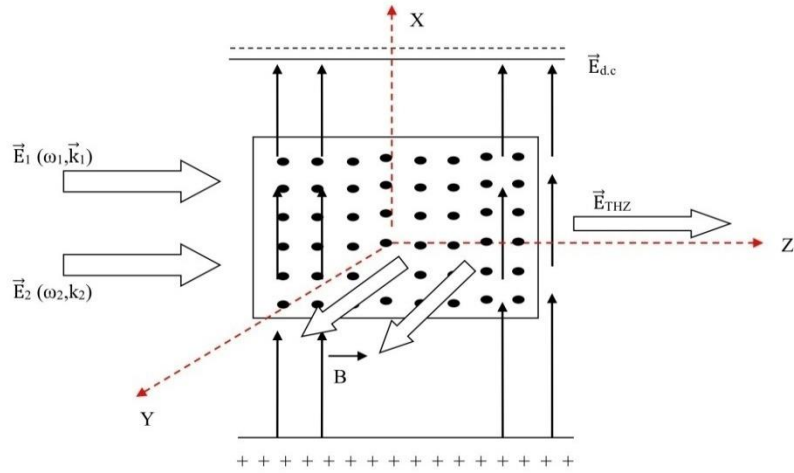
(*Scheme of THz generation irradiating Lasers in magnetized Plasma in the presence of D.C. electric field*)

(Figure: 1)

They also exert static Ponderomotive force

$F_{pq} = e \vec{V} \phi_{pq}$ and beat frequency ponderomotive force

$F_{p\omega} = e \vec{V}_{p\omega}$

$$\varphi_{p\omega} = \frac{e\, A_{10} A_{20}}{2\, m\, (i\omega_1 - v_e)(i\omega_2 - v_e)} \left\{ 1 + \left(\frac{\mu_1 + \mu_2}{2}\right) e^{\iota qx} \right\} e^{-\iota(\omega t - k_2 x)}$$

(5)

$$\varphi_{p\omega} = \frac{e}{4 m T_e} \left\{ \frac{A_{10}^2 \mu_1}{(\iota\omega_1 - v_e)} + \frac{A_{20}^2 \mu_2}{(\iota\omega_2 - v_e)^2} \right\} e^{\iota qx}$$

(6)

T_e , the equilibrium temperature of electrons

The beat frequency ponderomotive force, collisional force and magnetic field force will provide oscillatory velocity to electrons.
By using equations of motion,

4

$$\vec{V}_P^{NL} = \frac{\vec{F}_P^{NL}}{m(\upsilon - \iota\omega)} - \frac{\vec{F}_P^{NL}\vec{\omega}_c}{m(\upsilon - \iota\omega)^2} - \frac{\omega_c^2}{(\upsilon - \iota\omega)^2}\vec{V}_P^{NL}$$

$$(7)$$

$\vec{\omega}_c = e\,\vec{B}_y/m$ is cyclotron frequency of electrons

$$\vec{V}_x^{NL} = \frac{(\upsilon - \iota\omega)(F_x\hat{x} + F_z\hat{z})}{[m(\upsilon - \iota\omega)^2 + \omega_c^2]} + \frac{\omega_c F_z\hat{x} - \omega_c F_x\hat{z}}{[m(\upsilon - \iota\omega)^2 + \omega_c^2]}$$

$$(8)$$

The components of velocity along X and Z axis

$$\vec{V}_x^{NL} = \frac{(\upsilon - \iota\omega)F_x}{m(\upsilon - \iota\omega)^2 + \omega_c^2} + \frac{\omega_c}{m(\upsilon - \iota\omega)^2 + \omega_c^2}F_z$$

$$(9)$$

And

$$\vec{V}_z^{NL} = \frac{(\upsilon - \iota\omega)F_z}{m(\upsilon - \iota\omega)^2 + \omega_c^2} - \frac{\omega_c}{m(\upsilon - \iota\omega)^2 + \omega_c^2}F_x$$

$$(10)$$

$Put\ [(\upsilon - \iota\omega)^2 + \omega_c^2] = \omega_\alpha^2$

$$\vec{V}_x^{NL} = \frac{(\upsilon - \iota\omega)F_x}{m\omega_\alpha^2} + \frac{\omega_c}{m\omega_\alpha^2}F_z$$

$$(11)$$

$$\vec{V}_z^{NL} = \frac{(\upsilon - \iota\omega)F_z}{m\omega_\alpha^2} + \frac{\omega_c}{m\omega_\alpha^2}F_x$$

$$(12)$$

$$\begin{aligned}
\vec{V}_x^{NL} = {} & \frac{(\upsilon - \iota\omega)}{m\omega_\alpha^2}\left(\frac{e^2 A_{10}A_{20}(\mu_1 + \mu_2)}{4m(\iota\omega_1 - \upsilon_e)(\iota\omega_2 + \upsilon_e)}\right)e^{-\iota(\omega t - kz - qx)}(iq)\hat{x} \\
& + \frac{\omega_c}{m\omega_\alpha^2}\left(\frac{e^2 A_{10}A_{20}}{2m(\iota\omega_1 - \upsilon_e)(\iota\omega_2 + \upsilon_e)}\right)e^{-\iota(\omega t - kz)}(ik)\hat{z} \\
& + \frac{\omega_c}{m\omega_\alpha^2}\left(\frac{e^2 A_{10}A_{20}(\mu_1 + \mu_2)}{4m(\iota\omega_1 - \upsilon_e)(\iota\omega_2 + \upsilon_e)}\right)e^{-\iota(\omega t - kz - qx)}(iq)\hat{z}
\end{aligned}$$

$$(13)$$

5

129

$$= \frac{\iota[(v - \iota\omega)q\,\hat{x} + \omega_c k\,\hat{z}]}{4m^2\omega_\alpha^2(\iota\omega_1 - v_e)(\iota\omega_2 + v_e)}\left(e^2 A_{10}A_{20}(\mu_1 + \mu_2)\right)e^{-\iota(\omega t - kz - qx)}$$
$$+ \frac{\iota\omega_c k\,\hat{z}}{2\omega_\alpha^2(\iota\omega_1 - v_e)(\iota\omega_2 + v_e)}(e^2 A_{10}A_{20})e^{-\iota(\omega t - kz)}$$

$$\vec{V}_z^{NL} = \frac{(v - \iota\omega)}{m\omega_\alpha^2}\left(\frac{e^2 A_{10}A_{20}(ik)\hat{z}}{2m(\iota\omega_1 - v_e)(\iota\omega_2 + v_e)}\right)e^{-\iota(\omega t - kz)}$$
$$+ \frac{(v - \iota\omega)}{m\omega_\alpha^2}\left(\frac{e^2 A_{10}A_{20}(\mu_1 + \mu_2)(ik)}{4m(\iota\omega_1 - v_e)(\iota\omega_2 + v_e)}\right)e^{-\iota(\omega t - kz - qx)}(iq)\hat{z}$$
$$- \frac{\omega_c}{m\omega_\alpha^2}\left(\frac{e^2 A_{10}A_{20}(\mu_1 + \mu_2)(iq)}{4m(\iota\omega_1 - v_e)(\iota\omega_2 + v_e)}\right)e^{-\iota(\omega t - kz - qx)}(iq)\hat{x}$$

$$(14)$$

$$= \frac{\iota[(v - \iota\omega)k\,\hat{z} - \omega_c q\,\hat{x}]}{4m^2\omega_\alpha^2(\iota\omega_1 - v_e)(\iota\omega_2 + v_e)}\left(e^2 A_{10}A_{20}(\mu_1 + \mu_2)\right)e^{-\iota(\omega t - kz - qx)}$$
$$+ \frac{\iota(v - \iota\omega)k\,\hat{z}}{2\omega_\alpha^2(\iota\omega_1 - v_e)(\iota\omega_2 + v_e)}(e^2 A_{10}A_{20})e^{-\iota(\omega t - kz)}$$

Along X-axis

$$\vec{n}_{w,k}^{NL} = \frac{n_0^0 e^2 A_{10}A_{20}[ik^2]\omega_c}{2m^2\omega\omega_\alpha^2(\iota\omega_1 - v_e)(\iota\omega_2 + v_e)}e^{-\iota(\omega t - kz)}$$

$$\vec{n}_{w,k+q}^{NL} = \frac{n_0^0 e^2 (A_{10}A_{20})(\mu_1 + \mu_2)}{4m^2(\iota\omega_1 - v_e)(\iota\omega_2 + v_e)} - \frac{\iota[(v - \iota\omega)^2 q^2 + \omega_c k^2]}{\omega\omega_\alpha^2}e^{-\iota(\omega t - kz - qx)}$$

$$(15)$$

Along Z-axis

$$\vec{n}_{w,k}^{NL} = \frac{n_0^0 e^2 A_{10}A_{20}[ik^2](v - \iota\omega)}{2m^2\omega\omega_\alpha^2(\iota\omega_1 - v)(\iota\omega_2 + v)}e^{-\iota(\omega t - kz)}$$

$$= \frac{n_0^0 e^2 (A_{10}A_{20})(\mu_1 + \mu_2)}{4m^2(\iota\omega_1 - v)(\iota\omega_2 + v)} - \frac{\iota[(v - \iota\omega)^2 k^2 + \omega_e^2 q^2]}{\omega\omega_\alpha^2}e^{-\iota(\omega t - kz - qx)}$$

$$(16)$$

Non linear current density at ω, k erases due to coupling between

(i)   Equilibrium plasma density n_0^0 and non linear velocity $\vec{n}_{w,k}^{NL}$

(ii) Non linear density perturbation $\vec{n}_{w,k}^{NL}$ and dc electrons velocity $\vec{V}_{d.c}$

(iii) Zero frequency transverse density ripple $n_{0,q}$ and non linear velocity $\vec{n}_{\omega,w,k}^{NL}$

$$\vec{J}_{\omega,k}^{NL} = -n_{o,q}^* \, e \, \vec{V}_{\omega,\vec{k}+\vec{q}}^{NL} \; - \; n_0^0 \, e \, \vec{V}_{\omega,\vec{k}}^{NL} \; - \; \vec{n}_{\omega,\vec{k}}^{NL} \, e \, \vec{V}_{d.c}$$

$\underrightarrow{- n_{o,q}^* \, e \, \vec{V}_{\omega,\vec{k}+\vec{q}}^{NL}}$:-

$$= \frac{-n_0^0 e^3}{4mT_e} \left\{ \frac{A_{10}^2 \mu_1}{(\iota\omega_1 - v_e)^2} + \frac{A_{20}^2 \mu_2}{(\iota\omega_2 + v_e)^2} \right\} e^{-iqx} \left(e^2 A_{10} A_{20} (\mu_1 + \mu_2) \right) \frac{i[(v - \iota\omega)q\hat{x} + \omega_c k\hat{z}]}{4m^2 \omega_\alpha^2 (\iota\omega_1 - v_e)(\iota\omega_2 + v_e)} e^{-\iota(\omega t - kz - qx)}$$

$$= \frac{-n_0^0 e^3}{4mT_e} \left\{ \frac{A_{10}^2 \mu_1}{(\iota\omega_1 - v_e)^2} + \frac{A_{20}^2 \mu_2}{(\iota\omega_2 + v_e)^2} \right\} e^{-iqx} \left(e^2 A_{10} A_{20} (\mu_1 + \mu_2) \right) \frac{i[(v - \iota\omega)k\hat{z} + \omega_c q\hat{x}]}{4m^2 \omega_\alpha^2 (\iota\omega_1 - v_e)(\iota\omega_2 + v_e)} e^{-\iota(\omega t - kz - qx)}$$

$$= \frac{-n_0^0 e^3}{4mT_e} \left\{ \frac{A_{10}^2 \mu_1}{(\iota\omega_1 - v_e)^2} + \frac{A_{20}^2 \mu_2}{(\iota\omega_2 + v_e)^2} \right\} e^{-iqx} \frac{\left(e^2 A_{10} A_{20} (\mu_1 + \mu_2) \right)}{4m^2 \omega_\alpha^2 (\iota\omega_1 - v_e)(\iota\omega_2 + v_e)} i[(v - \iota\omega - \omega_c)q\hat{x} + ((v - \iota\omega)\omega_c)k\hat{z}] e^{-\iota(\omega t - kz)}$$

$$= -n_0^0 e^3 \frac{A_{10} A_{20} (\iota)[(v - \iota\omega + \omega_c)k\hat{z}]}{2m^2 \omega_\alpha^2 (\iota\omega_1 - v_e)(\iota\omega_2 + v_e)} e^{-\iota(\omega t - kz)}$$

$\underrightarrow{-n_{\omega,k}^{NL} \, e \, \vec{V}_{d.c}}$:-

$$= \frac{-n_0^0 e^3 A_{10} A_{20} [ik^2] \omega_c}{2m^2 \omega \, \omega_\alpha^2 (\iota\omega_1 - v_e)(\iota\omega_2 + v_e)} \left(\frac{-e\vec{E}_{d.c}}{mv_e} \right) e^{-\iota(\omega t - kz)}$$

$$= \frac{-n_0^0 e^3 A_{10} A_{20} [ik^2](v - \iota\omega)}{2m^2 \omega \, \omega_\alpha^2 (\iota\omega_1 - v_e)(\iota\omega_2 + v_e)} \left(\frac{-e\vec{E}_{d.c}}{mv_e} \right) e^{-\iota(\omega t - kz)}$$

$$= \frac{-n_0^0 e^4 A_{10} A_{20} \vec{E}_{d.c}}{2m^3 \omega \, \omega_\alpha^2 (\iota\omega_1 - v_e)(\iota\omega_2 + v_e)} ik^2 [\omega_c + v - \iota\omega] e^{-\iota(\omega t - kz)}$$

$\vec{J}_{X\,\omega,k}^{NL}$

$$= \frac{-n_0^0 e^4 A_{10} A_{20} [i]}{2m^3 \omega_\alpha^2 (\iota\omega_1 - v_e)(\iota\omega_2 + v_e)} \left\{ \frac{K^2 \vec{E}_{d.c}[(v - \iota\omega + \omega c)]}{\omega v_e} - \frac{eq(\mu_1 + \mu_2)}{8T_e} \left(\frac{A_{10}^2 \mu_1}{(\iota\omega_1 - v_e)^2} + \frac{A_{20}^2 \mu_2}{(\iota\omega_1 + v_e)^2} \right) (v - \iota\omega - \omega_c) \right\} e^{-\iota(\omega t - kx)}$$

(17)

$\vec{J}^{NL}_{z\,\omega,k}$

$$= \frac{-n_0^0 e^4 A_{10} A_{20}[i]}{2m^3 \omega_\alpha^2 (i\omega_1 - v_e)(i\omega_2 + v_e)} \left\{ \frac{ek(\mu_1 - \mu_2)}{8T_e} \left(\frac{A_{10}^2 \mu_1}{(\iota\omega_1 - v_e)^2} + \frac{A_{20}^2 \mu_2}{(\iota\omega_1 + v_e)^2} \right)(v - \iota\omega + \omega_c) \right.$$
$$\left. + \frac{mk[(v - \iota\omega) + \omega_c]}{e} \right\} e^{-\iota(\omega t - kz)}$$

(18)

III. Generation of THz radiations

The wave equation governing the propagation of THz waves can be written as:-

$$-\nabla^2 \vec{E} + \nabla.\left(\nabla.\vec{E} \right) = \frac{4\pi\iota\omega}{c^2} \vec{J}^{NL} + \frac{\omega^2}{c^2} \bar{\varepsilon} \vec{E}$$

In the presence of magnetic field along Y-axis in collisional plasma, dielectric constant assumes the form of anisotropic Tensor $\bar{\varepsilon}$

X and Z components of THz field are

$$-\frac{\omega^2}{c^2} \epsilon_{zz} E_z - \frac{\omega^2}{c^2} \epsilon_{zx} E_x = \frac{+4\pi\iota\omega}{c^2} \vec{J}^{NL}_z$$

And

$$-2ik'\frac{\partial E_x}{\partial z} + k'^2 E_x - \frac{\omega^2}{c^2} \epsilon_{xz} E_z - \frac{\omega^2}{c^2} \epsilon_{xx} E_x = \frac{+4\pi\iota\omega}{c^2} \vec{J}^{NL}_x$$

$$-2ik'\frac{\partial E_x}{\partial z} + \left(k'^2 - \frac{\omega^2}{c^2} \left(\epsilon_{xx} + \frac{\epsilon_{zx}^2}{\epsilon_{zz}} \right) \right) E_x = \frac{+4\pi\iota\omega}{c^2} \left(\vec{J}^{NL}_x + \frac{\epsilon_{zx}}{\epsilon_{zz}} \vec{J}^{NL}_z \right)$$

By using phase matching condition

$$k'^2 - \frac{\omega^2}{c^2} \left(\epsilon_{xx} + \frac{\epsilon_{zx}^2}{\epsilon_{zz}} \right) = 0$$

$$k'^2 = \frac{\omega^2}{c^2} \left\{ 1 - \frac{\omega_P^2(v - \iota\omega)}{\iota\omega\omega_\alpha^2} + \frac{(-\omega_c^2 \omega_P^4)}{\frac{\omega^2 \omega_\alpha^4}{1 - \frac{\omega_P^2(v - \iota\omega)}{\iota\omega\omega_\alpha^2}}} \right\}$$

$$k_1 - k_2 + q = \frac{\omega}{c} \left\{ 1 - \frac{\omega_P^2}{\iota\omega\omega_\alpha^2} \left((v - \iota\omega) - \frac{\omega_c^2 \omega_P^2}{\iota\omega\omega_\alpha^2 - \omega_P^2(v - \iota\omega)} \right) \right\}^{1/2}$$

132

By Using above Phase matching condition electric field component along the X-axis

$$E_x = \frac{-2\pi\omega}{k'c^2}\left\{ j^{NL}_{x\,\omega,k} + \frac{\epsilon_{zx}}{\epsilon_{zz}} j^{NL}_{z\omega,k} \right\} z$$

$$E_x = \frac{-2\pi\omega z}{k'c^2}\left(\frac{-n_0^0 e^4 A_{10} A_{20}[\iota]}{2m^3\omega_a^3(\iota\omega_1 - v_e)(\iota\omega_2 + v_e)}\right)\left(\frac{K^2\vec{E}_{d.c}(v - \iota\omega + \omega_c)}{\omega v_e} - \frac{eq(\mu_1+\mu_2)}{8T_e}\frac{A_{10}^2\mu_1}{(\iota\omega_1 - v_e)^2} + \frac{A_{20}^2\mu_2}{(\iota\omega_2 + v_e)^2}\right)(v$$
$$- \iota\omega + \omega_c) + \frac{\omega_c\omega_P^2}{\iota\omega\omega_a^2 - \omega_P^2(v-\iota\omega)}\left\{\frac{ek(\mu_1+\mu_2)}{8T_e}\left\{\frac{A_{10}^2\mu_1}{(\iota\omega_1-v_e)^2} + \frac{A_{20}^2\mu_2}{(\iota\omega_2+v_e)^2}\right\}\right\}(v - \iota\omega + \omega_c)$$
$$+ \frac{mK}{e}(v - \iota\omega + \omega_c)$$

$$(19)$$

The normalized THz amplitude

$$\frac{eE_x}{m\omega_P C} = \frac{\omega'z'V_{10}'V_{20}'\iota}{4k''\omega^{02}(\iota\omega_{P1} - v_e')(\iota\omega_{P2} + v_e')}\left\{\frac{K_0^2 E_{d.c}'(v_0' - \iota\omega' + \omega_c')}{\omega'v_e'}\right.$$
$$+ \left(\frac{K_0}{8}\left(\frac{\omega_c'}{\iota\omega'\omega^{02} - (v_e' - \iota\omega')}\right) - \frac{q'}{8}\right)\frac{(\mu_1+\mu_2)}{V_{th}'}\left(\frac{V_{10^2}'\mu_1}{(\iota\omega_{P1} - v_e')^2} + \frac{V_{20^2}'\mu_2}{(\iota\omega_{P2} + v_2')^2}\right)(v_e' - \iota\omega' - \omega_c')$$
$$\left. + \left(\frac{\omega_c'}{\iota\omega'\omega^{02} - (v_e' - \iota\omega')}\right)(v_e' - \iota\omega' - \omega_c')\right\}$$

$$(20)$$

Where $V_{10}' = eA10/m\omega pC$, $V_{20}' = eA20/m\omega pC$, $\omega' = \omega/\omega p$, $z' = \omega pZ/c$, $\omega p1 = \omega1/\omega2$. $\omega p2 = \omega2/\omega p$

$v_e' = vc/\omega p$, $E_{d.c}' = e\,E_{d.c}'\,/\,m\omega pC$. $K^0 = CK/\omega p$, $K'' = CK'/\omega p$, $\omega_c' = \omega c/\omega p$, $q' = Cq/\omega p$

$V_{th}' = V_{th}\,/\,C$

$\omega_1 = 2.4\,x\,10^{14}\,rad/s$, $\omega_2 = 2.1\,x\,10^{14}\,rad/s$, $E_{d.c}' = 0.053$, $\omega_P = 2.0\,x10^{13}\,rad/s$, $\mu_1 = \mu_2 = 0.3$, q'= 0.3

$\omega' = 2.0 \to 5.0$ $V_{10}' = V_{20}' = 0.005 \to 0.01$, $\omega_{p1} = 12$, $\omega_{p2} = 10.5$, $v_e = 1.5\,x\,10^{13}\,rad/s$, B = 5 T

$\omega_c = 0.879\,x\,10^{12}\,rad/s$, $\omega_c' = 0.04$, $v_e' = 0.75$, $K_1 = 0.8\,x\,10^6\,m$, $K_2 = 0.7\,x\,10^6\,m$, $K^0 = 1.5$

q' = 0.3, $q = 0.2\,x\,10^5\,m$, K' = 1.2 $x\,10^5$, K'' = 1.8, Z' = 100, $V_{th}' = 0.0067$

9

6.   Jyoti Rajput, Niti kant , Harjit Singh, Vikas Nanda, " Resonant third harmonic generation of a short pulse laser in plasma by applying a wiggler magnetic field." Optics Communications Volume 282, issue 23, 1 December 2009, Pages-4614-4617.

7.   Jyoti Rajput, Niti kant and Arvinder Singh, " Electron acceleration due to a circularly polarized laser pulse on a downward plasma density ramp in the presence of an azimuthal magnetic field."AIP Conference Proceedings Volume 2006, Issue 1 10.1063/1.5051281.

8.   Niti Kant, Jyoti Rajput, Arvinder Singh. "Electron acceleration from rest to GeV energy by chirped axicon Gaussian laser pulse in vaccum in the presence of wiggler magnetic field." Volume 26, March 2018, Pages 16-22

9.   L. Bhasin, V.K. Tripath, "THz generation from Laser filaments in the presence of static electric field in plasma", Phys. Plasma 18,123106.

10.   Prateek Varohnety, Vivek sajal, Prashant chuhan, Ravinder Kumar and Navneet .K. Sharma, "Effects of Transverse static by heating of two Transversely modulated Gaussian Laser beams in plasma". Laser and particle beams (2014) 32, 375-381

11.   S. Tzortakis, M. Franco, Y.B. Andre, A. Chiron, B. Lenourouz, B. Prade and A. Mysyrowicz, 1989 Phys. Rev. E 63 F 3505

12.   A. Couairon. 2003 Phys. Rev. A 68015

13.   R. MeLaughlin, A. Corohia, M.B. Johnston Q. Chen, C.M. Clesla, D.D. Araone, G.A.C. Jones, E.H. Linfield, A.G. d and M. Papper 2000, Appl. Phys. Letter 76 2038

14.   A. Hourd, Y.Liu, B. Prade, V.T. Tikhanchuk and A. Myoyzovie Phys. Rev Lett. 100, 255006(2008)

15.   H.C. Wu, Z.M. Sheng, Q.L. Dose M. Ku and J. Zhang 2001, Physq., Rev. E 75016407

16.   Niti Kant, Jyoti Rajput, Pankaj Giri, Arvinder Singh. "Effect of axial magnetic field on axicon laser-induced acceleration."Volume 18, March 2016, Pages 20-25.

17.   Arvinder Singh, Jyoti Rajput and Niti Kant. "Combined influence of azimuthal and axial

magnetic fields on resonant electron acceleration in plasma." Published 26 October 2017

Laser Physics, Volume 27, Number 11.

Resonant Terahertz Generation by the Interaction of Laser Beams with Magnetized Anharmonic Carbon Nanotube Array

Sandeep Kumar[1] · Shivani Vij[2] · Niti Kant[1] · Vishal Thakur[1]

Abstract

In this novel scheme, a theoretical analysis of resonant terahertz (THz) generation in the array of magnetized anharmonic carbon nanotubes (CNTs) is presented. Two laser beams with frequencies (ω_1, ω_2) and wavenumbers (k_1, k_2) propagate through the array of vertically aligned anharmonic CNTs in the presence of an applied static magnetic field. It provides different displacements to the various electrons of CNTs. Due to this, restoration force varies nonlinearly with the displacements of electrons and hence results in anharmonicity. This anharmonicity plays a significant role in the enhancement of absorption of laser beams by the electrons of CNTs. The nonlinear restoration force produces the current which is responsible for the THz generation. It is observed that the applied magnetic field (170 to 235 kG) helps in the enhancement of the THz generation by increasing the nonlinearity of the system. The impact of dimensions, inter-tube separation, and density of CNTs on the THz amplitude has also been analyzed.

Keywords Carbon nanotube · Nonlinear restoration force · Anharmonicity · Inter-tube separation · Magnetic field

Introduction

In this modern world, THz technology has attained great importance due to compact and highly efficient THz sources for various applications in many fields like security protection [1], medical sciences [2–4], and broadband communication [5]. The various researchers have proposed several schemes for THz wave generation to provide compact, efficient, and reliable THz sources. For this purpose, they have used different mechanisms to enhance the amplitude of THz radiation. Some of these are by beating of two chirped-pulse laser beams in spatially periodic density plasma [6], the interaction of laser filaments in the presence of a static electric field in a magnetized collision plasma [7], laser coupling to an anharmonic CNT array [8], nonlinear mixing of laser beams [9], and by applying a magnetic field on an array of CNTs [10–12]. The CNTs are considered very reliable and effective sources for THz generation, due to their compact size, large current density, high electrical conductivity, and excellent combination of transverse-longitudinal dimensions. The CNTs are considered a more favorable medium for the efficient generation of terahertz radiation [13]. Moreover, CNTs are also helpful in the strong absorption of the laser beam [14] due to which generated THz amplitude is enhanced. Titova et al. [15] have proposed the generation of THz radiation by using single-walled CNTs, excited by femtosecond laser beams. Batrakov et al. [16] and Portnoi et al. [17] have explained and reviewed THz generation processes in CNTs to increase the efficiency of THz generation. Wang and Wu [18] studied the properties of THz radiation experimentally, emitted by CNT antenna. Dragoman and Dragoman [19] have studied the characteristics of metallics, single-walled CNTs as a THz antenna. Dagher et al. [20] have studied the amplification of THz radiation in metallic CNTs under the influence of the D.C. magnetic field and observed enhancement in the normalized amplitude of THz radiation.

In the present paper, we propose a new scheme for THz generation by irradiating two co-propagating laser beams of nearly equal frequencies on vertically aligned hollow anharmonic CNTs in the presence of an external static magnetic field. In this, we are using an array of CNTs to ease the propagation of THz radiation. A single-walled

✉ Vishal Thakur
  vishal20india@yahoo.co.in

[1] Department of Physics, Lovely Professional University, G.T. Road, Phagwara - 144411, Punjab, India

[2] Department of Applied Sciences, DAV Institute of Engineering & Technology, Jalandhar 144008, India

🙎 Springer

carbon nanotube is generally modeled as a hollow cylinder [21] to calculate electrical and optical conductivity. But the response of these nanotubes towards the transverse electric and magnetic fields is assumed as solid cylindrical tubes [22–24]. This assumption is reasonable because the diameter of CNTs is very small and the density of atoms is very high. The array of anharmonic CNTs is grown over the glass dielectric surface. Here, restoration force of electrons of CNTs is a non-linear function of electron displacements in CNTs. In the 2nd segment of the paper, we derive nonlinear current density by using the concept of resonance absorption. In the 3rd segment, THz wave dynamics is provided by using standard equations of wave propagation. In the last segment, a discussion of results with the conclusion is provided.

Nonlinear Current Density

Consider an array of vertically aligned anharmonic CNTs grown over the dielectric surface of glass ($\epsilon_r = 2.5$). This arrangement of CNTs can be obtained by the chemical vapor deposition (CVD) process. It is because, in the CVD process, radius, length, wall number, and alignment of CNTs can be easily controlled [25, 26]. There are n_c number of CNTs per unit area given by $n_c = 1/d^2$, where d is known as inter-tube separation. The term n_0 is the number density of free electrons of CNTs. The inner and outer radii of each CNT are denoted by a and b respectively. The length of CNT is represented by L, parallel to the y-axis, and perpendicular to the x–z plane as shown in Fig. 1. The external magnetic field $\vec{B}$ is applied along the y-axis, parallel to the axis of CNTs. The laser beams with nearly equal angular frequencies (ω_1, ω_2) and wavenumbers

(k_1, k_2) propagate through an array of anharmonic CNTs with electric field profiles,

$$\vec{E}_j = \hat{x} A_j e^{-i(\omega_j t - k_j z)} ; j = 1,2 \tag{1}$$

The laser beams ionize the atoms of CNTs and impart finite oscillatory velocity to the free electrons of CNTs. The electrons of CNTs get separated from the ion cylinder with a displacement of $\vec{\Delta}$. When the displacement $\vec{\Delta}$ is perpendicular to the axis of CNT, a space-charge electric field is created. This field is represented by the overlapped region of the electron cylinder and ion cylinder in Fig. 2. The net space charge electric field $\vec{E}$ is the vector sum of the space-charge electric field due to ion cylinder $\vec{E}_{ion}$ and electron cylinder $\vec{E}_{ele}$.

$$\vec{E} = \vec{E}_{ion} + \vec{E}_{ele} \tag{2}$$

The interior space-charge electric field due to ion cylinder at a point (r, φ, z) is

$$\vec{E}_{ion} = \frac{n_0 e (r^2 - a^2)}{2\epsilon} \frac{\vec{r}}{r^2} \tag{3}$$

where, e is the electronic charge and $\epsilon = \epsilon_0 \epsilon_r$ is known as the electric permittivity of the medium. The interior space-charge electric field due to the electron cylinder shifted by displacement $\vec{\Delta}$ with the respect to the ion cylinder is given as,

$$\vec{E}_{ele} = \frac{-n_0 e}{2\epsilon} \left[\left| \vec{r} - \vec{\Delta} \right|^2 - a^2 \right] \left[\frac{\vec{r} - \vec{\Delta}}{\left| \vec{r} - \vec{\Delta} \right|^2} \right] \tag{4}$$

Substituting Eqs. (3) and (4) in Eq. (2), the net space charge electric field at the point (r, φ, z) would be
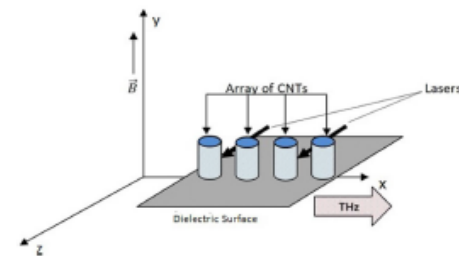

Fig. 1 Schematic of THz generation by the interaction of laser beams with vertically aligned anharmonic carbon nanotube array in the presence of an external magnetic field
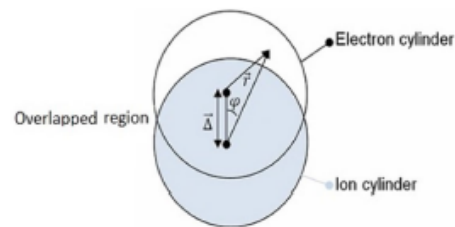

Fig. 2 Shifting of the electron cylinder by distance $\vec{\Delta}$ with respect to the ion cylinder

137

$$\vec{E} = \frac{n_0 e (r^2 - a^2)}{2\epsilon} \frac{\vec{r}}{r^2} - \frac{n_0 e}{2\epsilon_0} \left[\left| \vec{r} - \vec{\Delta} \right|^2 - a^2 \right] \left[\frac{\vec{r} - \vec{\Delta}}{\left| \vec{r} - \vec{\Delta} \right|^2} \right] \quad (5)$$

The displacement of the electrons parallel to the CNT axis is zero but non-zero along the perpendicular direction (x-axis). Therefore, the expression of x-component of space charge electric field can be derived from Eq. (5),

$$E_x = \frac{n_0 e}{2\epsilon} \left[\left(1 + \frac{a^2}{r^2} \right) \Delta_x + \left(\frac{5\cos\varphi}{r} + \frac{4\cos^2\varphi}{r} - \frac{(r^2 - a^2)}{r^3} \cos\varphi \right) \Delta_x^2 \right] \quad (6)$$

Corresponding to the x-component of space charge electric field, the restoring force for each electron along the x-axis can be obtained by using the relation, $F_x = -eE_x$,

$$F_x = \frac{-n_0 e^2}{2\epsilon} \left[\left(1 + \frac{a^2}{r^2} \right) \Delta_x + \left(\frac{5\cos\varphi}{r} + \frac{4\cos^2\varphi}{r} - \frac{(r^2 - a^2)}{r^3} \cos\varphi \right) \Delta_x^2 \right] \quad (7)$$

Due to anharmonicity, the restoration force is not the same for all the electrons. Some of the electrons experience a weak restoration force, whereas others experience a strong restoration force. Hence, we need to calculate the φ (average) and the r (average) of restoration force to obtain its linear (F_{Lx}) and nonlinear components (F_{NLx}).

$$\langle F_{Lx} \rangle = -\frac{n_0 e^2}{2\epsilon} \frac{\int_a^b \left(1 + \frac{a^2}{r^2} \right) 2\pi r . dr}{\int_a^b 2\pi r . dr} \Delta_x \text{ and } \langle F_{NLx} \rangle = -\frac{n_0 e^2}{2\epsilon} \left(\frac{1}{2\pi} \right) \int_0^{2\pi} \left(\frac{5\cos\varphi}{r} + \frac{4\cos^2\varphi}{r} - \frac{(r^2 - a^2)}{r^3} \cos\varphi \right) d\varphi \Delta_x^2$$

Solving these, net average restoration force is given by

$$\langle F_{Lx} \rangle + \langle F_{NLx} \rangle = \frac{-m\omega_P^2}{2\epsilon_r} \Delta_x \left[1 + \beta + \alpha \Delta_x \right] \quad (8)$$

where, $\omega_P = \left[n_0 e^2 / m\epsilon_0 \right]^{1/2}$ is the plasma frequency and m is the electronic rest mass. $\beta = 2 log_e (b/a) / \left(b^2 / a^2 - 1 \right)$ and $\alpha = 4 / (b + a)$ are known as characteristic parameters and anharmonicity factors respectively. Both the terms are responsible for nonlinear mixing in the response. The numerical values of both β and α depend upon the inner and outer radii of CNTs.

As the static magnetic field $\vec{B}$ is applied along the y-axis, therefore, magnetic force $F_B = e \left(\vec{v} \times \vec{B} \right) / c$ can be resolved into their x and z components, $F_{Bx} = -ev_z B/c$ and $F_{Bz} = ev_x B/c$ respectively.

Under the influence of electric fields of the lasers beams, an external static magnetic field $\vec{B}$, and space charge electric field, the displacement of electrons in CNTs is governed by the following equations:

$$\frac{d^2 \Delta_x}{dt^2} + \frac{\omega_P^2}{2\epsilon_r} \left(1 + \beta + \alpha \Delta_x \right) \Delta_x + \frac{F_{Bx}}{m} + \upsilon \frac{d\Delta_x}{dt} = \frac{-eE_x}{m} \quad (9)$$

$$\frac{d^2 \Delta_z}{dt^2} + \frac{F_{Bz}}{m} + \upsilon \frac{d\Delta_z}{dt} = \frac{-eE_z}{m} \quad (10)$$

where, υ represents electron collision frequency, which is lesser than ω.

Simplifying Eqs. (9) and (10), we get

$$-\omega^2 \Delta_x + \frac{\omega_P^2}{2\epsilon_r} \left(1 + \beta + \alpha \Delta_x \right) \Delta_x + i\omega\omega_c \Delta_z - i\omega\upsilon\Delta_x = \frac{-eE_x}{m} \quad (11)$$

$$-\omega^2 \Delta_z - i\omega\omega_c \Delta_x - i\upsilon\omega\Delta_z = \frac{-eE_z}{m} \quad (12)$$

where $\omega_c = eB/mc$ is known as the cyclotron frequency of plasma electrons.

By solving Eqs. (11) and (12), we get

$$\Delta_z = \frac{1}{m} \left[\frac{eE_z - im\omega\omega_c \Delta_x}{\omega^2 + i\upsilon\omega} \right] \quad (13)$$

By substituting Δ_z in Eq. (11), and ignoring the anharmonicity, we can calculate Δ_x

$$-\omega^2 \Delta_x + \frac{\omega_P^2}{2\epsilon_r} \left(1 + \beta + \alpha \Delta_x \right) \Delta_x + \frac{i\omega\omega_c}{m}$$
$$\left[\frac{ieE_z - im\omega\omega_c \Delta_x}{\omega^2 + i\upsilon\omega} \right] - i\upsilon\omega\Delta_x = \frac{-eE_x}{m} \quad (14)$$

$$\Delta_x = \frac{e \left[E_x + \frac{i\omega\omega_c E_z}{\omega^2 + i\upsilon\omega} \right]}{m \left[\omega^2 - \frac{\omega_P^2}{2\epsilon_r} (1 + \beta) - \frac{\omega^2 \omega_c^2}{(\omega^2 + i\upsilon\omega)} + i\upsilon\omega \right]} \quad (15)$$

🖄 Springer

As explained above, the displacement of electrons in CNTs is finite for the field perpendicular to the CNT axis and 0 for the field along the axis. Therefore, the term E_Z is taken as 0.

$$\Delta_x = \frac{eE_x}{m\left[\omega^2 - \frac{\omega_p^2}{2\epsilon_r}(1+\beta) - \frac{\omega^2\omega_c^2}{(\omega^2 + \iota\nu\omega)} + \iota\nu\omega\right]} \quad (16)$$

The anharmonicity factor α is responsible for nonlinear mixing in the electron response towards the incident laser beams. If we neglect the nonlinear terms, then electron displacement due to laser beams is given as,

$$\Delta_j = \frac{eE_j}{m\left[\omega_j^2 - \frac{\omega_p^2}{2\epsilon_r}(1+\beta) - \frac{\omega_j^2\omega_c^2}{(\omega^2 + \iota\nu\omega)} + \iota\nu\omega_j\right]} \quad (17)$$

With the help of Eqs. (9) and (16), the non-linear term provides electron displacement Δ_x at frequency $\omega = (\omega_1 - \omega_2)$ and becomes responsible for THz generation.

$$\left[\omega^2 - \frac{\omega_p^2}{2\epsilon_r}(1+\beta) - \frac{\omega^2\omega_c^2}{(\omega^2 + \iota\nu\omega)} + \iota\nu\omega\right]\Delta_x = -\frac{\alpha\omega_p^2\Delta_1\Delta_2^*}{4\epsilon_r} \quad (18)$$

$$\Delta_x = \frac{-\alpha\omega_p^2\Delta_1\Delta_2^*}{4\epsilon_r\left[-\omega^2 + \frac{\omega_p^2}{2\epsilon_r}(1+\beta) - \iota\nu\omega + \frac{\omega^2\omega_c^2}{(\omega^2 + \iota\nu\omega)}\right]} \quad (19)$$

Due to this displacement (Δ_x) of electrons, plasma electrons start oscillating with THz oscillatory velocity given by $v_{\omega x} = -\iota\omega\Delta_x$. The THz oscillatory velocity is further responsible for the generation of non-linear THz current density $J'^{NL}_{\omega x}$.

$$J'^{NL}_{\omega x} = -en_o v_{\omega x} \quad (20)$$

The nonlinear current density $J'^{NL}_{\omega x}$ is non-zero over the cross-section $\pi(b^2 - a^2)$ and 0 over the area d^2. Thus, the average nonlinear THz current density due to the array of CNTs is

$$J^{NL}_{\omega x} = -\pi en_o n_c (b^2 - a^2) v_{\omega x} \quad (21)$$

THz Wave Dynamics

The standard equation for the generation of THz waves is

$$\nabla^2 E_{\omega x} + k^2 E_{\omega x} = \frac{-4\pi\iota\omega}{c^2} J^{NL}_{\omega} \quad (22)$$

From the above Eq. (22), we can write the x-component as

$$\frac{\partial^2 E_{\omega x}}{\partial z^2} + k^2 E_{\omega x} = \frac{-4\pi\iota\omega}{c^2} J^{NL}_{\omega x} \quad (23)$$

where, $k^2 = \frac{\omega^2}{c^2}\left[\epsilon_r - \pi(b^2 - a^2)n_c \frac{\omega_p^2}{\left[\omega^2 - (1+\beta)\frac{\omega_p^2}{2\epsilon_r} - \frac{\omega^2\omega_c^2}{\omega^2 + \iota\nu\omega}\right]}\right]$

On solving Eq. (23), we get a terahertz electric field $E_{\omega x}$ given below

$$E_{\omega x} = \left[\pi(b^2 - a^2)n_c\right]\frac{1}{\epsilon_r}\left[\frac{n_0 e^2}{m\epsilon_0\omega_1^2}\right]\left[\frac{eA_2A_1}{m\omega_2 c}\right]\left[\frac{\omega_p^2}{-\omega^2 + (1+\beta)\frac{\omega_p^2}{2\epsilon_r} - \iota\nu\omega + \frac{\omega^2\omega_c^2}{\omega^2 + \iota\nu\omega}}\right]$$
$$\left[\frac{\omega_1^2}{-\omega_1^2 + (1+\beta)\frac{\omega_p^2}{2\epsilon_r} - \iota\nu\omega_1 + \frac{\omega_c^2\omega_1^2}{\omega_1^2 + \iota\nu\omega_1}}\right]\left[\frac{\omega_2^2}{-\omega_2^2 + (1+\beta)\frac{\omega_p^2}{2\epsilon_r} + \iota\nu\omega_2 + \frac{\omega_c^2\omega_2^2}{\omega_2^2 + \iota\nu\omega_2}}\right]$$
$$\left[\frac{\omega^2}{\left[k_\omega^2 - (k_1 + k_2)^2\right]c(b+a)\iota\omega_2}\right] \quad (24)$$

The normalized THz electric field equation is

$$\frac{E_{\omega x}}{A_1} = \left[\pi(b^2 - a^2)n_c\right]\frac{1}{\epsilon_r}\left[\frac{n_0 e^2}{m\epsilon_0\omega_1^2}\right]\left[\frac{eA_2}{m\omega_2 c}\right]$$
$$\left[-\frac{\omega^2}{\omega_p^2} + \left(\frac{1+\beta}{2\epsilon_r}\right) - \iota\left(\frac{\omega}{\omega_p}\right)\left(\frac{\nu}{\omega_p}\right) + \frac{\omega_c^2/\omega_p^2}{1 + \iota\nu/\omega}\right]^{-1}$$
$$\left[1 + \iota\frac{\nu}{\omega_1} - \left(\frac{\omega_p^2}{\omega_1^2}\right)\left(\frac{(1+\beta)}{2\epsilon_r}\right) - \frac{\omega_c^2/\omega_1^2}{1 + \iota\nu/\omega_1}\right]^{-1} \quad (25)$$
$$\left[1 - \iota\frac{\nu}{\omega_2} - \left(\frac{\omega_p^2}{\omega_2^2}\right)\left(\frac{(1+\beta)}{2\epsilon_r}\right) - \frac{\omega_c^2/\omega_2^2}{1 + \iota\nu/\omega_2}\right]^{-1}$$
$$\left[\frac{\omega^2/\omega_2^2}{\left[k_\omega^2 - (k_1 + k_2)^2\right]c(b+a)/\omega_2}\right]$$

Discussion and Conclusion

Numerical simulations are performed with the following set of laser beams and CNT parameters. The carbon dioxide laser beams of frequencies $\omega_1 = 2 \times 10^{14}$ rad/s and $\omega_2 = 1.85 \times 10^{14}$ rad/s have been chosen in such a way that frequency difference lies in the region of THz. The corresponding wavelengths of laser beams are $\lambda_1 = 9.45\,\mu m$ and $\lambda_2 = 10.20\,\mu m$. The intensities of both laser beams are $I \sim 10^{13}$ W/cm^2 and $e\,A_2/m\,\omega_2 c = e\,A_2/m\,\omega_2 c = 0.03$. The length of CNT is 1 μm with an inner radius of 20.0 nm, and

139

Fig. 3 Variation of normalized terahertz amplitude with normalized THz frequency at different values of external magnetic field $B = 170$ kG, 195 kG, 235 kG for $\beta = 0.4622$ and $\alpha = 0.06$ nm^{-1}. Inset graph; plot similar to figure, in the absence of a static magnetic field
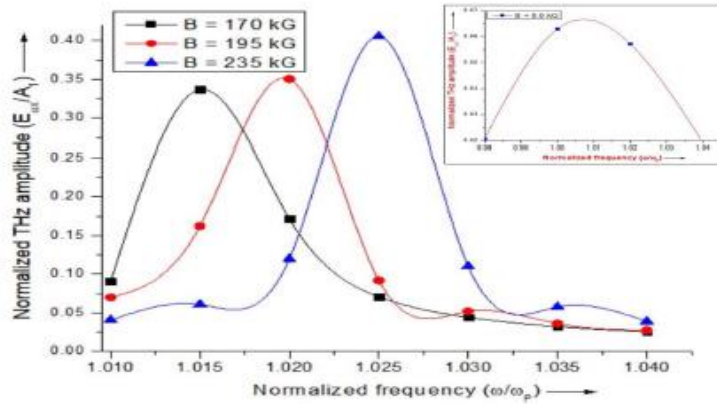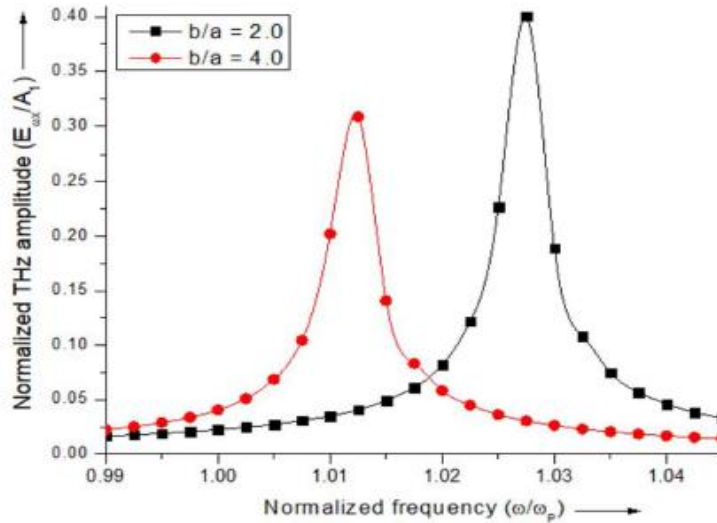

outer radius of 40.0 nm. Corresponding to these dimensions of CNTs, characteristic parameter $\beta = 0.4622$ and anharmonicity factor $\alpha = 0.06$ nm^{-1}. The relative permittivity of a dielectric surface is 2.5 and the applied static magnetic field lies in the range 170 to 235 kG.

In Fig. 3, we have plotted the graph between normalized THz amplitude and normalized frequency for different values of external static magnetic field $B = 140$ kG, 200 kG,

and 230 kG. From Fig. 3, it is observed that each curve shows an increase in normalized THz amplitude with the increase of normalized THz frequency and attains its maximum value. After attaining the maximum value, normalized THz amplitude shows a decrease with the increase of normalized frequency. The curve shows the maxima at frequency, $\omega = \omega_P \sqrt{(1 + \beta)/2\epsilon_r + (\omega_c^2/\omega_P^2)}$. This is the

Fig. 4 Variation of normalized terahertz amplitude with normalized THz frequency for different values of characteristic parameter β and anharmonicity factor α at the optimized value of external magnetic field $B = 235$ kG

Springer

frequency where surface plasmon resonance occurs. At this resonance frequency, absorption of lasers by the electrons of CNT becomes maximum; and hence, THz wave of maximum amplitude is produced. Also, the external magnetic field is used to enhance the normalized THz amplitude. It is due to the reason that the applied magnetic field increases the nonlinearity of the system. Similar results were shown by Jain et al. [11] where they have applied a magnetic field on an array of CNTs embedded on the metal surface. It is further observed from this figure that with the increase of the external magnetic field, the surface plasmon resonance point gets shifted towards the higher value of normalized frequency. This is due to the dependence of surface plasmon resonance frequency on the external magnetic field. Hence, it is observed that surface plasmon resonance condition does not only depend upon dimensions of CNTs but also depends upon the external magnetic field. The inset figure of Fig. 3 is plotted in the absence of a static magnetic field; other parameters are the same as in Fig. 3. We observe an increase in the normalized THz amplitude, in the presence of a static magnetic field as compared to the absence of a magnetic field. This also shows the significance of a static external magnetic field in our proposed theory.

To study the effect of dimensions of CNTs on the normalized THz amplitude, we have plotted a graph between normalized THz amplitude and normalized frequency as shown in Fig. 4. In the first case, external and internal radii

of CNTs are 40.0 nm and 20.0 nm, whereas in the second case these are 36.0 nm and 12.0 nm. Corresponding to the first case $b/a = 2.0$, $\beta = 0.4622$, $\alpha = 0.06$ nm^{-1}, whereas, corresponding to the second case $b/a = 4.0$, $\beta = 0.1848$, $\alpha = 0.08$nm^{-1}. The value of normalized THz amplitude is observed to decrease with the increase in the value of b/a. THz amplitude is more for $b/a = 2.0$ (first case) as compared to $b/a = 4.0$ (second case). The physical mechanism of this observation is as follows: with the lesser value of b/a for CNTs, there is more absorption of laser beams by CNTs. A similar observation was made by Vij et al. [10] where they observed direct dependence of THz amplitude on the radii of CNTs. Watanabe et al. [27] have also shown the direct dependence of the THz electric field on the radii of CNTs in their experiment, in which they generated intense THz pulse excitons by using CNTs. Also, a shift in the surface plasmon resonance point is observed towards the lower side of THz frequency at the lower value of b/a. This shift can be well explained from the expression of surface plasmon resonance conditions.

In Fig. 5, we have shown a variation of normalized THz amplitude with normalized frequency at different values of inter-tube separation $d = 60.0$ nm, 75.0 nm, 90.0 nm, whereas other parameters are the same as those of Fig. 3. From the three curves of Fig. 5, it is observed that the normalized THz amplitude shows maxima at the lower value of inter-tube separation 60.0 nm. This is because at the lower value of inter-tube separation, the number density

Fig. 5 Variation of normalized terahertz amplitude with normalized THz frequency at different values of inter-tube separation at the optimized value of external magnetic field $B = 235$ kG for characteristic parameter $\beta = 1.064$ and $\alpha = 0.06$ nm^{-1}
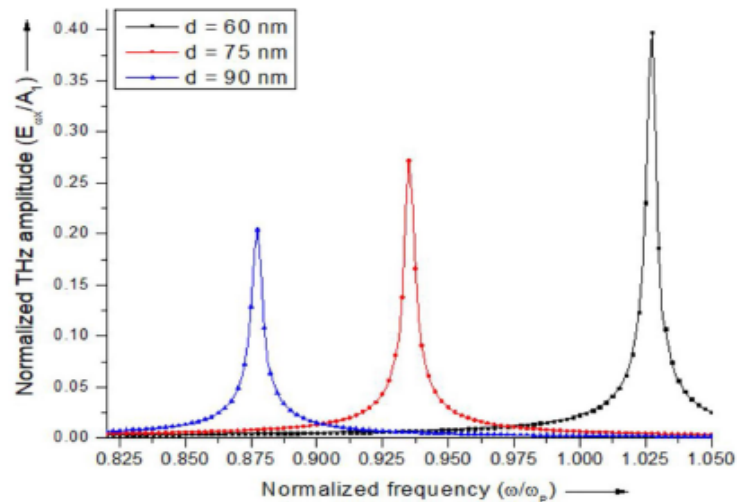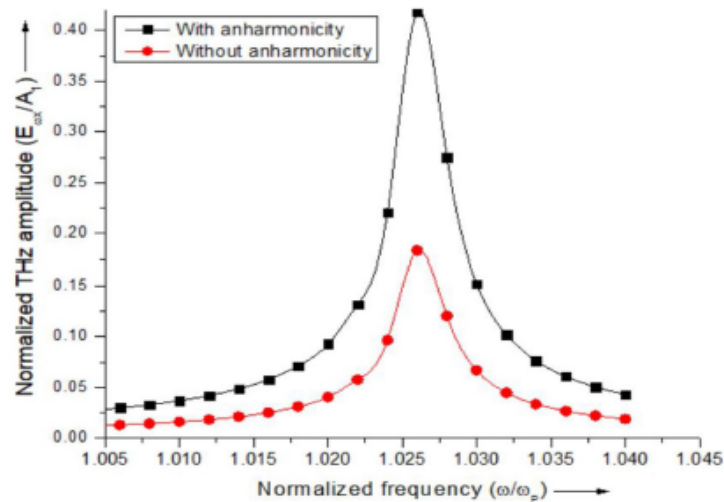
Fig. 6 Variation of normalized terahertz amplitude with normalized THz frequency, with and without anharmonicity at the optimized value of external magnetic field $B = 235$ kG and other parameters are the same as those of Fig. 3

of CNTs increases, and hence nonlinearity of the array of CNTs behaving as plasma increases. The same observation was made by Kumar et al. [28]. From the graph, it is also observed that the surface plasmon resonance shifts towards the left with the decrease in the inter-tube separation.

In Fig. 6, we have shown the effect on normalized THz amplitude by considering the anharmonicity and without considering the anharmonicity in the CNTs. From the curves, it is clear that by considering the anharmonicity, there is a significant increase in the normalized amplitude of THz radiation. From Fig. 6, it is observed that normalized THz amplitude shows a nearly 2.0 times increase in anharmonic CNTs as compared to the case where anharmonicity is not considered. Hence, the THz amplitude is enhanced significantly by considering anharmonicity as compared to considering the ponderomotive nonlinearity only. One more very important observation which we have made from this figure is that the surface plasmon resonance is broadened. It is very useful when we are using this THz source for communication purposes because with the broadening of surface plasmon resonance frequency, bandwidth is increased.

Conclusion

The surface plasmon resonance peaks expand and broaden due to the anharmonic behavior of an array of CNTs in the presence of a static magnetic field. It also results in the enhancement of normalized THz amplitude. Under the influence of electric fields exerted by laser beams, electrons of CNTs experience restoration force to induce the nonlinear current. This nonlinear current is further responsible for the generation of THz radiations. The normalized THz field gets resonantly enhanced at the surface plasmon resonance frequency. One can tailor this resonance condition $\omega = \omega_P \sqrt{(1 + \beta)/2\varepsilon_r + (\omega_c^2/\omega_P^2)}$ for the enhancement of normalized THz amplitude by changing the values of characteristic parameter β and external magnetic field B. It is also observed that the normalized THz amplitude shows a significant variation with the change of values of the applied external magnetic field, inter-tube separation, dimensions, and the density of CNTs, by considering the anharmonicity.

Declarations

Consent to Participate Not applicable.

Consent for Publication Not applicable.

Conflict of Interest The authors declare no competing interests.

🌀 Springer

142

References

1. Baker C, Lo T, Tribe WR, Cole BE, Hogbin MR, Kemp MC (2007) Proc. IEEE 95:1559
2. Orlando AR, Galierano GP (2009) J Infrared Millim Terahertz Waves 30:1308
3. Siegel PH (2002) IEEE Trans Microwave Theory Tech 50:910
4. Dragoman D, Dragomen M (2004) Prog Quantum Electron 28:1
5. Ishigaki K, Shiraishi M, Suzuki S, Asada M (2012) Nishiyama N and Arai S Electronics letters 48:582
6. Mehta A, Rajput J, Kang K, Kant N (2020) Laser Phys 30:045402
7. Kumar S, Vij S, Kant N (2021) Mehta A and Thakur V EPJ Plus 136:148
8. Sharma S, Vijay A (2018) Phys Plasmas 25:023114
9. Sharma S, Vijay A (2019) Optik 199:163381
10. Vij S, Kant N and Thakur V (2019) Plasmonics 14:1051
11. Jain S, Parashar J, Kurchania R (2013) Int Nano Lett 3:5326
12. Mehta A, Kant N (2019) Proc SPIE 10917-109170R
13. Zhang Q, Haroz E H, Jin Z, Ren L, Wang X, Arvidson RS, Luttge A, Kono J (2013) Nano Lett 13:5991
14. Giannini V, Vecchi G, Rivas JG (2010) Phys Rev Lett 105:266801
15. Titova LV, Pint CL, Zhang Q, Hauge RH (2015) Kono J and Hegmann F A Nano Lett 15:3267
16. Batrakov KG, Kibis OV, Kuzhir P, Da Costa MR, Portnoi ME (2010) J Nanophotonics 4:041665
17. Portnoi ME, Kibis OV, Da Costa MR (2008) Superlattices Microstruct 43:399–407
18. Wang Y, Wu Q (2008) Chin Opt Lett 8:770
19. Dragoman D, Dragoman M (2004) Physics E 24:282
20. Dagher M, Chamanara N, Sounas D, Martel R, Caloz C (2012) IEEE Trans. Nanotech 11:463
21. Reich S, Thomson C, Maultzsch J (2004) Carbon nanotubes: Basic concepts and physical properties. Wiley VCH
22. Lu W, Wang D (2007) Chen L. Nano Lett 7:2729
23. Liu S, Tripathi VK (2004) Phys Rev B 70:115414
24. Kumar M, Tripathi VK (2013) Phys Plasmas 20:023302
25. Dai H (2002) Surf Sci 500:218
26. Muñoz E, Maser WK, Benito AM, Martínez MT, de la Fuente GF, Righi A, Sauvajol JL, Anglaret E, Maniette Y (2000) Appl Phys A 70:145
27. Watanabe S, Minami N, Shimano R (2011) Opt Express 19:1528
28. Kumar A, Kumar P (2016) Phys Plasmas 23:103302

143

Resonant terahertz generation by cross-focusing of Gaussian laser beams in the array of vertically aligned anharmonic and magnetized CNTs

Sandeep Kumar [a], Shivani Vij [b], Niti Kant [a], Vishal Thakur [a] ✍ ✉

Show more ⌄

+ Add to Mendeley   ⌝ Share   🔓 Cite

Get rights and content

Abstract

In this novel scheme of terahertz (THz) generation, the effect of cross-focusing of Gaussian laser beams in the array of vertically aligned anharmonic carbon nanotubes (CNTs) has been studied. The static magnetic field is applied transverse to the axis of CNTs to magnetize the CNTs. The nonlinearity in the system arises due to the ponderomotive force exerted by the laser beams on the electrons of CNTs. The plasma in the CNTs rearranges itself due to this ponderomotive nonlinearity, which gives rise to the cross-focusing of both laser beams. The nonlinear current at THz frequency appears in the array of CNTs on account of the ponderomotive nonlinearity and anharmonicity of the system. The anharmonicity plays a pivotal role in the enhancement of THz generation. The normalized amplitude of THz radiation shows a notable enhancement with the increase of the externally applied static magnetic field (90 kG to 330 kG), dimensions of CNTs, and inter-tube separation. The cross-focusing of two laser beams in the magnetized collisional plasma makes a significant enhancement in the THz generation with the help of anharmonicity.

Introduction

In the contemporary technical world, terahertz technology has explored many new research opportunities in various potential fields like imaging [1], [2], medicine [3] biological chemical sensing [4], communication [5], and explosive detection [6]. The numerous schemes for THz generation have been introduced by the researchers to provide packed, compact, highly efficient, and reliable THz sources. To attain this, they have used different mechanisms, techniques, and theories. Some of these are; by applying external static and wiggler magnetic fields on the array of CNTs [7], [8], by nonlinear mixing of lasers [9], by using filamentation under the influence of external magnetic and electric fields applied at the right angle to each other [10], by using laser coupling to anharmonic CNTs array [11] and by using a thin semiconductor slab with density ripple under the influence of external magnetic field [12]. The CNTs have extraordinary thermal and electrical conductivity with the advantage of compact size, which makes these nanotubes effective and reliable THz sources. Titova et al. [13] have shown the THz generation by using single walled carbon nanotubes (SWCNTs) with femtosecond lasers. Ahmad et al. [14] generated THz radiation from multi-ion plasma by using two-color laser self-focusing. The study of the cross-focusing in collisional plasma in the presence of a static external electric field has a significant impact on the THz generation [15]. The intense laser beams can undergo cross-focusing in the plasma by the various nonlinear interaction mechanisms. Akhmanov et al. [16] and Sodha et al. [17] have provided the theoretical models to study the self-focusing of intense laser beams in the plasma by applying an external magnetic field and without applying the magnetic field. Sharma [18] has studied the self-focusing and filamentation of the laser beam in plasma under the effect of the external static magnetic field. The effect of external magnetic field on the cross focusing of two co-propagating Gaussian laser beams in plasma has been studied and it was observed that the focusing of one beam affects the other and vice versa [19], [20], [21], [22].

In this manuscript, we have proposed a theoretical model for THz generation by irradiating two cross-focused and co-propagating Gaussian laser beams on vertically aligned hollow anharmonic CNTs in the presence of an external static magnetic field (shown in Fig. 1). The array of CNTs is embedded on the silicon carbide glass dielectric surface, having a refractive index of 2.5. This array is synthesized by using the plasma-enhanced chemical vapor deposition (PECVD) method. The CNTs are coated with non-conductive polymer to suppress the mutual interactions of CNTs and to enhance the THz generation. The mutual interactions between laser beams, THz radiations, and CNTs in the form of plasma can decrease the efficiency of output THz radiations. Therefore THz efficiency has been calculated by using optimized CNT and Gaussian laser beam parameters including the mutual effects.

Each CNT is characterized by inner radius a, outer radius b, length L, and free-electron density n_0 corresponding to the plasma frequency $\omega_P = \left(n_0 e^2/m\varepsilon_0\right)^{1/2}$, where e and m represent electronic charge and rest mass respectively. In the array, there are N_c number of CNTs per unit area given by $N_c = 1/d^2$, where d is the inter-tube distance. A single-walled CNT is used as a hollow cylinder in most of the experimental works [23] but as far as the response of this CNT towards the electric and magnetic fields of laser is concerned, it behaves like a solid cylindrical tube [24]. The static magnetic field is applied mutually perpendicular to the direction of co-propagation and polarization of laser beams. In the present scheme, we have used preformed plasma (array of CNTs in the form of plasma). The laser beam interacts with the array of CNTs and energy is absorbed by the inner wall of each CNT to ionize its atoms to form plasma. The ponderomotive force acts on the electrons of CNTs to produce nonlinearity and the plasma of CNTs gets rearranged along the direction of the applied static magnetic field. This ponderomotive nonlinearity carries the main responsibility to produce the cross-focusing of laser beams in the magnetized collisional plasma. In the 2nd section of the paper, we explain the cross-focusing phenomenon of two Gaussian laser beams. In the 3rd section, we have provided the theoretical model for the generation of THz radiation. In the 4th section of this paper, the discussion is summarized, and the conclusion is provided.

Section snippets

Cross focusing of lasers beams

In the proposed scheme, we consider two Gaussian laser beams with slightly different frequencies (ω_1, ω_2) and wavenumbers (k_1, k_2), polarized along x-direction and co-propagating along the z-direction as shown in Fig. 1. The static magnetic field B is applied along the y-direction that is mutually perpendicular to the direction of propagation of lasers and the axis of CNTs. The electric field profiles of laser beams are provided as $\vec{E}_j = \hat{x} E_{jx\,0} e^{-i(k_j z - \omega_j t)}$; $\quad j = 1, 2.$where, $E_{jx\,0}$ represent the amplitude of the ...

Terahertz generation

The electrons of CNTs in the presence of static magnetic field experience a non-linear ponderomotive force at beat frequency $\omega = \omega_1 - \omega_2$ and wave number $k = k_1 - k_2$. The ponderomotive force at beat wave frequency is given as

$$\vec{F}_{PM} = -\frac{e^2 \nabla\left(\vec{E}_1 \vec{E}_2^*\right)}{2m(i\omega_1 + \nu)(-i\omega_2 + \nu)}; \qquad E_1 E_2^* = \left(1 - \frac{\varepsilon_{1\approx 0}\delta_{2\approx 0}^*}{\varepsilon_{1\approx 0}\varepsilon_{2\approx u}^*}\right) E_{1x0} E_{2x0}^* e^{-i(kz - \omega t)}.$$ As the static magnetic field is applied along the y-axis, therefore x and z-components of the beat frequency ponderomotive force (F_{PMx} and F_{PMz}) can be expressed as:

$$F_{PMx} = \frac{e^\circ E_{1,00} E_{2,00}}{2m(i\omega_1 + \nu)(-i\omega_2 + \nu)\sqrt{f_1 f_2}} \left(1 - \frac{\varepsilon_1}{}\right)\dots$$

Results and discussion

One can solve the Eq. (11) numerically by using Runge–Kutta (RK) method. For this purpose, the following initial conditions are employed (i) $f_1|_{\zeta-0} = f_2|_{\zeta-0} = 1$. (ii) $\frac{df_1}{d\zeta}\big|_{\zeta=0} = \frac{df_2}{d\zeta}\big|_{\zeta=0} = 0$. To carry out the numerical computation and analysis, we have used the specific set of laser-plasma and CNT parameters: $\omega_1 = 2.4 \times 10^{14}$ rad /s, $\omega_2 = 2.1 \times 10^{14}$ rad /s, $\lambda_1 = 0.80$ μm, $\lambda_2 = 0.70$ μm, the intensity of laser beams $I_1 \sim I_2 = 10^{14}$ W/cm^2, radii of the laser beams $r_{10} = 20$ μm and $r_{20} = 40$ μm. The inner and outer radii of CNTs are 40 nm and...

Conclusion

In this proposed scheme, the THz generation is well enhanced by the cross focusing of two Gaussian laser beams in the vertical array of CNTs, under the influence of the static magnetic field. The nonlinear coupled differential equations have been derived by using PR and WKB approximation, to discuss the beam width parameters of laser beams. The focusing of each beam depends upon the applied static magnetic field and intensity of each laser beam. The normalized THz amplitude shows significant...

Declaration of Competing Interest

The authors declare that they have no known competing financial interests or personal relationships that could have appeared to influence the work reported in this paper....